Dissertation
submitted to the Department of Earth Sciences
of the Freie Universität Berlin

Responses of regional sedimentary archives to Late Quaternary climate change

Luminescence dating of coastal, lacustrine and aeolian deposits from northern China and Germany

JINGRAN ZHANG

张 静 然

Freie Universität Berlin

Responses of regional sedimentary archives to Late Quaternary climate change

Luminescence dating of coastal, lacustrine and aeolian deposits from northern China and Germany

Inaugural-Dissertation zur Erlangung des Doktorgrades

Dr. rer. nat.

im Fachbereich Geowissenschaften

der Freien Universität Berlin

vorgelegt von

JINGRAN ZHANG

张静然

aus Anhui, China

Berlin 2016

Erstgutachter: Prof. Dr. Manfred Frechen

Zweitgutachterin: Prof. Dr. Margot Böse

Tag der Disputation: 05.02.2016

Acknowledgements

This PhD project has been financially supported by the DAAD (German Academic Exchange Service) scholarship and carried out in the Leibniz Institute for Applied Geophysics (LIAG), in Hannover, Germany. I gratefully acknowledge the funding from DAAD and all the facilities provided by LIAG that made my PhD study possible.

I would like to express my sincere respect and thanks to my “Doktorvater” Prof. Manfred Frechen, who offered me the great opportunity to carry out my PhD research in Germany three years ago. It has been a great honor to be one of your PhD students. Through the whole period of my study, you are always supportive and make me feel free to do the work following my own will. I appreciate all you contributions of time, ideas, motivations and the other essential supports to fulfill this PhD. I would never forget your reactions after the "HF accident" I had shortly after I arrived in Germany. I was actually so scared and waiting for a "storm" in the office on the following Monday morning. But, you came into my office, hugged me saying “I’m very sorry that I didn't take good care of you” and never blamed me even for a single word. Your kindness and magnanimity are deeply touched me.

I would like to give my heartfelt thanks to Dr. Sumiko Tsukamoto for co-supervising my PhD. I feel very lucky that I could always come to you whenever and wherever I got stuck with my work. I very much appreciate for your critical reading and careful corrections for almost all the writings I have done in the past three years. I had also lots of great girl’s time together with you after work, celebrating for the papers, cooking together, having a glass of Alsterwasser, and of course the Tulip field-sightseeing in Schwaneberg should not be ignored…

I am also deeply indebted to all my colleagues from section S3 in LIAG for their generous help not only in my research but also in the daily life since the first day I joined in the group. Gudrun Drewes, Petra Posimowski, Sonja Riemenschneider, Sabine Mogwitz, Astrid Jaeckel and Ragna Bergman are thanked for your generous help in the OSL, gamma spectrometry and grain size lab. Frank Oppermann and Karsten Vollmer are thanked for your technical support for the computer stuff and some administrative work in the institute. Melanie Sierralta, Christine Thiel, Tobias Lauer and Astrid Techmer are

thanked for your inspiring discussions and suggestions about my research. Furthermore, I would like to give my special thanks to Sonja (of course Gerrit as well), who did and still doing me so many favors that make my life much easier in Germany. Thank you very much for all things you have done for me, as spokesman, translator and Deutsch Lehrerin...whatever I need.

I am very delighted for having the opportunity to join very fruitful collaborations with Prof. Frank Lehmkuhl and Veit Nottebaum from RWTH Aachen. Thank you very much for providing the loess samples from Qilian Shan and writing papers together with me. Special thanks are going to Prof. Lehmkuhl for inviting me to visit Aachen for two weeks in Dec 2013 and financing me to participate in the Montreal LED conference in July 2014. I enjoyed these two trips very much and certainly benefited a lot.

I'd like to thank Prof. Margot Böse from Freie Universität Berlin for the very constructive comments for my PhD and carefully reading and reviewing the dissertation. I have been to Lankwitz campus several times during my doctorate study. The colleges there are always very friendly and welcoming. Jacob Hardt is especially thanked for giving me very useful advices concerning administrative formalities in submitting this dissertation in the last days. And also thanks for making nice coffee whenever I visit.

I want to mention particularly my office-mates Dr. Eike Rades, Dr. Chia-han Zeng, Gabi Barta, Ede Kenzler and Li Yan, who share not only the office but also the friendship and knowledge with me. You made the room A47 a joyful place for me. I would also like to thank all the "Garding" group members, especially Dr. Alf Grube, Maria Proborukmi and Christel Adam, for all the constructive discussions and exchanging ideas which helped me understand more and better about the Garding core that I work with.

Many thanks go to Prof. Jia Yulian, who is always supportive and cares about me since I became your Master student. Your help in the field trip in China during my PhD is much appreciated. Dr. Chen Jianhui is thanked for the help in processing the DEM maps of Huangqihai Lake.

The last but not least, Dr. Hao Long, my best friend and beloved husband, is so much appreciated for your faithful support, constant encouragement and unconditional love. Thank you with all my heart and soul for being with me in this amazing life.

Life is a long journey. Looking back upon the past three years, pursuing a PhD is indeed painful but also enjoyable; it has been certainly a life-changing experience for me. I am sure that these three years must be one of the brightest and most rememberable time in my whole life. Thousands of thanks again to all of you!

Jingran Zhang

20.05.2015

Hannover

Table of content

Acknowledgements ..... **i**
Table of content ..... **iv**
List of figures ..... **vii**
List of tables ..... **x**
Abstract **1**
Kurzfassung **3**
Chapter 1 Introduction **6**
1.1 Introduction 7
1.1.1 Luminescence dating 8
1.1.2 Research questions and objectives 15
1.1.3 Outline of the dissertation 21
Reference 22
Chapter 2 Late Quaternary loess accumulation in Qilian Shan, northern China **36**
2.1 Late Pleistocene and Holocene loess sedimentation in central and western Qilian Shan (China) revealed by OSL dating 37
Abstract 37
2.1.1 Introduction 38
2.1.2 Regional setting and section description 39
2.1.3 Luminescence dating 46
2.1.4 Discussion 53
2.1.5 Conclusions 58
References 59
Chapter 3 Late Quaternary sedimentary processes in German North Sea coast **68**
3.1 OSL and ^{14}C chronologies of a Holocene sedimentary record (Garding-2 core) from the German North Sea coast 69
Abstract 69
3.1.1 Introduction 70
3.1.2 Geological setting and core description 72
3.1.3 Methods 75
3.1.4 Results 78
3.1.5 Comparison between OSL and ^{14}C chronologies 85

3.1.6 Transgression and sediment accumulation history during the past 16 ka 87
3.1.7 Conclusions 91
References 92
Chapter 4 Late Quaternary lake evolution of Huangqihai in northern China 99
4.1 Lake level reconstruction of Huangqihai Lake in northern China since MIS 3 based on pulsed optically stimulated luminescence dating 100
Abstract 100
4.1.1 Introduction 101
4.1.2 Regional setting 102
4.1.3 Material and methods 104
4.1.4 Results 113
4.1.5 Discussion 119
4.1.6 Conclusion 126
Reference 126
Chapter 5 Post-IR IRSL dating of K-rich feldspar and polymineral fine grains . 133
5.1 Application of the post-IR IRSL dating in the Garding-2 core sediment from the German North Sea coast 134
Abstract 134
5.1.1 Introduction 135
5.1.2 Samples and experimental details 136
5.1.3 Equivalent doses 139
5.1.4 Bleachability and residual dose 140
5.1.5 Dose recovery test 144
5.1.6 Fading test 145
5.1.7 Comparison of pIRIR ages with independent age control 151
5.1.8 Conclusions 152
References 153
5.2 D_e plateau and its implications for post-IR IRSL dating of polymineral fine grains 159
Abstract 159
5.2.1 Introduction 160
5.2.2 Samples and experimental details 161
5.2.3 Luminescence characteristics 164

5.2.4 The pIRIR D_e plateau and its implications 169
5.2.5 Conclusions 174
References 174
Chapter 6 Conclusions and outlooks 179
6.1 Conclusions 180
6.1.1 Luminescence age determination and validation 180
6.1.2 Environmental implications of the obtained chronologies 184
6.2 Outlooks of the future research 186
6.2.1 Suggestions regarding luminescence methodology 186
6.2.2 Further work on Garding drilling project 188
Reference 188
Appendix 1: Curriculum vitae 191
Appendix 2: Publications 192
Appendix 3: Conference contributions 194
Appendix 4: Eidesstattliche Erklärung 196

List of figures

Fig. 1.1 Overview map showing the localities of the three study areas.. 8
Fig. 1.2 Sketch of a simple band gap energy model of optically stimulated luminescence (OSL). 10
Fig. 1.3 The emission spectra from quartz and feldspar as well as the corresponding stimulation and detection wave length for OSL measurements. 11
Fig. 1.4 Geomorphological map of Huangqihai Lake 20
Fig. 2.1 (a) Map of China. (b) Enlarged Map showing the Qilian Shan area and the locations of the sampling sections. 40
Fig. 2.2 Loess covered landscape in Qilian Shan area and typical loess sections.. 41
Fig. 2.3 Graphical logs of the loess sections. OSL ages of 23 loess samples are shown. 45
Fig. 2.4 OSL decay curves and dose-response curves for sample (a) LUM-2940 and (b) LUM-2944.. 48
Fig. 2.5 Equivalent dose, dose recovery ratio, thermal transfer and recycling ratios as a function of preheat temperature for sample (a) LUM-2940 and (b) LUM-2944, respectively.. 49
Fig. 2.6 (a) Measured to given doses ratio for the dose recovery test on all samples. ... 50
Fig. 2.7 Dose response curves for one representative aliquot of sample (a) LUM-2939, (b) LUM-2938 and (c) LUM-2952, respectively..... 54
Fig. 3.1 A satellite image of the North Sea area (Google Earth).. 73
Fig. 3.2 A photograph of the core with the locations of the sedimentary units.. 74
Fig. 3.3 Results from the preheat plateau, dose recovery and thermal transfer tests..... 79
Fig. 3.4 The D_e distributions for medium and small aliquots of samples (a) LUM-2678 and (b) LUM-2728..... 80
Fig. 3.5 The summary of the dose rate data..... 82
Fig. 3.6 Lithology and chronology of the Garding-2 core..... 83
Fig. 4.1 (a) Map showing the location of Huangqihai Lake in northern China. (b) DEM map showing the catchment of Huangqihai Lake 103
Fig. 4.2 DEM map showing the sampling sites around the Huangqihai Lake.. 104
Fig. 4.3 (a) Photograph of the TGM site. (b) Sedimentary log and photo of section TGM. 106

Fig. 4.4 The photo and sedimentary log of section TJY1. 107
Fig. 4.5 The sedimentary log and the OSL age of section TJY2. 108
Fig. 4.6 The photos and sedimentary log of section TJY3. 113
Fig. 4.7 Decay curve and dose–response curve of a representative aliquot from sample LUM-3036 and LUM-3043.. 114
Fig. 4.8 Comparison of normalized OSL decay curves between the calibration quartz and sample LUM-3036 and LUM-3043 from the current study.. 115
Fig. 4.9 Dose recovery ratios of all samples. 117
Fig. 4.10 Abanico plot showing the De distribution of four representative samples: LUM-3035, LUM-3039, LUM-3041 and LUM-3047.. 118
Fig. 4.11 The chronostratigraphy of all studied sections from the current study and from Zhang et al. (2011, 2012). 121
Fig. 4.12 (a) Reconstructed Holocene temperature stack (30–90°N) (b) proxy temperature stacks (30–60°N) since deglaciation; (c) synthesized EASM precipitation from Gonghai Lake; (d) speleothem δ ^{18}O records from Dongge Cave; (e) schematic Holocene lake level history of Huangqihai Lake. 125
Fig. 5.1 The D_es for (a) IR_{50} and (b) pIRIR signals obtained from different preheat/stimulation temperatures. 140
Fig. 5.2 Residual doses of the IR_{50} and pIRIR signals.. 142
Fig. 5.3 The dose recovery ratio for (a) IR_{50} and (b) pIRIR signals obtained from different preheat/stimulation temperatures. 144
Fig. 5.4 Laboratory fading tests of (a) IR_{50} and (b) pIRIR signals obtained at different preheat/stimulation temperatures. 146
Fig. 5.5 Fading rate (*g*-value) determination of a representative aliquot of sample LUM-2699.. 148
Fig. 5.6 Natural signals and dose response curves for (a) IR_{50} and (b) pIRIR signals obtained from sample LUM-2761.....150
Fig. 5.7 Comparison between the IR_{50} and pIRIR ages and the corresponding quartz OSL ages.....151
Fig. 5.8 (a) Normalized test dose intensity of the IR_{50} and pIRIR signals.....164
Fig. 5.9 Residual doses of (a) IR_{50} and (b) pIRIR signals. 166
Fig. 5.10 The measured fading rates (g-value) of (a) IR_{50} and (b) pIRIR signals obtained at different preheat (stimulation) temperatures.. 167

Fig. 5.11 The dose recovery ratios for (a) IR_{50} and (b) pIRIR signals obtained at different preheat (stimulation) temperatures for three samples..... 168

Fig. 5.12 Equivalent dose (D_e) determined for four samples using different measurement conditions..... 172

Fig. 5.13 Fading corrected pIRIR and IR_{50} ages of sample (a) LUM-2941, (b) LUM-2940 and (c) LUM-2938.. 173

List of tables

Table 2.1 Summary of radionuclide concentrations, dose rates, Des and OSL ages for all samples. 52

Table 3.1 Summary of the U, Th and K contents, observed water contents, dose rates, D_e values and OSL ages for the Garding-2 core. 84

Table 3.2 Sample data and ^{14}C ages for the Garding-2 core. 85

Table 4.1 The POSL measurement protocol. 110

Table 4.2 Summary of the OSL sample information, dose rate data and water content. 112

Table 4.3 Summary of data showing D_e distribution statistics and age determinations of the measured quartz OSL samples in the study.. 116

Table 4.4 Summary of the AMS ^{14}C ages. 119

Table 5.1 Summary of the U, Th and K contents and the dose rates. 137

Table 5.2 The pIRIR single-aliquot-regenerative-dose (SAR) protocols used in this study. 139

Table 5.3 D_es and ages of $pIRIR_{150}$, $pIRIR_{225}$ and $pIRIR_{190}$ for all the samples 141

Table 5.4 The U, Th, K content and the calculated dose rate of the samples under study. 162

Table 5.5 The modified single-aliquot-regenerative-dose (SAR) protocol for post-IR IRSL dating. 163

Table 5.6 The D_e (Gy) values obtained from the IR_{50} and pIRIR signals under various preheat temperatures. 169

Table 5.7 Summary of pIRIR and IR_{50} ages. 171

Table 6.1 Overview of luminescence dating information of three sedimentary archives under study in this dissertation.. 181

Abstract

Chronology is the backbone of history. Geochronology plays the same role in geosciences research. The optically stimulated luminescence (OSL) dating is one of the most intensively and commonly applied numerical dating techniques in determining the age of Late Quaternary sediments. This dissertation focuses both on quartz OSL dating applications of Late Quaternary sediments to refine the chronological framework of regional sedimentary records and on methodological development in feldspar luminescence dating. For that reason, three sedimentary archives were chosen from northern China and Germany. Given validation of any dating method by comparison with other methods is necessary, radiocarbon dating is carried out as independent age control whenever possible. The research samples were collected from three different sedimentary archives, which are the Garding-2 core (240 m) drilled in the Eiderstedt Peninsula from the German North Sea coast, loess in central and western Qilian Shan in northwestern China and Huangqihai Lake from the East Asian monsoon marginal area in northern China.

The quartz OSL dating using single-aliquot regenerative-dose (SAR) protocol is primarily carried out for all three case studies. For the Garding-2 core, sand-sized quartz fractions are extracted from the uppermost 26 m of the core. The luminescence performance demonstrated that the quartz OSL signals from the coastal sediments were sufficiently bleached prior to deposition. The OSL ages coupled with ^{14}C ages are proven to be reliable and robust. For the loess sediments from the central and Qilian Shan area, fine-grained quartz fractions are used to conduct OSL dating. Relatively larger uncertainty of the quartz OSL ages is observed for some of the loess samples due to their low OSL sensitivity, which probably related to a short sedimentation history of the particles from the source region to depositional site. The routine quartz OSL dating encounters major problems in dating the samples from Huangqihai Lake due to the chemical irremovable feldspar contamination and the samples from the deeper part of the Garding-2 core because of the quartz signal saturation. To deal with the feldspar contamination, a post-IR OSL dating protocol using pulsed stimulation is employed to discriminate against the unwanted feldspar signals. Typical quartz OSL signals are observed after pulsing indicating that the feldspar contamination can be sufficiently removed. The obtained

pulsed OSL ages are generally in stratigraphic order in the geographical context and agree with independent age control from four radiocarbon ages.

By applying the suitable dating protocols of quartz OSL, the chronological frameworks of each sedimentary archive are established. The 16 ka coastal sedimentary record generated from the Garding-2 core reveals that after last deglaciation the transgression started in the early Holocene and the sea level reached the core site at around 8.3 ka and continued to rise with a decelerated rate until around 3 ka. In northern China, the OSL chronology of loess demonstrates that the deposition of dust was widespread since the last deglaciation (~13 ka) until ~3.6 ka in the northern piedmont of the central and western Qilian Shan area. During the last glacial period, loess sedimentation is only sporadically and episodically registered which is dated back at least to ~80 ka. The OSL ages obtained from a series of outcrops from Huangqihai Lake in northern China indicated a lake highstand during the early Holocene (~10−8 ka). The previously reported high lake level during MIS 3 that extensively occurred in northern and western China is not supported by the current record.

As an alternative dosimeter, feldspar has much higher saturation doses compared to quartz, which shows great potential in extending the age range of luminescence dating and thus allowing the determining of older geological events (likely back to Mid-Pleistocene). The recently developed post-IR IRSL (pIRIR) dating of feldspar at elevated temperature is tested using either sand-sized K-rich feldspar or polymineral fine grains from the Garding-2 core sediment and the Qilian Shan loess. The pIRIR and the corresponding IR_{50} signals are systematically investigated under various preheat and stimulation temperatures in terms of residual dose, fading rate and dose recovery measurements. Previously reported general behaviours of the pIRIR signal are confirmed, e.g. the higher preheat and stimulation temperatures are used, the higher residual and lower fading can be expected. The pIRIR dating of feldspar yields ages up to more than 400 ka without saturation, which is very promising for the investigation of the deeper part of the Garding-2 core. The pIRIR D_e plateau is observed for the polymineral fine grains from four loess samples with different ages. However, the dating implication of the pIRIR D_e plateau cannot be fully understood so far. Further investigations are still imperative in order to unveil the fundamental mechanisms of the pIRIR signal.

Kurzfassung

Die nummerische Altersbestimmung ist die Basis für eine verlässliche zeitliche Rekonstruktion von Sedimentarchiven in den Geowissenschaften. Die Optisch Stimulierte Lumineszenz (OSL)-Datierungsmethode ist eine in den letzten Jahrzehnten etablierte und weit verbreitete Altersbestimmungsmethode, mit der das Ablagerungs- oder Sedimentationsalter von (spät) quartären Sedimenten bestimmt werden kann. Der methodische Schwerpunkt dieser Dissertation liegt auf der Anwendung von Quarz-OSL für oberpleistozäne und holozäne Sedimente sowie die methodische Weiterentwicklung der Lumineszenz-Datierung von Feldspäten. Die Validierung der hier angewandten Datierungsmethode durch Vergleich mit anderen anerkannten und verlässlichen Altersbestimmungsmethoden ist notwendig; aus diesem Grund wird in dieser Arbeit, wann immer geeignetes Material zur Verfügung steht, die ^{14}C-Altersbestimmungsmethode zur unabhängigen Alterskontrolle angewendet. Sedimentproben aus drei unterschiedlichen Sedimentarchiven werden bearbeitet: aus dem Garding-2 Sedimentkern (240 m Endteufe), der auf der Eiderstedter Halbinsel unweit der Nordseeküste erbohrt wurde, Lösse aus den zentralen und westlichen Qilian Bergen im nordwestlichen China sowie Sedimente vom Huangqihai See im nördlichen China, in einer Region aus dem Grenzbereich des ostasiatischen Monsuns.

An allen drei Fallstudien wurde die Quarz-OSL-Datierung unter Anwendung des „single-aliquot regenerative-dose“ (SAR) Messprotokolls durchgeführt. Aus dem Kern der Bohrung Garding-2 wird die Quarz-Grobkornfraktion aus Proben der obersten 26 m extrahiert. Die Lumineszenz-Qualitätstests zeigen, dass das Quarz-OSL Signal der küstennahen Sedimente vor der letzten Ablagerung ausreichend gebleicht worden ist, somit diese Datierungsvoraussetzung erfüllt ist. Der aus der Kombination von OSL- und ^{14}C-Altern abgeleitete zeitliche Rahmen ist robust und beweist die sehr gute Verlässlichkeit von OSL-Datierungen dieser Sedimente aus Norddeutschland. Für die Lösse aus den zentralen und westlichen Qilian Bergen wird die Quarz-Feinkornfraktion zur Datierung verwendet. Für einige Lößproben wird eine relativ große Streuung der OSL-Alter aufgrund der geringen Sensitivität der Quarze aus diesem Gebiet festgestellt. Diese geringe OSL-Sensitivität ist wahrscheinlich in der kurzen Sedimentationsgeschichte der Sedimentpartikel begründet, d.h. wenige Erosions- und Ablagerungszyklen. Die routinemäßige OSL-Datierung der Quarz-Grobkornfraktion aus

dem Huangqihai-Seegebiet weist massive Datierungsprobleme aufgrund chemisch nicht löslicher Feldspat-Kontaminationen auf. Um das Problem der Feldspat-Kontamination zu lösen, wird ein post-IR OSL-Datierungsprotokoll mit gepulster Stimulation erstmalig für diese Sedimente entwickelt und angewendet. Hierdurch ist eine eindeutige Unterscheidung zwischen dem Quarz-Signal und dem in diesem Fall „unerwünschten" Feldspat-Signal möglich. Nach dem „Pulsing" werden Quarz-Signale aufgezeichnet; sie beweisen, dass die Feldspat-Kontamination ausreichend eliminiert wurde. Die berechneten „gepulsten" OSL-Alter sind im geographischen Kontext stratigraphisch konsistent und stimmen mit der unabhängigen Alterskontrolle durch ^{14}C-Alter gut überein.

Durch die Anwendung geeigneter Quarz-OSL Datierungsprotokolle werden robuste chronologische Zeitrahmen für die drei untersuchten Sedimentarchive erstellt. Der bearbeitete Teil des Bohrkerns Garding-2 umfasst zeitlich die letzten 16.000 Jahre. Die ^{14}C- und OSL-Datierungen zeigen übereinstimmend, dass die Meerestransgression die Bohrlokalität um etwa 8.300 Jahren vor heute erreichte. Danach stieg der Meeresspiegel weiter (mit geringerer Rate) bis ca. 3.000 Jahre vor heute an. Die OSL-Datierungsergebnisse aus dem nördlichen China zeigen, dass die Staubablagerungen und die Lößentstehung von ca. 13.000 Jahren vor heute bis ca. 3.600 Jahren vor heute im nördlichen Vorland der Qilian Berge weit verbreitet gewesen sind. Lösse des letzten Glazial sind dagegen nur sporadisch mit Altern bis etwa 80.000 Jahren vor heute nachweisbar. Die OSL-Alter von mehreren Aufschlüssen am Huangqihai im nördlichen China beweisen einen Seespiegel-Hochstand während des frühen Holozäns (ca. 10.000 bis 8.000 Jahren vor heute). Der in früheren Arbeiten für das nördliche und westliche China weitverbreitete und postulierte Seespiegelhochstand während des MIS 3 konnte durch die Untersuchungen für den Huangqihai nicht nachgewiesen werden.

Feldspäte eignen sich aufgrund ihrer höheren Sättigungsdosen des Lumineszenzsignals im Vergleich zu Quarz als alternative Dosimeter und zeigen somit großes Potential für die Ausweitung der Datierungsgrenze der OSL bis in das Mittel-Pleistozän. Das kürzlich entwickelte post-IR IRSL (pIRIR)-Protokoll für Feldspäte bei höheren Temperaturen wird für die Grob- und Feinkornfraktion an Sedimenten der Bohrung Garding-2und an Lössen aus den Qilian Bergen detailliert untersucht. Die pIRIR- und das korrespondierende IR_{50}-Signal wurden bei verschiedenen Vorheiz- und

Stimulationstemperaturen systematisch untersucht (Residualdosis, Fading-Rate, Dose recovery etc.). Für die pIRIR-Signale konnte bestätigt werden, dass je höher die Vorheiz- und Stimulationstemperaturen sind, desto größer ist die Residualdosis (unbleichbarer Rest) und desto geringer ist die Fading-Rate. Die pIRIR-Datierung von Feldspäten erreicht für Proben aus dem tieferen Abschnitt der Bohrung Garding-2 Sedimentationsalter von mehr als 400.000 Jahren (ohne die Sättigung zu erreichen). Dies sind vielversprechende Resultate für die weitere Untersuchung von Proben der Bohrung Garding-2. Das pIRIR Äquivalentdosis-Plateau von polymineralischen Feinkornproben (Löss aus den Qilian Bergen) wurde für Proben unterschiedlichen Alters nachgewiesen. Jedoch sind die Datierungskonsequenzen noch nicht vollständig verstanden. Weitere Untersuchungen sind notwendig, um die fundamentale Mechanismen und Prozesse der pIRIR-Signale zu verstehen.

Chapter 1 Introduction

1.1 Introduction

The Late Quaternary has been a period of major climatic and environmental changes, typically characterized by the long-term glacial-interglacial cycles. Our knowledge of these past periodic variations is of crucial importance to understanding the natural state of the global climatic systems and subsequently to predicting the future. Various kinds of archives, such as ice cores (e.g. Petit et al., 1999; EPICA community members, 2004; Kawamura et al., 2007; Jouzel et al., 2007), deep sea drilling cores (e.g. Imbrie et al., 1984; Bassinot et al., 1994; Lisiecki and Raymo, 2005) and terrestrial sediments (e.g. Heller and Liu, 1982; Colman et al., 1995; Guo et al., 2002; An et al., 2012), provide complementary information about the palaeoclimatic and palaeoenvironmental variations of the past. Among these climatic records, terrestrial archives, such as lake deposits and loess, have been intensively and increasingly investigated, since they are widely preserved in various climatic and geographical settings. General chronological frameworks of the global scale climatic variations in the Quaternary have been well established by e.g. the deep marine sediment and the polar ice cores. In contrast, the age frameworks of the regional sedimentary records responding to climate changes are more complex and remain disputable in many areas, which need further investigations. To reconstruct and understand the palaeoclimatic and palaeoenvironmental changes, reliable chronological frameworks that can provide information on timing and rate of these changes are needed. A wide variety of geochronological tools or methods can be employed to quantitatively and/or qualitatively estimate the age of geological materials spanning from billions of years to historical records (Walker, 2005). The optically stimulated luminescence (OSL) dating is one of the most intensively and commonly applied numerical dating techniques in determining the age of late Quaternary sediment.

In this dissertation, three study sites are selected, targeting a drilling core (Garding-2 Core) retrieved from the German North Sea coast, loess from central and western Qilian Shan and lake sediments from Huangqihai Lake, northern China (Fig. 1.1), where the chronological researches concerning regional sedimentary responses to Late Quaternary climate change are controversial. The primary aim is to investigate the performance of quartz OSL dating on a variety of depositional environment. By applying appropriate OSL dating techniques, more reliable and robust chronological frameworks are established in order to clarify and refine the regional sedimentary processes during the

Late Quaternary. In addition, the recently developed post-IR IRSL dating protocol of feldspar was investigated with the interest of dating much older sediment (Early to Mid-Pleistocene) for the future work. In the following part of this chapter, the basic mechanism and the state of art of luminescence dating are briefly reviewed. Then, the three objectives were introduced separately and associated scientific questions were highlighted. Subsequently, the outline of the dissertation was listed.

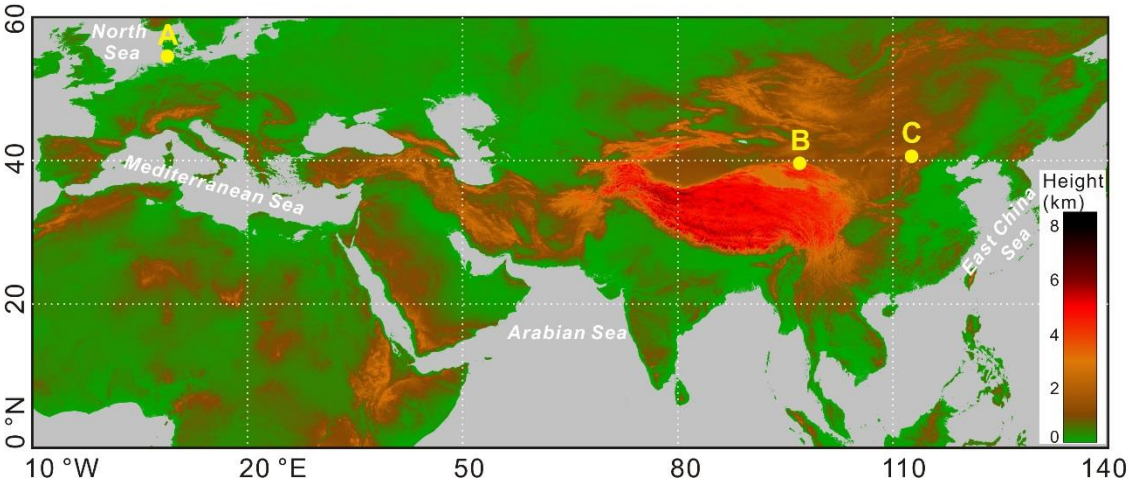

Fig. 1.1 Overview map showing the localities of the three study areas (*source: http://www.cgiar-csi.org*). A: the Grading-2 core, which is located the German North Sea coast on the Eiderstedt Peninsula, Schleswig-Holstein, Germany. B: the Qilian Shan range, northwestern China, where the loess sediment from this dissertation were found. C: the Huangqihai Lake, located on the northern margin of the East Asian monsoonal area in the southern part of Inner Mongolia, northern China.

1.1.1 Luminescence dating

Luminescence dating determines the time elapsed since the sediment was last exposed to sunlight or heat. The possibility of using luminescence to dating sediment was first proposed by Daniels et al. (1953). There are two main luminescence techniques used for dating: thermoluminescence (TL) (Aitken et al., 1964; Aitken, 1985) and optically stimulated luminescence (OSL) (Huntley et al., 1985; Aitken, 1998). TL was introduced for dating application earlier, which initially developed for dating heated materials, such as ancient ceramics (e.g. Aitken et al., 1964) and later applied in dating sediment as well (e.g. Morozov et al., 1968; Wintle and Huntley, 1979, 1980; Wintle, 1981). OSL dating

was first introduced by Huntley et al. (1985) using visible (blue/green) light stimulation for quartz. Three years later, the optical dating was applied to date feldspar using the infrared stimulated luminescence (IRSL) signal which yielded promising results (Hütt et al., 1988). It is noteworthy that besides the TL and OSL dating, other types of luminescence dating techniques, such as the InfraRed-RadioFluorescence (IR-RF) dating (e.g. Trautmann et al., 1999; Krbetschek et al., 2000; Erfurt and Krbetschek, 2003; Buylaert et al., 2012) have also been developed. In the last few decades, the luminescence dating has experienced a rapid stage of expansion in dating application to geological and archaeological studies (Preusser et al., 2008).

1.1.1.1 Basic mechanism of luminescence dating

Although the explicit mechanism of luminescence (either thermally or optically) is not well understood so far, the essential basis of luminescence dating is the ejection of trapped electrons in a crystalline material and the subsequent measurement of the photons resulting from the electron-hole recombination (Aitken, 1985). It involves a series of processes: ionizing radiations produces unpaired electrons and holes; some of these electrons and holes are captured in different traps (lattice defects and impurities); thermal or optical stimulation evicts a trapped electron, and instantaneously, the evicted electron reaches a luminescence center, recombine with a trapped hole and emit light.

In nature, mineral grains with defects and impurities will accumulate the energy of the ionizing radiation flux mostly provided by U/Th series nuclides, K and Rb in the sediment (in the form of alpha, beta and gamma radiations), as well as by cosmic rays. This energy is stored in the form of electrons and holes that have been trapped at defects in the crystal lattice. The longer the burial, the more absorbed energy from irradiations is stored in the crystal lattice. It is noteworthy that the absorbed dose cannot increase indefinitely but will reach a saturation value (saturation dose), since the number of traps (both for electrons and holes) is limited. Once the mineral grains are briefly exposed to light or heat, the latent signal (luminescence clock) is set to zero. The signal will gradually build up again starting at the moment that the mineral grains are reburied. The fundamental assumption of luminescence dating is that the luminescence signal can be sufficiently reset or zeroed

by exposure to daylight prior to deposition. This is an event commonly termed 'bleaching' and occurs in many processes of erosion, transportation or deposition.

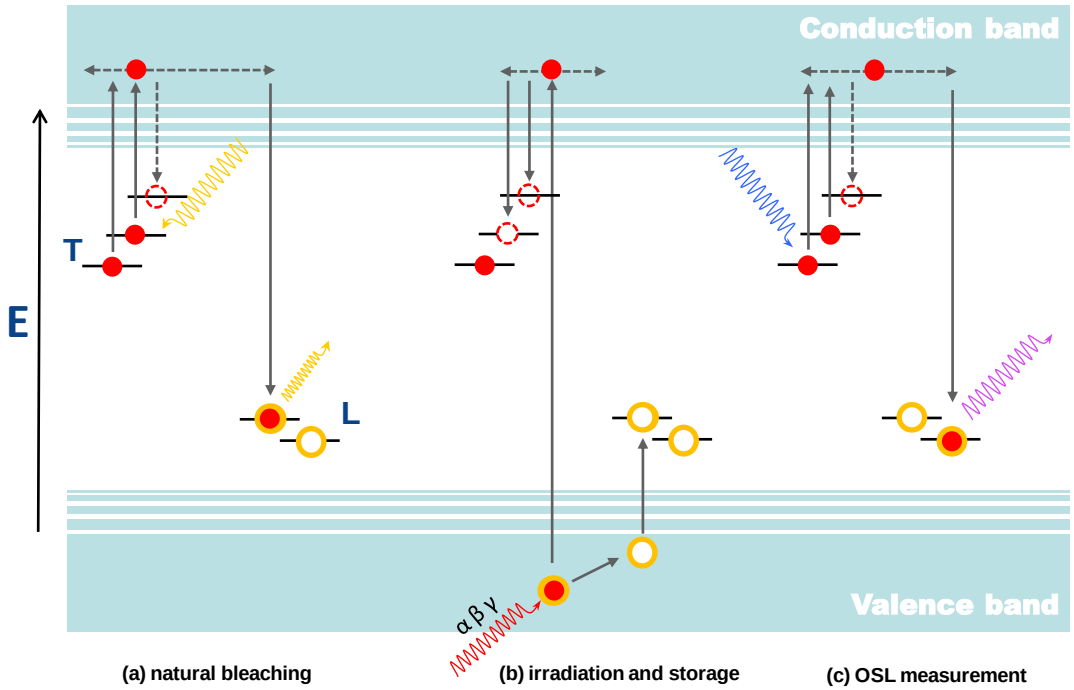

Fig. 1.2 Sketch of a simple band gap energy model of optically stimulated luminescence (OSL). Light-sensitive (OSL) electron traps are shown in red circles, the hole traps are shown in yellow circles. T is the electron trap. L is the luminescence center (modified from *Aitken, 1998 and Rhodes, 2011*).

The total absorbed dose since the last exposure event (in the interest of dating) is usually referred as equivalent dose (ED or D_e) or palaeodose. The rate that the D_e has accumulated is proportional to the rate at which energy is absorbed from the radioactivity in the environment (Aitken, 1985, 1998). The luminescence age thus can be calculated using the following equation.

$$\text{Age (ka)} = \frac{\text{Equivalent dose (Gy)}}{\text{Dose rate (Gy/ka)}}$$

where the equivalent dose is the total radiation dose absorbed by the minerals buried in sediments; and dose rate is the dose contributed by the natural radioactivity and cosmic rays per thousand years.

The equivalent dose can be measured in the laboratory using the luminescence reader in terms of TL or OSL procedures. The two commonly used minerals as palaeodosimeter are quartz and feldspar (Aitken, 1998) that are virtually ubiquitous in terrestrial sediments, although a variety of minerals show the phenomenon of luminescence. As quartz has a strong emission centred on 365 nm (near UV) while many types of feldspars have a strong emission centred on 410 nm (violet), different stimulation and detection windows for quartz and feldspar measurements are used (Fig. 1.3). For quartz measurement, the luminescence signal is stimulated by blue LED (with a peak emission at 470 nm) and detected through a 7.5 mm thick UV filter. The feldspar measurement is commonly carried out using Infrared (IR) stimulation in the region of 800–900 nm (with a peak emission at 870 nm) and often detected through the so-called blue filter pack in the blue region. The emitted luminescence is detected by a photomultiplier tube (PMT), which has maximum detection efficiency between 200 and 400 nm, making it suitable for both quartz and feldspar signal detections.

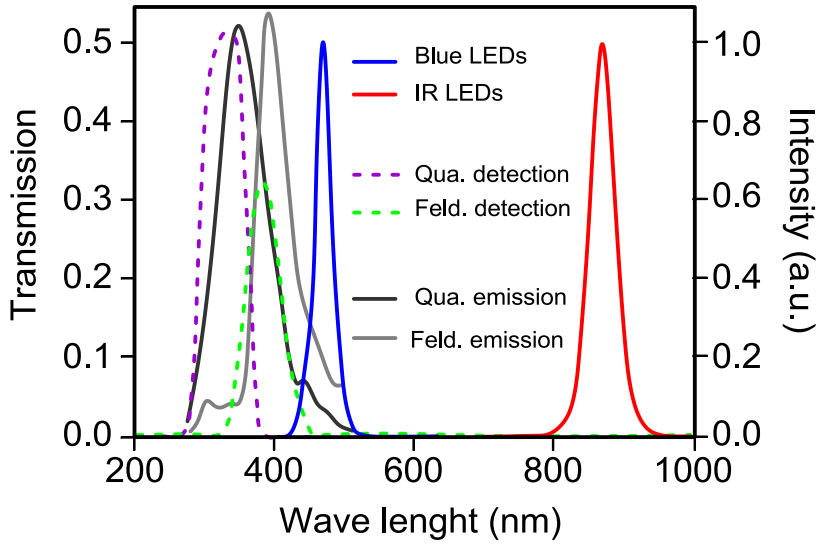

Fig. 1.3 The emission spectra from quartz and feldspar as well as the corresponding stimulation and detection wave length for OSL measurements. The transmission characteristics of Hoya U-340 (quartz detection) and the blue filter pack of CN7-59 in combination with BG39 (feldspar detection). (Modified from *The Risø TL/OSL Reader Guide book*)

The most commonly used approach for D_e determination is the single-aliquot regenerative-dose (SAR) protocol improved by Murray and Wintle (2000), and first proposed by Murray and Roberts (1998). In the SAR protocol, the natural dose and a number of laboratory regenerated doses are mostly measured on single aliquot. Both

natural and regenerative signal are normalized with a subsequent test dose which applies to monitor and correct for a potential sensitivity change. D_e can then be calculated from the ratio of the natural and regenerated luminescence signals to the test dose signals (Murray and Wintle, 2003).

The dose rate can be obtained by either measuring directly the natural radioactive emissions or analysing the concentrations of radionuclides (U, Th and K) in the sediment. A variety of methods is available to determine the dose rate of samples, such as the gamma spectrometry (applied in this thesis), neutron activation analysis (NAA), and alpha counting (Aitken, 1985). The measured radionuclide concentrations have to be converted into individual contributions of alpha, beta and gamma dose rate using conversion factors provided by e.g. Guérin et al. (2011). The small amount irradiation contributed by cosmic rays can be calculated depending on the geographical position, the altitude and the burial depth (Prescott and Stephan, 1982). Another factor to be considered is the dose attenuation (Zimmerman, 1971), caused by moisture content in the interstices of sediment, which must be determined as the water absorbs part of the radiation that would otherwise reach the grains. For the fine-grained minerals or un-etched quartz and feldspar, the alpha value should be also taken into consideration (Aitken, 1985) for total dose rate calculations.

1.1.1.2 Developments and challenges of luminescence dating

Luminescence dating is one of the most useful and applicable dating methods for determining the age of a broad range of landforms and sediments on time-scales from 10^1 to 10^5 years, encompassing the entire late Quaternary. The great advantage of OSL dating over other methods is the direct association of the depositional event. Nevertheless, Aitken (1998) had pointed out that the validity and accuracy of the luminescence results may be judged, when the other methods, radiocarbon dating in most of the case, can be useful in providing dating constraints. After decade's rapid development, this circumstance is not significantly changed for luminescence dating. It is generally because of that the luminescence properties of sediments are highly variable from site to site and even from sample to sample (Aitken, 1998). The variety in environment and post-depositional features of samples can be also reflected in the variety and complexity of the

luminescence signals. From the dating application point of view, universal applicable dating procedure for all kind of sediments is thus not existed. More attention should be paid to the selection of the most suitable dating procedure and the evaluation of the luminescence age before making use of it.

In the past decade most retrospective luminescence dosimetry research has focused on developing methods based on quartz (Thomson et al., 2008). Quartz is known to be more resistant to weathering, easier to be bleached and more stable in contrast to the signal from feldspar (Huntley and Lamothe, 2001). However, the often encountered problems of quartz OSL dating, such as partial bleaching, foreign mineral (mostly feldspar) contaminations, poor luminescence sensitivity and early saturation, can make the obtained age less reliable. Attempts have been made to overcome these associated problems. To deal with partial bleaching, small aliquots and/or the single-grain technique (Murray and Roberts, 1997; Duller 2008) were applied to identify the dose population most likely to have been well bleached at burial. Moreover, statistic approaches such as the minimum age model (MAM) (Galbraith et al., 1999) have been also used to determine the true burial age for incomplete bleached samples (e.g. Alappat et al., 2010; Lütgens et al., 2010, 2011). The contamination by other minerals may make the usage of the quartz OSL signal problematic (e.g. Roberts, 2007). To remove feldspar contamination, the post-IR blue OSL (also known as "double-SAR") protocol (Banerjee et al., 2001; Roberts and Wintle, 2001) has been attempted to isolate the pure quartz signal by depleting the feldspar signal with IR stimulation prior to the blue OSL. However, the double-SAR protocol is not always capable of isolating a quartz-dominated signal (Roberts 2007; Zhang et al., 2007) and further treatment such as fading correction is still necessary in some cases to derive reliable ages (e.g. Vasiliniuc et al., 2013). The OSL dating using pulsing instead of continuous wave stimulation is adopted to discriminate against feldspar signal when measuring feldspar contaminated quartz, since the majority of feldspar signal decays significantly faster than that from quartz after the LED pulses switch off (Denby et al., 2006 and the reference therein).

It is widely recognized that the reliability of radiocarbon dating quickly degrades toward the ends of its dating limit (Pigati et al., 2007), so does luminescence dating. The quartz dose response curve generally saturates at (before) ~300 Gy (e.g. Wang et al., 2006; Buylaert et al., 2007; Timar et al., 2010), corresponding to a practical age range from

~50 ka up to ~200 ka depending on the natural dose rate. Such early saturation of the quartz OSL signal hampers its application in dating samples beyond this age range. The application of quartz OSL dating is accordingly restricted to the Late Glacial time scale. As an alternative dosimeter to quartz, the luminescence signal of feldspar saturates at much higher dose (up to thousand Gy), which shows great potential in dating much older materials. Furthermore, feldspar generally has much higher luminescence intensity than quartz. This property is of particular interest when the quartz OSL intensity is too dim to utilize. Unfortunately, one of the intrinsic properties of the feldspar known as "anomalous fading" (Wintle, 1973) can give rise to massive signal loss which is responsible for age underestimation. This phenomenon has long held back the use of feldspars in luminescence dating applications. The commonly accepted explanation for the malign fading phenomenon is athermal wave-mechanical tunnelling in term of quantum mechanics (Aitken, 1985).

The luminescence dating of feldspar has mostly been conducted using IR stimulation at lower temperature (e.g. 50 °C) with detection in the blue blue-violet wavelength region since it was first reported by Hütt et al. (1988). Typically, an age underestimation of 30−40% could be observed caused by anomalous fading. As a result, different models have been developed to correct for or minimize the effect of anomalous fading (e.g. Huntley and Lamothe, 2001; Lamothe et al., 2003; Kars et al., 2008). However, inherent assumptions have been adopted in those correction models, including that the laboratory measured fading rate is relevant to geological time (e.g. Huntley and Lamothe, 2001; Lamothe et al., 2003; Morthekai et al., 2008), which make the fading corrected age greatly dependent on assumptions and not always reliable (Wallinga et al., 2007; Li and Li, 2008; Kars et al., 2008). Promising advances have been achieved in developing protocols for extracting non- or less fading components from feldspars, such as pulsed IRSL dating (Tsukamoto et al., 2006), isochron IRSL dating (Li et al, 2008) and post-IR elevated temperature IRSL (pIRIR) dating (e.g. Thomsen et al., 2008; Buylaert et al., 2009; Li and Li, 2011; Stevens et al., 2011; Thiel et al., 2011; Fu and Li, 2013; Li et al., 2014 and the references there in). Among them, the pIRIR protocol has attracted most of the attention and been increasingly used for age determination especially for older samples. This recently developed approach brought the feldspar dating a big step forward, since the pIRIR signal shows remarkably lower fading rate than conventional low temperature IRSL signals. There are two kinds of pIRIR protocols, known as the two step pIRIR and

multi-elevated-temperature pIRIR (MET-pIRIR). The two step pIRIR protocol (hereafter pIRIR) carries out twice IR stimulations, a low temperature IR stimulation mostly at 50 °C followed by another elevated temperature IR stimulation (e.g. 150 °C; 225 °C and 290 °C). The MET-pIRIR protocol, as its name implies, adopts a series of stimulations at progressively increasing elevated temperatures from 50 °C to 300 °C (Li et al., 2013). Jain and Ankjærgaard (2011) proposed a comprehensive model for feldspar luminescence based on time-resolved luminescence technique, suggesting that the athermal stability of the pIRIR signal is expected to increase with the preheat and stimulation temperatures. In other words, the higher the stimulation temperature is, the lower the fading is. Meanwhile, signals stimulated at higher temperature become harder to bleach (Buylaert et al., 2009; Li and Li, 2011; Kars et al., 2014) resulting in considerable residual doses, which may cause significant age overestimation especially for young samples. It is therefore problematic to select suitable measurement conditions for the pIRIR protocol in order to sample the most bleachable and less fading signals. Although protocols using lower stimulation temperature (150 °C−180 °C) are accordingly modified to dating young (Holocene) sample (e.g. Reimann et al., 2011; Madsen et al., 2011; Fu and Li, 2013; Long et al., 2014), the problem is not yet solved since so far there are no satisfactory standards addressing how to select a suitable preheat and stimulation temperature for the samples within different age ranges.

1.1.2 Research questions and objectives

1.1.2.1 Late Quaternary loess accumulation in Qilian Shan, northern China

Continental loess deposits are one of the most important archives to reconstruct the climate fluctuations during the Quaternary (Kukla, 1987; Hovan et al., 1989; Rutter et al., 1991; Liu and Ding, 1993). For example, loess-palaeosol sequences on the Chinese Loess Plateau provide excellent records of long-term palaeoclimate variations throughout the last 2.4 Ma (e.g., Liu, 1985; Kukla, 1987; Kukla and An, 1989). Recently, more attention has been paid to the loess in the source proximal region in northwestern China, where loess deposits are commonly observed but unevenly distributed. Loess in this area can have a thickness from some tens of centimeters to a few meters (e.g. Derbyshire et al., 1998; Stauch et al., 2012; Stokes et al., 2003; Küster et al., 2006; Chen et al., 2013). Qilian

Shan, located on the northeast margin of the Tibetan Plateau, plays a very important role in the loess deposition in northwestern China. It serves as not only one of the major dust source regions but also as an important pathway in arid/semi-arid Central and East Asia (Derbyshire et al., 1998; Sun, 2002). Nevertheless, the research on the Qilian Shan loess is rather limited and the knowledge of loess accumulation in the central and western Qilian Shan was restricted to the time span since 13−11 ka until present (Stokes et al., 2003; Küster et al., 2006). Loess deposits prior to this period have not yet been reported. However, the loess deposition on the main Loess Plateau demonstrates that dust has been transported continuously from northern China to the Loess Plateau during the entire Quaternary (Derbyshire, et al., 1998). Therefore, a question is raised whether there is evidence for "older" loess accumulated in the Qilian Shan area. Furthermore, the correlation between the loess accumulation and the local/regional climate and environmental changes, is also of great interest. Compared with the adjacent Loess Plateau, the climatic condition is hasher and the geological setting is different in the central and western Qilian Shan area. All loess sequences that investigated in the current study are lack of palaeosol formation. It is therefore noteworthy that the implication of the loess accumulation in the remote Qilian Shan area might be different from the Chinese Loess Plateau, where the loess-palaeosol sequence were widely accepted as very sensitive indicator of global and regional climate changes, in particularly glacial/interglacial cycles (e.g. Liu, 1985).

Loess is considered as the ideal material for luminescence dating because the grains experienced a long time exposure to sun light during aeolian transportation which should result in complete bleaching of the luminescence signal prior to deposition. Since the 1980s, luminescence dating has been intensively applied to date loess sediment worldwide producing direct numerical chronologies (e.g. Wintle et al., 1984; Frechen et al., 1997, 1999, 2001; Roberts and Wintle, 2001; Stevens et al., 2007; Buylaert et al., 2008). Along the central and western Qilian Shan front, loess and/or loess-like sediments are widespread and deposited up to few meters between altitudes of ~2000 m and ~3800 m a.s.l. Twenty-three loess samples from eleven sections located in the central and western Qilian Shan have been collected for OSL dating. The characteristics of fine-grained quartz OSL are investigated. The quartz OSL ages are derived to explore the loess accumulation history in the central and western part of Qilian Shan area. Apart from this, the performance of feldspar luminescence is systematically examined in order to further

understand the temperature dependency of pIRIR signals using polymineral fine grains. A series of preheat and stimulation temperature combinations are applied in D_e plateau, fading test, dose recovery test and residual test. Taking the corresponding quartz OSL dates as age control, the reliability of the obtained pIRIR ages and its implications under various preheat and stimulation temperatures are discussed.

1.1.2.2 Late Quaternary sedimentary processes in German North Sea coast

Coasts are dynamics systems, which are sensitive in response to climate and sea level changes at different time and space scales (Cowell et al., 2003). Identification of the local relative sea-level history and the sedimentary process in the coastal area from individual locations has long been one of the major objectives of coastal research. The North Sea is a shallow continental shelf sea with an average water depth of 94 m, which is located between Great Britain, Scandinavia, Germany, the Netherlands, Belgium, and France. (Schwarzer et al., 2008). It has an open transition to the Atlantic Ocean via English Channel to the Southwest. The Sea floor in the German North Sea sector is built up mainly of loose Quaternary deposits (Zeiler et al., 2008). The climate in the North Sea area is strongly influenced by the inflow of oceanic water from the Atlantic Ocean and by the large scale westerly air circulation which frequently contains low pressure systems (OSPAR Commission, 2000). The general outline of the North Sea basin came into being at the end of the Tertiary period (Streif, 2004). The coastline of the North Sea has dramatically shifted under the influences of glaciations and the sea level fluctuations during the Quaternary. For example, during the Last Glacial Maximum (LGM) when the global sea level was about ~130 m lower than today, the entire North Sea area was exposed and the coastline was retreated for approximately 600 km westward from its present day position (Jelgersma, 1979; Streif, 2002). It has been reported that since the last deglaciation the transgression of the North Sea started at about 18 ka and has continued until today (Streif 2004 and the references therein). However, the detailed sea-level change pattern and sediment accumulation history since the last deglaciation along the Southern North Sea coast is still controversial (Behre, 2007; Bungenstock and Weerts, 2010; Baeteman et al., 2011).

The German sector of the North Sea is under intensive study since last century in geology, archaeology, climatology and natural resources' exploitation, etc. Among these aspects, the coastal evolution and the sea level fluctuation histories (e.g. Streif, 2004; Behre, 2007) are of special interest. A 240 m long terrestrial sediment core, named Garding-2 core, was retrieved in 2011 from the Eiderstedt Peninsula in Schleswig-Holstein, Germany, in order to obtain a comprehensive record of the Quaternary sediment succession in Northern Germany. The preliminary lithostratigraphic investigations reveal that the sediment sequence starts from present and probably extends to the Early Pleistocene/Pliocene (Personal communication with Dr. Alf Grube). The core generally consists of marine, glacial and fluvial deposits. The coastal evolution and landscape changes are of great interest to this project, especially for the Holocene period. The uppermost 26 m sediments of the Garding-2 core, which were investigated in this study, varied from fluvial deposits to the marine-dominated (coastal) deposits, providing excellent record of the sea level and coastal evolution history. The primary investigation is to build up a reliable chronostratigraphy of this sediment succession by means of quartz OSL technique in order to refine the coastal sedimentary processes in the German North Sea sector since last deglaciation. The registered mollusc shells allow the application of AMS ^{14}C dating technique, which provides independent age control to cross-check and validate the robustness of the OSL chronology.

Besides, the application of the pIRIR dating technique is tested on both coarse grain K-feldspar and polymineral fine-grains of samples from different depth (down to 200 m with Tertiary age). The performance of different pIRIR signals is systematically examined. The potential of the pIRIR dating technique in establishing the chronological framework of the deeper part of Garding-2 core is accordingly discussed.

1.1.2.3 Late Quaternary lake evolution of Huangqihai in northern China

Inland terminal lakes are common sediment traps and sensitive to climate change. The lake surface fluctuations are direct indicators of regional hydrological variability and could provide a detailed record of regional and continental climatic variations (Street-Perrott and Harrison, 1984). Numerous lakes in northern China, especially in the Asian monsoon marginal area, have been investigated to reconstruct the lake evolution and

climatic history during the Late Quaternary. Controversy exists regarding the pattern of the Holocene climate change mainly revealed by lake archives in the Asian monsoon area. Some proposed that the climate in the mid-Holocene was continuously warm and wet (Holocene Optimum) (Shi et al., 1993) in the Asian monsoon area, while others recently argued that a dry mid-Holocene existed between ca. 7 and 5 ka (Chen et al., 2003a, b; Li et al., 2003). Herzschuh (2006) provided a detailed review of Holocene effective-moisture changes in the Asian monsoon regions and showed that the Holocene climate optimum with high precipitation occurred during the early Holocene in the Indian monsoon region, but possibly occurred during the mid-Holocene in the East Asian monsoon region. In a review by Chen et al. (2008), they concluded that all the selected well-dated monsoon records show a strong monsoon (high precipitation) in the early and mid-Holocene and a weak monsoon (low precipitation and dry climate) during the late Holocene both in the East Asian Monsoon and Indian Monsoon regions.

Conflicting evidences also exist in the chronologies of lake high stand during the Late Pleistocene. It is generally hypothesized that during the late MIS 3 the climate was much cooler and drier than in the Holocene (Martinson et al., 1987; Petit et al., 1999). However, in the last twenty years, a phenomenon has often been reported that the climate during the late MIS 3 (ca. 30−40 ka, the interstadial) in northwestern China, especially on the Tibetan Plateau, is not in phase with that of other regions in the world (Thompson et al., 1997). This climate anomaly has been supported by many lake records from northwestern China which showed that the highest lake level indicating the warm and wet climate occurred during the late MIS 3 (e.g. Pachur et al., 1995; Rhodes et al., 1996; Shi et al., 2001; Li, 2000; Zhang et al., 2004). The chronological data in those studies largely depended on radiocarbon dating. However, more recently, some studies revealed that high lake levels occurred beyond 70 ka instead of previously reported during Late MIS 3 according to the chronologies mainly relied on luminescence dating or U/Th dating (see the review by Long and Shen, 2015). This issue is undergoing intensive study and debate. Thus, the lake response to climate change during the Late Quaternary in northern China needs more investigations, especially on the chronological framework.

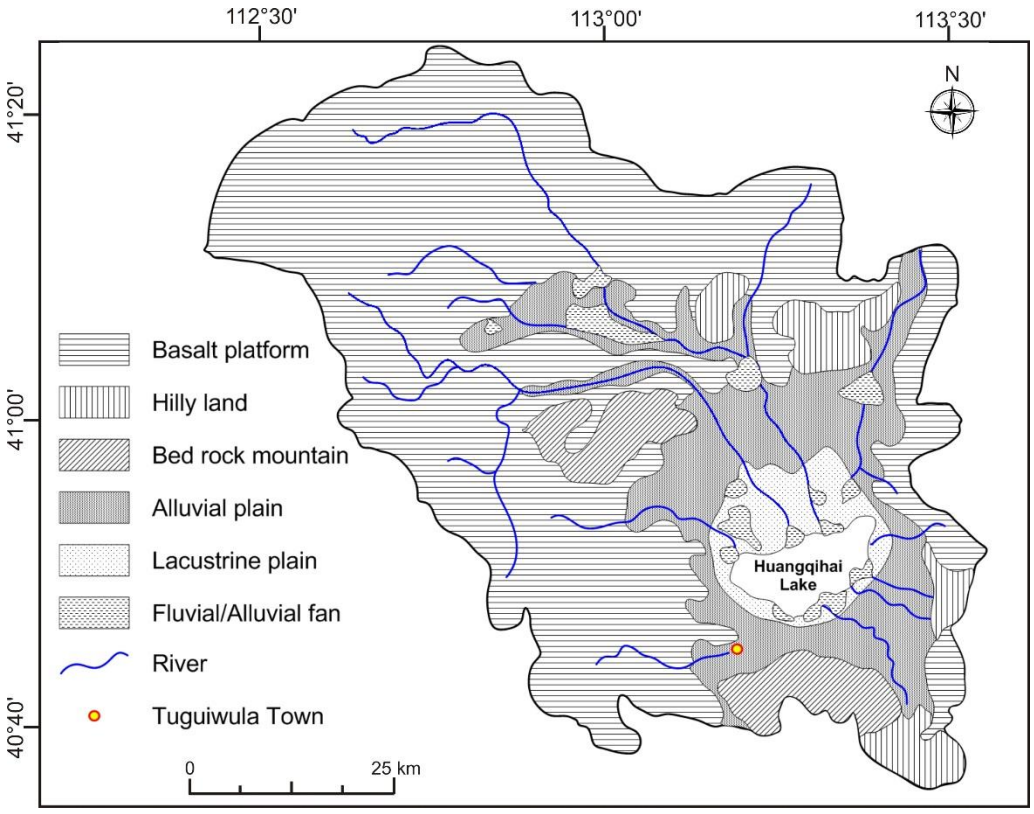

Fig. 1.4 Geomorphological map of Huangqihai Lake (modified from *Li and Wang, 1993*)

Huangqihai Lake is an inland terminal lake located at the northern margin of East Asian monsoon influenced area in Inner Mongolia. Its lake level fluctuation is very sensitive to the climate changes, which has been considered as an indicator of the East Asian monsoon variations (Li et al, 1992; Zhang et al., 2012). The geomorphological map of the drainage area is shown in Fig. 1.4. The bedrock within the basin is composed mostly of Tertiary volcanic rocks. Quaternary unconsolidated deposits are distributed in the lake basin and river valleys. The landscape in the catchment is dominated by basaltic tablelands and alluvial–lacustrine plains. The modern lake is fed by a few seasonal streams. Around the lake basin, a series of outcrops, consisting of either lake sediments or aeolian sediments, have been identified during several field campaigns since 2009. Quartz OSL dating using pulsed stimulation technique and AMS ^{14}C were employed to date these sedimentary archives, in order to reconstruct the lake evolution history during the late Quaternary. The age framework of the Huangqihai Lake evolution since MIS3 is refined.

1.1.3 Outline of the dissertation

This dissertation is composed of six chapters including the Introduction (*Chapter 1*) and Conclusions (*Chapter 6*). The main part constitutes a compilation of five manuscripts which have been published in or are preparing for submission to international scientific peer-reviewed journals. Repetitions are inevitable in some places (e.g. methods) of each manuscript. The five manuscripts are assigned into four chapters (*Chapter 2, 3, 4 and 5*). The brief overview of each case study is listed as below.

In *Chapter 2*, 23 loess samples from the northern piedmont of central and western Qilian Shan area have been OSL dated using fine-grained quartz. The chronology of the loess sedimentation has been extended back at least to ~81 ka, which is remarkably older than previously thought. The possible reasons for the discontinuous loess sedimentation in the central and western Qilian Shan area during the late Pleistocene have been discussed.

Chapter 3 consists of one manuscript on the study of 240 m Garding-2 core from the German North Sea coast. The well-established quartz OSL and AMS ^{14}C chronology for the uppermost 26 m deposits of Garding-2 core were presented. Based on twenty-five OSL ages and fourteen AMS ^{14}C ages, we obtained a well dated sedimentary record that covers a large part of the Holocene as well as the last deglaciation period (back to ~16 ka) in one succession of the German North Sea coastal area. In particular, the Holocene transgression history and the coastal sedimentary process were reconstructed and compared with former investigations in the southern North Sea area. Preliminary tests show that the quartz OSL signal might reach saturation at around 50-60 m depth. Since feldspar is a promising candidate for extending the luminescence dating limit due to its much higher saturation dose, the application of pIRIR dating using sand-sized potassium feldspar (K-feldspar) as well as polymineral fine grains from Garding-2 core has been tested in *Chapter 5.1*.

Chapter 4 presents the results of chronological and sedimentological investigations from five sediment outcrops around the Huangqihai Lake basin in northern China. 17 OSL and 4 AMS ^{14}C ages were obtained. Detailed depositional facies description and the corresponding environmental interpretation have been carried out. As most of the quartz samples are contaminated by feldspar, which could not be sufficiently removed by chemical treatment, the post-IR pulsed OSL dating technique has been applied. After

pulsing, the OSL signals show similar decay curves as that of typical pure quartz, indicating that the pulsed OSL technique is able to discriminate against the feldspar contamination. Based on the chronological and sedimentological evidences, the lake level fluctuations and the climate evolution history since the MIS 3 have been discussed and a lake level fluctuation curve has been synthesized.

Chapter 5 is assigned to deal with the pIRIR dating of feldspar. In *Chapter 5.1*, the most commonly used pIRIR protocols were tested with the samples from the Garding-2 core. The elevated stimulation temperature at 150 °C ($pIRIR_{150}$), 225°C ($pIRIR_{225}$) and 290°C ($pIRIR_{290}$) were selected to test the luminescence characteristics of a group of samples with various ages (from several ka to several hundred ka). The behaviour of different pIRIR signals and the corresponding IR_{50} signals, in term of residual, fading rate and dose recovery ratio, have been systematically examined. In *Chapter 5.2*, the characteristics of the pIRIR signal was further investigated using polymineral fine grains. Four loess samples from Qilian Shan with different ages have been selected. The pIRIR measurements of polymineral fine grains were conducted under a wide range of preheat temperature between 180 °C and 340 °C. The second pIRIR stimulation temperature was always −30 °C tracking the preheat temperature. A series of measurements, such as the dose recovery, fading and bleachability tests were carried out to examine the pIRIR characteristics. The ages obtained from a variety of preheat and pIRIR stimulation conditions exhibit a "plateau" for all the samples between 240 °C and 280 °C. The reliability of the pIRIR "plateau" ages and the possible explanations are discussed.

Reference

Aitken, M.J., Tite, M.S., Reid, J., 1964. Thermoluminescence dating of ancient ceramics. Nature 202, 1032–1033.

Aitken, M.J., 1985. Thermoluminescence dating. Academic Press, London.

Aitken, M.J., 1998. An introduction to optical dating: the dating of Quaternary sediments by the use of photon-stimulated luminescence. Oxford University Press, London.

Alappat, L., Vink, A., Tsukamoto, S., Frechen, M. 2010. Establishing the Late Pleistocene-Holocene sedimentation boundary in the southern North Sea using OSL dating of shallow continental shelf sediments. Proceedings of the Geologists' Association 121, 43–54.

An, Z.S., Colman, S.M., Zhou, W.J., Li, X.Q., Brown, E.T., Jull, A.J.T., Cai, Y.J., Huang, Y.S., Lu, X.F., Chang, H., Song, Y.G., Sun, Y.B., Xu, H., Liu, W.G., Jin, Z.D., Liu, X.D., Cheng, P., Liu, Y., Ai, L., Li, X.Z., Liu, X.J., Yan, L.B., Shi, Z.G., Wang, X.L., Wu, F., Qiang, X.K., Dong, J.B., Lu, F.Y., Xu, X.W., 2012. Interplay between the Westerlies and Asian monsoon recorded in Lake Qinghai sediments since 32 ka. Scientific Reports 2, 1–7.

Baeteman, C., Waller, M., Kiden, P., 2011. Reconstructing middle to late Holocene sea-level change: a methodological review with particular reference to 'A new Holocene sea-level curve for the southern North Sea' presented by K.-E. Behre. Boreas 40, 557–572.

Banerjee, D., Murray, A.S., Bøtter-Jensen, L., Lang, A., 2001. Equivalent dose estimation using a single aliquot of polymineral fine grains. Radiation Measurements 33, 73–93.

Bassinot, F. C. et al., 1994. The astronomical theory of climate and the age of the Brunhes-Matuyama magnetic reversal. Earth Planetary Science Letter 126, 91–108.

Behre, K. E., 2007. A new Holocene sea-level curve for the southern North Sea. Boreas 36, 82–102.

Blaauw, M., van Geel, B., Kristen, I., Plessen, B., Lyaruu, A., Engstrom, D.R., van der Plicht, J., Verschuren, D., 2011. High-resolution ^{14}C dating of a 25,000 year lake sediment record from equatorial East Africa. Quaternary Science Review 30, 3043–3059.

Bungenstock, F., Weerts, H. J. T., 2010. The high-resolution Holo- cene sea-level curve for Northwest Germany: global signals, local effects or data-artefacts? International Journal of Earth Sciences 99, 1687–1706.

Buylaert, J.P., Vandenberghe, D., Murray, A.S., Huot, S., De Corte, F., Van den haute, P., 2007. Luminescence dating of old (470 ka) Chinese loess: a comparison of single-aliquot OSL and IRSL techniques. Quaternary Geochronology 5, 9–14.

Buylaert, J.P., Murray, A.S., Vandenberghe, D., Vriend, M., De Corte, F., Van den haute, P., 2008. Optical dating of Chinese loess using sand-sized quartz: Establishing a time frame for Late Pleistocene climate changes in the western part of the Chinese Loess Plateau. Quaternary Geochronology 3, 99–113.

Buylaert, J.P., Murray, A.S., Thomsen, K.J., Jain, M., 2009. Testing the potential of an elevated temperature IRSL signal from K-feldspar. Radiation Measurements 44, 560–565.

Buylaert, J.P., Jain, M., Murray, A.S., Thomsen, K.J., Lapp, T., 2012. IR-RF dating of sand-sized K-feldspar extracts: A test of accuracy. Radiation Measurements 47, 759−765.

Chen, C.T.A., Lan, H.C., Lou, J.Y., et al. 2003b. The dry Holocene megathermal in Inner Mongolia. Palaeogeography, Palaeoclimatology, Palaeoecology 193, 181–200.

Chen, F.H., Wu, W., Holmes, J.A., Madsen, D.B., Zhu, Y., Jin, M., Oviatt, C.G., 2003. A Mid- Holocene drought interval as evidenced by lake desiccation in the Alashan Plateau, Inner Mongolia, China. Chinese Science Bulletin 48, 1401–1410

Chen, F., Yu, Z., Yang, M., Ito, E., Wang, S., Madsen, D.B., Huang, X., Zhao, Y., Sato, T., Birks, H.John B., Boomer, I., Chen, J., An, C., Wünnemann, B., 2008. Holocene moisture evolution in arid central Asia and its out-of-phase relationship with Asian monsoon history. Quaternary Science Reviews 27, 351–364.

Chen, Y.W., Li, S.H, Sun, J.M., Fu, B.H., 2013. OSL dating of offset streams across the Altyn Tagh Fault: Channel deflection, loess deposition and implication for the slip rate. Tectonophysics 594, 182–194.

Cowell, P. J., Stive, M. J. F., Niedoroda, A. W., De Vriend, H. J., Swift, D. J. P., Kaminsky, G. M., Capobianco, M., 2003. The coastal tract. Part 1: A conceptual

approach to aggregated modelling of low-order coastal change. Journal of Coastal Research 19, 812-827

Colman, S.M., Peck, J.A., Karabanov, E., Carter, S.M., Bradbury, J.P., King, J.W., Williams, D.F., 1995. Continental climate response to orbital forcing from biogenic silica records in Lake Baikal. Nature 378, 769–771.

Daniels, F., Boyd, C.A., Saunders, D.F., 1953. Thermoluminescence as a research tool. Science 117, 343–349.

Denby, P.M., Bøtter-Jensen, L., Murray, A.S., Thomsen, K.J., Moska, P., 2006. Applications of pulsed OSL to the separation of the luminescence components from a mixed quartz/feldspar sample. Radiation Measurements 41, 774–779.

Derbyshire, E., Meng, X.M., Kemp, R.A., 1998. Provenance, transport and characteristics of modern aeolian dust in western Gansu Province, China, and interpretation of the Quaternary loess record. Journal of Arid Environments 39, 497–516.

Duller, G.A.T., 2008. Single-grain optical dating of Quaternary sediments: why aliquot size matters in luminescence dating. Boreas 37, 589–612.

EPICA community members, 2004. Eight glacial cycles from an Antarctic ice core. Nature 429, 623–628.

Erfurt, G., Krbetschek, M.R., 2003. Studies on the physics of the infrared radio-luminescence of potassium feldspar and on the methodology of its application to sediment dating. Radiation Measurements 37, 505−510.

Frechen, M., Horváth, E., Gábris, G, 1997. Geochronology of middle and upper Pleistocene loess sections in Hungary. Quaternary Research 48, 291–312.

Frechen, M., Zander, A., Cílek, V., Ložek, V., 1999. Loess chronology of the Last Interglacial/Glacial cycle in Bohemia and Moravia, Czech Republic. Quaternary Science Review 18, 1467–1493.

Frechen, M., Van Vliet Lanoe, B., Van den Haute, P., 2001. The Upper Pleistocene loess record at Harmignies, Belgium high resolution terrestrial archive of climate forcing. Palaeogeogr. Palaeoclimatol. Palaeoecol. 173, 175–195.

Fu, X., Li, S.H., 2013. A modified multi-elevated-temperature post-IR IRSL protocol for dating Holocene sediments using K-feldspar. Quaternary Geochronology 17, 44–45.

Galbraith, R.F., Roberts, R.G., Laslett, G.M., Yoshida, H., Olley, J.M., 1999. Optical dating of single and multiple grains of quartz from Jinmium Rock Shelter, northern Australia: Part 1, experimental design and statistical models. Archaeometry 41, 339–364.

Guérin, G., Mercier, N., Adamiec, G., 2011. Dose-rate conversion factors: update. Ancient TL 29, 5–8.

Guo, Z.T., Ruddiman, W.F., Hao, Q.Z., Wu, H.B., Qiao, Y.S., Zhu, R.X., Peng, S.Z., Wei, J.J., Yuan, B.Y., Liu, T.S., 2002. Onset of Asian desertification by 22 Myr ago inferred from loess deposits in China. Nature 416, 159–162.

Heller, F., Liu, T.S., 1982. Magnetostratigraphical dating of loess deposits in China. Nature 300, 431–433.

Herzschuh, U., 2006. Palaeo-moisture evolution in monsoonal Central Asia during the last 50000 years. Quaternary Science Reviews 25, 163–178.

Hovan, S.A., Rea, D.K., Pisias, N.G., Shackleton, N.J., 1989. A direct link between the China loess and marine $\delta^{18}O$ records: aeolian flux to the north Pacific. Nature 340, 296–298.

Huntley, D.J., Godfrey-Smith, D.I. and Thewalt, M.L.W., 1985. Optical dating of sediments. Nature 313, 105–107.

Huntley, D.J., Lamothe, M., 2001. Ubiquity of anomalous fading in K-feldspars and the measurement and correction for it in optical dating. Canadian Journal of Earth Science 38, 1093–1106.

Hütt, G., Jaek, I., and Tchonka, J., 1988. Optical dating: K-feldspars optical response stimulation spectra. Quaternary Science Reviews 7, 381–385

Imbrie, J., Hays, J.D., Martinson, D.G., McIntyre, A., Mix, A.C., Morley, J.J., Pisias, N.G., Prell, W.L., Shackleton, N.J., 1984. The orbital theory of Pleistocene climate: support from a revised chronology of the marine $\delta^{18}O$ record. In: Berger, A.L. et al. (Eds.), Milankovitch and Climate, Part 1. Reidel, The Netherlands, pp. 269–305.

Jain, M., Ankjaergaard, C., 2011. Towards a non-fading signal in feldspar: insight into charge transport and tunnelling from time-resolved optically stimulated luminescence. Radiation Measurements 46, 292–309.

Jelgersma, S., 1979. Sea-level changes in the North Sea basin. In Oele, E., Schüttenhelm, R. T. E., Wiggers, A. J., (eds.): The Quaternary History of the North Sea, Acta Universitatis Upsaliensis, Symposium Universitatis Upsaliensis Annum Quingentesimum Celebrantis, 233–248. University of Uppsala, Uppsala.

Jouzel, J., Masson-Delmotte, V., Cattani, O., Dreyfus, G., Falourd, S., Hoffmann, G., Nouet, J., Barnola, J.M., Chappellaz, J., Fischer, H., Gallet, J.C., Johnsen, S., Leuenberger, M., Loulergue, L., Luethi, D., Oerter, H., Parrenin, F., Raisbeck, G., Raynaud, D., Schwander, J., Spahni, R., Souchez, R., Selmo, E., Schilt, A., Steffensen, J.P., Stenni, B., Stauffer, B., Stocker, T., Tison, J.L., Werner, M., Wolff, E.W., 2007. Orbital and millennial Antarctic climate variability over the last 800,000 years. Science 317, 793–796.

Kars, R. H., Wallinga, J. and Cohen, K. M., 2008. A new approach towards anomalous fading correction for feldspar IRSL dating- tests on samples in field saturation. Radiation Measurements 43, 786–790.

Kars, R.H., Reimann, T., Ankjærgaard, C.,Wallinga, J., 2014. Bleaching of the post-IR IRSL signal: new insights for feldspar luminescence dating. Boreas 43, 780–791.

Kawamura, K., Parrenin, F., Lisiecki, L., Uemura, R., Vimeux, F., Severinghaus, J.P., Hutterli, M.A., Nakazawa, T., Aoki, S., Jouzel, J., Raymo, M.E., Matsumoto, K., Nakata, H., Motoyama, H., Fujita, S., Goto-Azuma, K., Fujii, Y., Watanabe, O., 2007.

Northern Hemisphere forcing of climatic cycles in Antarctica over the past 360,000 years. Nature 448, 912–917.

Krbetschek, M.R., Trautmann, T., Dietrich, A., Stolz, W., 2000. Radioluminescence dating of sediments: methodological aspects. Radiation Measurements 32, 493−498.

Kukla, G., 1987. Loess stratigraphy in Central China. Quaternary Science Reviews 6, 191–219.

Kukla, G., An, Z.S., 1989. Loess stratigraphy in Central China. Palaeogeography, Palaeoclimatology, Palaeoecology 72, 203–225.

Küster, Y., Hetzel, R., Krbetschek, M., Tao, M., 2006. Holocene loess sedimentation along the Qilian Shan (China): significance for understanding the processes and timing of loess deposition. Quaternary Science Reviews 25, 114–125.

Lamothe, M., Auclair, M., Hamzaoui, C., Huot, S., 2003. Towards a prediction of longterm anomalous fading of feldspar IRSL. Radiation Measurements 37, 493–498.

Li, B., Li, S. H., 2008. Investigations of the dose-dependent anomalous fading rate of feldspar from sediments. Journal of Physics D: Applied Physics 41: 225502 (15pp).

Li, B., Li, S.H., Wintle, A.G., Zhao, H., 2008. Isochron dating of sediments using luminescence of K-feldspar grains. J. Geophysical Research-Earth Surface 113, F02026.

Li, B., Li, S.H., 2011. Luminescence dating of K-feldspar from sediments: a protocol without anomalous fading correction. Quaternary Geochronology 6, 468–479.

Li, B., Roberts, R.G., Jacobs, Z., 2013. On the dose dependency of the bleachable and non-bleachable components of IRSL from K-feldspar: Improved procedures for luminescence dating of Quaternary sediments. Quaternary Geochronology 17, 1–13.

Li, B., Jacobs, Z., Roberts, R.G., Li, S.H., 2014. Review and assessment of the potential of post-IR IRSL dating methods to circumvent the problem of anomalous fading in feldspar luminescence. Geochronometria 41, 178–201.

Li, B.Y., 2000. The last greatest lakes on the Tibetan Plateau. Acta Geographica Sinica 55, 174–182 (in Chinese with English abstract).

Li, X.Q., Zhou, W.J., An, Z.S., Dodson, J., 2003. The vegetation and monsoon variation at the desert-loess transition belt at Midiwan in northern China for the last 13ka. The Holocene 13, 770–784.

Lisiecki, L.E., Raymo, M.E., 2005. A Pliocene-Pleistocene stack of 57 globally distributed benthic $\delta^{18}O$ records. Paleoceanography 20, 1–17.

Liu, T.S., 1985. Loess and the Environment. China Ocean Press, Beijing.

Liu, T.S., Ding, Z.L., 1993. Stepwise coupling of monsoon circulations to global ice volume variations during the late Cenozoic. Global and Planetary Change 7, 119–130.

Long, H., Lai, Z.P., Wang, N.A., Zhang, J.R., 2011. A combined luminescence and radiocarbon dating study of Holocene lacustrine sediments from arid northern China. Quaternary Geochronology 6, 1–9.

Long, H., Shen, J., Tsukamoto, S., Chen, J.H., Yang, L.H., Frechen, M., 2014. Dry early Holocene revealed by sand dune accumulation chronology in Bayanbulak Basin (Xinjiang, NW China). The Holocene 24, 614–626.

Long, H., Shen, J., 2015. Underestimated ^{14}C-based chronology of late Pleistocene high lake-level events over the Tibetan Plateau and adjacent areas: Evidence from the Qaidam Basin and Tengger Desert. SCIENCE CHINA Earth Sciences 58, 183–194.

Lüthgens, C., Krbetschek, M.R., Böse, M., Fuchs, M.C., 2010. Optically stimulated luminescence dating of fluvioglacial (sandur) sediments from north-eastern Germany. Quaternary Geochronology 5, 237−243.

Lüthgens, C., Böse, M., Lauer, T., Krbetschek, M., Strahl, J., Wenske, D., 2011. Timing of the last interglacial in Northern Europe derived from Optically Stimulated Luminescence (OSL) dating of a terrestrial Saalian-Eemian-Weichselian sedimentary sequence in NE-Germany. Quaternary International 241, 79−96.

Madsen, A.T., Murray, A.S., Andersen, T.J., Pejrup, M., Breuning-Madsen, H., 2005. Optically stimulated luminescence dating of young estuarine sediments: a comparison with ^{210}Pb and ^{137}Cs dating. Marine Geology 214, 251–268.

Madsen, A.T., Buylaert, J.P., Murray, A.S., 2011. Luminescence dating of young coastal deposits from New Zealand using feldspar. Geochronometria 38, 378–390.

Martinson, D.G., Pisias, W.G., Hays, J.D., Imbrie, J., Moore, T.C., Shackleton, N.J., 1987. Age dating and the orbital theory of the ice age: development of a high resolution 0 to 300,000 year chronostratigraphy. Quaternary Research 27, 1–29.

Morozov, G.V., 1968. The relative dating of Quaternary Ukrainian sediments by the thermoluminescence method. Eighth International Quaternary Association Congress, Paris, p. 167, U.S. Geological Survey Library, Washington DC, Cat. No. 208M8280.

Morthekai, P., Jain, M., Murray, A. S., Thomsen, K. J., Bøtter-Jensen, L., 2008. Fading characteristics of martian analogue materials and the applicability of a correction procedure. Radiation Measurements 43, 672–678.

Murray, A.S., Roberts, R.G., 1997. Determining the burial time of single-grains of quartz using optically stimulated luminescence. Earth and Planetary Science Letters 152, 163–180.

Murray, A.S., Roberts, R.G., 1998. Measurement of the equivalent dose in quartz using a regenerative-dose single-aliquot protocol. Radiation Measurements 29, 503–515.

Murray, A.S., Wintle, A.G., 2000. Luminescence dating of quartz using an improved single aliquot regenerative-dose protocol. Radiation Measurements 32, 57–73.

Murray, A.S., Wintle, A.G., 2003. The single aliquot regenerative dose protocol: potential for improvements in reliability. Radiation Measurements 37, 377–381.

OSPAR Commission. 2000. Quality Status Report 2000 for the North-East Atlantic: Chapter 2 Geography, Hydrography and Climate. http://www.ospar.org/eng/doc/pdfs/qec2.pdf.

Pachur, H.J., Wunnemann, B., Zhang, H.C., 1995. Lake evolution in the Tengger Desert, Northwestern China, during the last 40,000 years. Quaternary Research 44, 171–180.

Petit, J.R., Jouzel, J., Raynaud, D., Barkov, N.I., Barnola, J.-M., Basile, I., Bender, M., Chappellaz, J., Davis, M., Delaygue, G., Delmotte, M., Kotlyakov, M., Legrand, M., Lipenkov, V.Y., Lorius, C., Pepin, L., Ritz, C., Saltzman, E., Stievenard, M., 1999. Climate and atmospheric history of the past 420,000 years from the Vostok ice core, Antarctica. Nature 399, 429–436.

Pigati, J.S., Quade, J., Wilson, J., Jull, A.J.T., Lifton, N.A., 2007. Development of low-background vacuum extraction and graphitization systems for 14C dating of old (40−0 ka) samples. Quaternary International 166, 4−14.

Prescott, J. R., Stephan, L. G., 1982. The contribution of cosmic radiation to the environmental dose for thermoluminescene dating-Latitude, altitude and depth dependences. PACT 6, 17–25.

Preusser, F., Degering, D., Fuchs, M., Hilgers, A., Kadereit, A., Klasen, N., Krbetschek, M., Richter, D., Spencer, J.Q.L., 2008. Luminescence dating: basics, methods and application. E&G Quaternary Science J. 57, 95–149.

Reimann, T., Tsukamoto, S., Naumann, M., Frechen, M., 2011. The potential of using K-rich feldspars for optical dating of young coastal sediments e a test case from Darss-Zingst peninsula (southern Baltic Sea coast). Quaternary Geochronology 6, 207–222.

Reimer, P.J., Baillie, M.G.L., Bard, E., Bayliss, A., Beck, J.W,, Blackwell, P.G., Bronk, R.C., Buck, C.E., Burr, G.S., Edwards, R.L., Friedrich, M., Grootes, P.M., Guilderson, T.P., Hajdas, I., Heaton, T.J., Hogg, A.G., Hughen, K.A., Kaiser, K.F., Kromer, B., McCormac, F.G., Manning, S.W., Reimer, R.W., Richards, D.A., Southon, J.R., Talamo, S., Turney, C.S.M., van der Plicht, J., Weyhenmeyer, C.E., 2009. IntCal09 and Marine09 radiocarbon age calibration curves, 0–50000 years cal BP. Radiocarbon 51, 1111–1150.

Rhodes, E.J., 2011. Optically stimulated luminescence dating of sediments over the past 200,000 Years. Annual Review Earth Planetary Science 39, 461−488.

Roberts, H.M., 2007. Assessing the effectiveness of the double–SAR protocol in isolating a luminescence signal dominated by quartz. Radiation Measurements 42, 1627–1636.

Roberts, H.M., Wintle, A.G., 2001. Equivalent dose determinations for polymineralic fine-grains using the SAR protocol: application to a Holocene sequence of the Chinese Loess Plateau. Quaternary Science Reviews 20, 859–863.

Rutter, N., Ding, Z.L., Evans, M.E., Liu, T.S., 1991. Baoji-type pedostratigraphic section, Loess Plateau, north-central China. Quaternary Science Reviews 10, 1−22.

Schwarzer, K., Ricklefs, K., Bartholomä, A., Zeiler, M., 2008. Geological development of the North Sea and the Baltic Sea. Die Küste, 74, 1–17.

Shi, Y., Kong, Z.,Wang, S., Tang, L.,Wang, F., Yao, T., Zhao, X., Zhang, P., Shi, S., 1993. Mid-Holocene climates and environments in China. Global and Planetary Change 7, 219–233.

Shi, Y.F., Yu, G., Liu, X.D., Li, B.Y., Yao, T.D., 2001. Reconstruction of the 30–40 ka BP en- hanced Indian monsoon climate based on geological records from the Tibetan Pla- teau. Palaeogeography, Palaeoclimatology, Palaeoecology 169, 69–83.

Stauch, G., IJmker, J., Pötsch, S., Zhai, H., Hilgers, A., Diekmann, B., Dietze, E., Hartmann, K., Opitz, S., Wünnemann, B., Lehmkuhl, F., 2012. Aeolian sediments on the north-eastern Tibetan Plateau. Quaternary Science Reviews 57, 71–84.

Stevens, T., Thomas, D.S.G., Armitage, S.J., Lunn, H.R., Lu, H., 2007. Reinterpreting climate proxy records from late Quaternary Chinese loess: a detailed OSL investigation. Earth-Science Reviews 80, 111−136.

Stevens, T., Markovic, S.B., Zech, M., Hambach, U., Sümegi, P., 2011. Dust deposition and climate in the Carpathian Basin over an independently dated last glacial-interglacial cycle. Quaternary Science Reviews 30, 662–681.

Stokes, S., Hetzel, R., Bailey, R.M., Tao, M., 2003. Combined IRSL-OSL single aliquot regeneration (SAR) equivalent dose (De) estimates from source proximal Chinese loess. Quaternary Science Reviews 22, 975−983.

Street-Perrott, F.A., Harrison, S.P., 1984. Temporal variation in lake levels since 30,000 yr B.P. –An index of the global hydrological cycle. In: Hansen, J.E., Takahashi, T. (Eds.), Climate Processes and Climate Sensitivity, Geophysical Monograph Series 29, American Geophysical Union, Washington, DC, pp. 118–129.

Streif, H.J., 2002. Nordsee und Küstenlandschaft-Beispiel einer dynamischen Landschaftsentwicklung. In Akademie der Geowissenschaften zu Hannover, Heft 20, 134−149.

Streif, H., 2004. Sedimentary record of Pleistocene and Holocene marine inundations along the North Sea coast of Lower Saxony, Germany. Quaternary International 112, 3–28.

Sun, J.M., 2002. Provenance of loess material and formation of loess deposits on the Chinese Loess Plateau. Earth and Planetary Science Letters 203, 845–859.

Thiel, C., Buylaert, J. P., Murray, A., Terhorst, B., Hofer, I., Tsukamoto, S., Frechen, M. 2011. Luminescence dating of the Stratzing loess profile (Austria)-Testing the potential of an elevated temperature post-IR IRSL protocol. Quaternary International 234, 23–31.

Thompson, L.G., Yao, T., Davis, M.E., Henderson, K.A., Mosley- Thompson, E., Lin, P.-N., Beer, J., Synal, H.-A., Cole-Dai, J., Bolzan, J.F., 1997. Tropical climate instability: the last glacial cycle from a Qinghai-Tibetan ice core. Science 276, 1821–1825.

Thomsen, K. J., Murray, A. S., Jain, M., Bøtter-Jensen, L. 2008. Laboratory fading rates of various luminescence signals from feldspar-rich sediment extracts. Radiation Measurements 43, 1474–1486.

Timar, A., Vandenberghe, D., Panaiotu, E.C., Panaiotu, C.G., Necula, C., Cosma, C., van den haute, P., 2010. Optical dating of Romanian loess using fine-grained quartz. Quaternary Geochronology 5, 143–148.

Trautmann, T., Krbetschek, M.R., Dietrich, A., Stolz, W., 1999. Feldspar radio-luminescence: a new dating method and its physical background. Journal of Lumininescence 85, 45−58.

Tsukamoto, S., Denby, P.M., Murray, A.S., Bøtter-Jensen, L., 2006. Time-resolved luminescence from feldspars: new insight into fading. Radiation Measurement 41, 790–795.

Vasiliniuc, Ş., Vandenberghe , D.A.G., Timar-Gabor, A. , Cosma, C., van den Haute, P., 2013. Combined IRSL and post-IR OSL dating of Romanian loess using single aliquots of polymineral fine grains. Quaternary International 293, 15–21.

Vink, A., Steffen, H., Reinhardt, L., Kaufmann, G., 2007. Holocene relative sea-level change, isostatic subsidence and the radial viscosity structure of the mantle of northwest Europe (Belgium, the Netherlands, Germany, southern North Sea). Quaternary Science Reviews 26, 3249–3275.

Walker, M., 2005. Quaternary Dating Methods. Wiley.

Wallinga, J., Bos, A. J. J., Dorenbos, P., Murray, A. S., Schokker, J. 2007. A test case for anomalous fading correction in IRSL dating. Quaternary Geochronology 2, 216–221.

Wang, X.L., Lu, Y.C., Zhao, H., 2006. On the performances of the single-aliquot regenerative-dose (SAR) protocol for Chinese loess: fine quartz and polymineral grains. Radiation Measurements 41, 1–8.

Walday, M., Kroglund, T., 2002. Europe's biodiversity-biogeographical regions and seas: Seas around Europe “The North Sea”. pp. 4. http://www.eea.europa.eu/publications/ report_ 2002_0524_154909.

Wintle, A.G., 1973. Anomalous fading of thermoluminescence in mineral samples. Nature 245, 143–144.

Wintle, A. G., Huntley, D.J., 1979. Thermoluminescence dating of a dee-sea sediment core. Nature 279, 710–712.

Wintle, A. G., Huntley, D.J., 1980. Thermoluminescence dating of ocean sediments. Canadian Journal of Earth Sciences, 17, 348–360.

Wintle, A.G., 1981. Thermoluminescence dating of late Devensian loesses in southern England. Nature 289, 479–480.

Wintle, A.G., Shackleton, N.J., Lautridou, J.P., 1984. Thermoluminescence dating of periods of loess deposition and soil formation in Normandy. Nature 310, 491–493.

Zeiler, M., Schwarzer, K., Ricklefs, K., 2008. Seabed Morphology and Seabed Sediments. Die Küste 74, 31–44, 2008.

Zhang, H.C., Peng, J,L., Ma, Y.Z., Chen, G.J., Feng, Z.D., Li, B., Fan, H.F., Chang, F.Q., Lei, G.L., Wünnemann, B., 2004. Late Quaternary palaeolake levels in Tengger Desert, NW China. Palaeogeography, Palaeoclimatology, Palaeoecology 211, 45–58.

Zhang, J.R., Lai, Z.P., Jia, Y.L., 2012. Luminescence chronology for late Quaternary lake levels of closed Huangqihai lake in East Asia monsoon marginal area in northern China. Quaternary Geochronology 10, 123–128.

Zhang, J.F., Fan, C.F., Wang, H., Zhou, L.P., 2007. Chronology of an oyster reef on the coast of Bohai Bay, China: constraints from optical dating using different luminescence signals from fine quartz and polymineral fine grains of coastal sediments. Quaternary Geochronology 2, 71–76.

Zimmerman, D.W., 1971. Thermoluminescence dating using fine grains from pottery. Archaeometry 13, 29–52.

Chapter 2 Late Quaternary loess accumulation in Qilian Shan, northern China

2.1 Late Pleistocene and Holocene loess sedimentation in central and western Qilian Shan (China) revealed by OSL dating

Jingran Zhang[1], Veit Nottebaum[2], Sumiko Tsukamoto[1], Frank Lehmkuhl[2], Manfred Frechen[1]

[1] Leibniz Institute for Applied Geophysics (LIAG); Stilleweg 2, 30655 Hannover, Germany

[2] Department of Geography, RWTH Aachen University; Templergraben 55, 52056 Aachen, Germany

Quaternary International, Vol. 372, pp. 120–129.

DOI: http://www.sciencedirect.com/science/article/pii/S1040618214010106

Abstract

The knowledge of loess accumulation in the central and western Qilian Shan was restricted to the time span since 13-11 ka until present. Loess deposits prior to this period have not yet been reported. In this study, 23 loess samples from the northern piedmont of central and western Qilian Shan area have been dated using fine-grained quartz optically stimulated luminescence (OSL) dating technique to set up a chronological framework for the loess sedimentation in this region. Our results demonstrate that the deposition of dust was widespread since the last deglaciation (~13 ka) until ~3.6 ka in the northern piedmont of the central and western Qilian Shan area. Furthermore, the chronology of the loess sedimentation has been extended back at least to ~81 ka, which is remarkably older than previously thought. The existence of suitable environmental conditions (e.g. vegetation cover) for loess accumulation can be deduced in the central and western Qilian Shan for the Holocene and late Pleistocene. However, the loess sedimentation has been revealed to be discontinuous before ~13 ka as indicated by its episodic occurrence.

Key word: loess; OSL dating; Qilian Shan; Late Pleistocene; Holocene

2.1.1 Introduction

The extensive Quaternary loess sequences from the Chinese Loess Plateau and adjacent areas in northwestern China have been widely documented and considered to be excellent archives for reconstructing the climate history of Central Asia for the past 2.4 Ma (Kukla and An, 1989; Liu and Ding, 1998). Most previous studies have focused on the central part of the Chinese Loess Plateau where up to ~400 m of interbedded loess-palaeosol sequences are present (e.g. Liu, 1985; An et al., 1991; Pye, 1995; Buylaert et al., 2008; Song et al., 2014). The Qilian Shan (*Shan* means mountain in Chinese), located along the northeastern margin of the Tibetan Plateau, plays an important role not only for the dust transport but also serves as one of the major dust source regions in arid/semi-arid Central and East Asia (Derbyshire et al., 1998; Sun, 2002). Loess deposits with varying thickness are commonly observed in the piedmont of Qilian Shan. In the eastern Qilian Shan close to the Chinese Loess Plateau, more than 200 m thick loess-palaeosol sequences have been well preserved for the period of the past ~0.8 Ma, which can be well correlated to the records of the Chinese Loess Plateau (Wu et al., 2001, 2002, 2005). The loess on various geomorphic surfaces has been also used to constrain ages of the overlying sediment (e.g. fluvial terraces) to investigate the tectonic and glacial activities as well as the climatic implications (e.g. Chen et al., 2013; Pan et al., 2013).

However, the studies on loess accumulation itself are still lacking especially in the more proximal central and western Qilian Shan. Two studies have been carried out to date loess deposits in the central and western Qilian Shan by applying optically stimulated luminescence (OSL) dating techniques (Stokes et al., 2003; Küster et al., 2006). In the central and western Qilian Shan, only a few meter of loess is preserved which is much thinner compared with the eastern Qilian Shan. Loess deposits on a series of river terraces near Zhangye City (central Hexi Corridor) have been dated by Stokes et al. (2003) to be commenced at ~8-9 ka and so restricted to the Holocene (interglacial) period. As the extraction of the fine-grained quartz fraction by 10 % HF was not successful to remove all feldspar signal, a double SAR protocol, with one step of IR stimulation before OSL stimulation (Banerjee et al., 2001; Roberts and Wintle, 2001), has been adopted in order to further remove the signal originated from feldspar. Based on sand-sized quartz OSL ages of the loess on river terraces at the western Qilian Shan front, Küster et al. (2006) confirmed the occurrence of Holocene loess ranging from 13 to 11 ka to the present. The

timing of the onset of loess accumulation revealed by these two studies shows several ka discrepancy. Küster et al. (2006) attributed this asynchrony to either the local differences in the history of loess deposition or the different OSL protocols applied. In contrast to the eastern Qilian Shan and the adjacent Chinese Loess Plateau, loess deposits older than the latest Pleistocene (13-11 ka) have not been reported in the central and western Qilian Shan.

Luminescence dating allows the direct determination of burial ages for sediments from a wide variety of depositional environments (Murray and Olley, 2002). This method has been extensively applied to date loess deposits throughout the world (e.g. Li and Wintle, 1992; Zhou et al., 1995; Frechen et al., 1999; Singhvi et al., 2001; Roberts, 2006; Stevens et al., 2006, 2007, 2008; Buylaert et al., 2008; Timar et al., 2010; Thiel et al., 2011; Schatz et al., 2012; Kreutzer et al., 2012; Chen et al., 2013; Kang et al., 2013; Marković et al., 2014). In the current study, OSL dating has been employed to date the loess collected from the northern piedmont of central and western Qilian Shan. The aim of this study is to examine the periods of dust accumulation in central and western Qilian Shan area based on the quartz OSL dating. The possible reasons for the discontinuity in loess sedimentation are also discussed.

2.1.2 Regional setting and section description

The Qilian Shan lies along the northeastern margin of the Tibetan Plateau (Fig. 2.1) with a maximum elevation of up to ~5700 m asl. It is constrained by two left-lateral strike-slip faults, Altyn Tagh Fault and Haiyuan Fault (Meyer et al., 1998). In the summit region, there are more than 3300 modern mountain glaciers with a total glacier area of 2063 km^2 with varying lower limit elevations of above ~4000 m asl (Wang, 1981). Many rivers (Changma River, Shiyou River, Baiyong River, Beida River, Heihe River, etc.) originate from the high mountain areas and flow into the Hexi Corridor, an elongated depression that is flanked by the Qilian Shan to the south and the Heli Shan and the Long Shou Shan to the north.

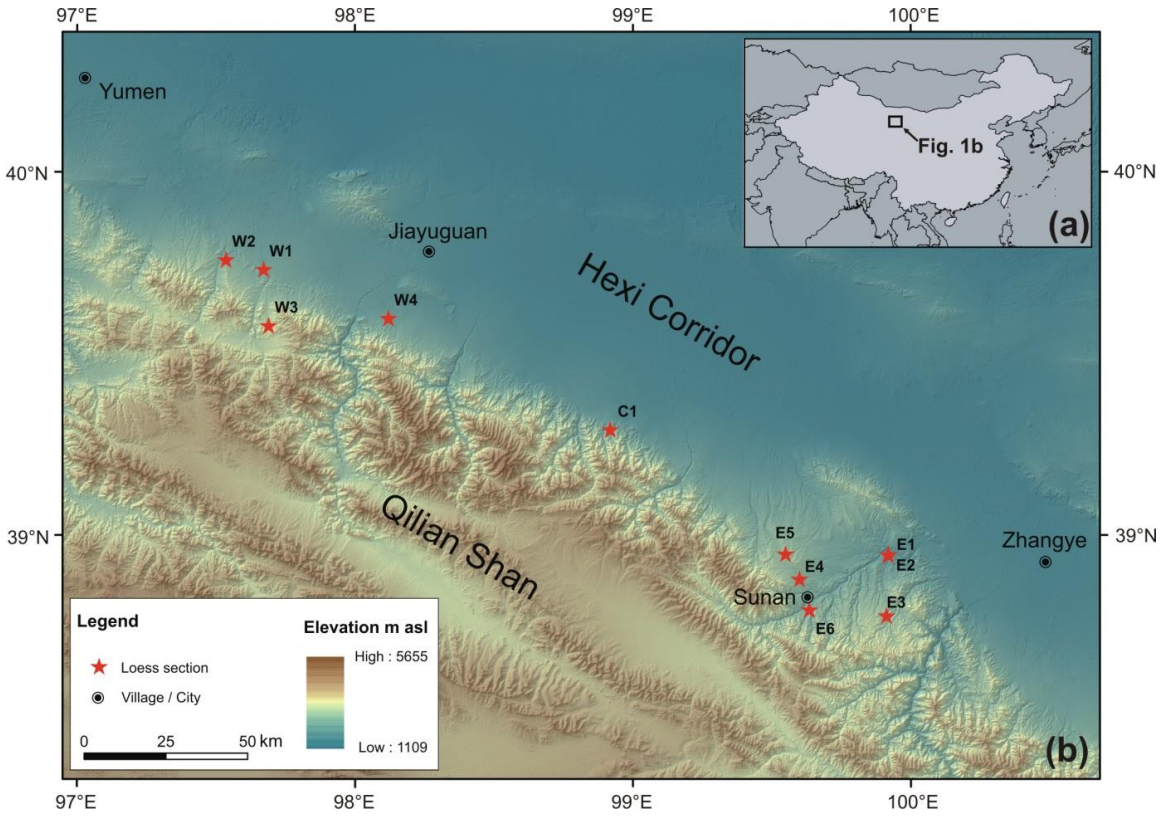

Fig. 2.1 (a) Map of China. The small square denotes the location of the study area (Qilian Shan). (b) Enlarged Map showing the Qilian Shan area and the locations of the sampling sections.

At the foreland of the Qilian Shan, a series of extensive and closely-adjacent alluvial fans mostly larger than 50 km^2 are present, built up mainly by gravels, sands and silts (Derbyshire et al., 1998). These silt-rich alluvial fans have been considered as an important source of aeolian silts deposited on the Chinese Loess Plateau (Derbyshire et al., 1998; Sun, 2002). The moisture is mostly brought by the SE-Asian Summer Monsoon between May and September (Bourque and Mir, 2012). A strong precipitation gradient from east to west exists. For example, Zhangye City (1483 m asl, central Qilian Shan) receives an annual precipitation of ~130 mm, whereas Yumen City (1527 m asl; western Qilian Shan) receives only ~67 mm (observed data between 1976 and 2005) (Bourque and Mir, 2012). The precipitation also increases with altitude owing to the orographic rainfall. In winter and spring time, NW Winter monsoon penetrates this area causing severe dust storms (Derbyshire et al., 1998; Ta et al., 2004). The dominant wind direction and the transport of wind-blown material north of the Qilian Shan are from northwest to southeast (e.g., Pye, 1995; Derbyshire, 2001). Dust deposition along the front of the

Qilian Shan is active today and an average rate of about 350 t/km^2/year has been reported in several major cities along the Hexi Corridor between 1986 and 2000 (Ta et al., 2004).

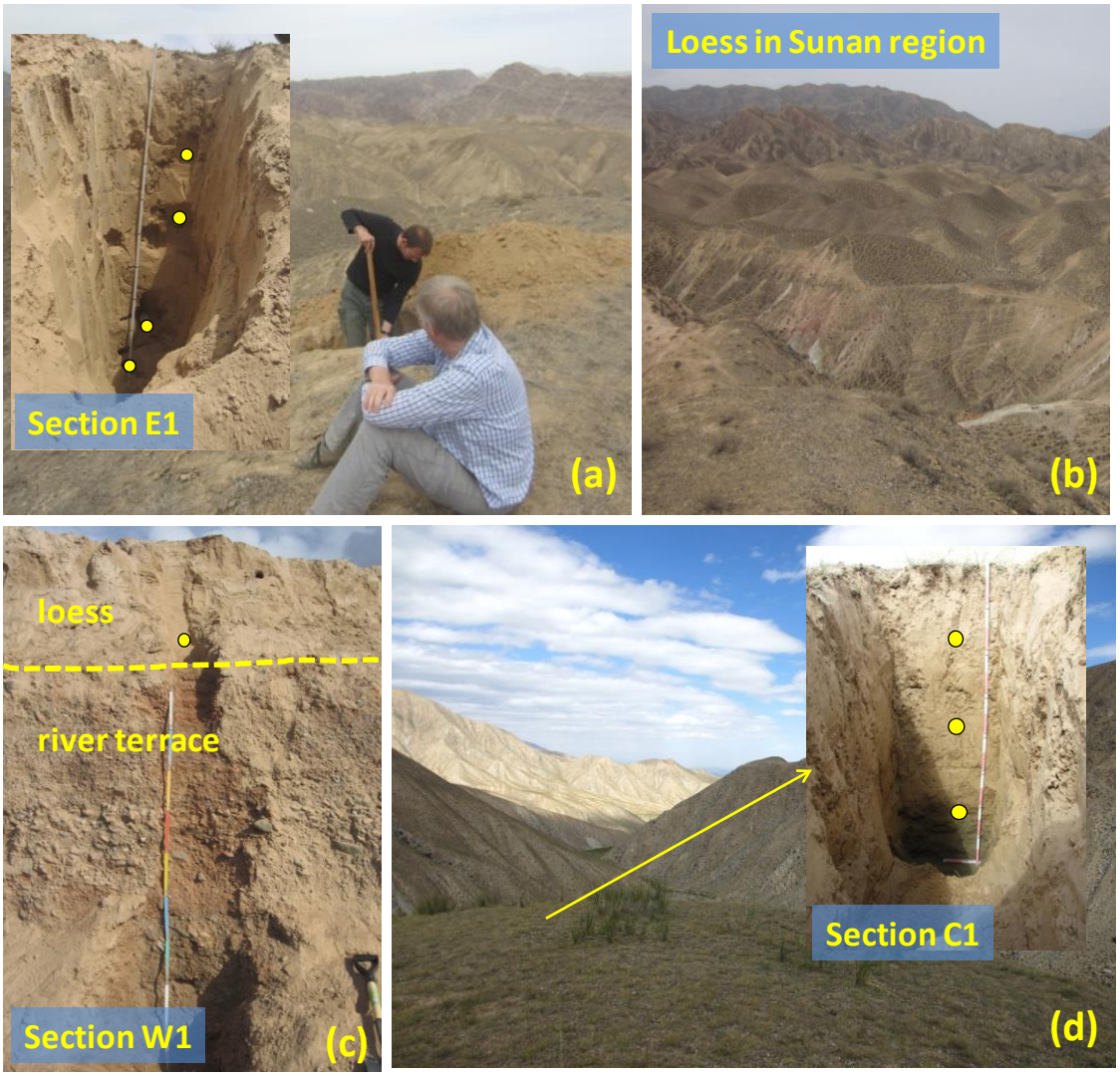

Fig. 2.2 Loess covered landscape in Qilian Shan area and typical loess sections. (a) Section E1 is located in a hill top position (Sunan region). (b) Loess covered landscape in Sunan region. The thickest loess sequence in Qilian Shan area is preserved to several meters. (c) Section W1 consists of primary silty loess and coarser fluvial deposits. The loess was accumulated on the river terrace. (d) Section C1, hilltop position next to a steeply incised valley in central Qilian Shan.

The field investigation in the current study spans over 230 km horizontal and 1.3 km vertical distance in the northern piedmont of central and western Qilian Shan. Loess

and/or loess-like sediments are widespread and deposited in varying thickness between altitudes of ~2000 m and ~3800 m asl (Fig. 2.2) (also see in Nottebaum et al., 2014). Except for the area around Sunan village, where the loess has accumulated up to several meters, the loess cover is generally less than 2 m thick, occurring not only on the river terraces but also on mountain slopes. No primary loess was found in the foreland region (below ~2000 m asl) (Nottebaum et al., 2014).

Twenty-three OSL samples from eleven sections were collected along an SE–NW transect. Sampling sites were selected after careful inspection of the geomorphological surrounding. Hilltop positions were preferred to reduce the risk of sampling layers affected by reworking, although there may be a higher chance of erosion. Samples for OSL dating were taken by hammering metal tubes of 6 cm diameter into freshly cleaned profiles. Samples for dosimetry measurements were taken from immediate surroundings of the OSL samples.

The studied sections are allocated to three different subdivisions of the study area along the central and western Qilian Shan front which referred to as the eastern part (Section E1, E2, E3, E4, E5 and E6), the central part (Section C1) and the western part (Section W1, W2, and W3). The profiles are located either on fluvial/alluvial terraces or at hilltop positions. Root penetration is present more or less in the loess from all sections. In contrast to most other loess regions, such as the Chinese Loess Plateau, no intercalated palaeosol layer was observed among the profiles under study. Results of further sedimentological investigations aiming for grain size variations in these sections are presented by Nottebaum et al. 2015. The sketches of these sections are shown in Fig. 2.3. The brief section descriptions are listed as below:

Section E1 (38°57’34.95N; 99°54’07.07’’E; ~2030 m asl) is located on a terrace of Liyuan River. This section consists of homogenous, yellowish silty loess (upper part) and gradually coarser fine sandy loess (lower part) (Fig. 2.2a) with a thickness of about 2 m. An increased number of carbonate concretions was observed below ~1 m. OSL samples were taken at 2.0 m (LUM-2938), 1.5 m (LUM-2939), 0.9 m (LUM-2940), and 0.5 m (LUM-2941) below surface.

Section E2 (38°57’38.46’’N; 99°54’01.85’’E; ~2020 m asl) is ~170 m to the northwest of Section E1, located on the right side of a steep tributary valley of Liyuan River. This

section consists of ~1 m homogenous yellowish loess. Some small gravels (<1 cm in diameter) are found at the bottom of the section. Fluvial deposits including gravels were observed in the adjacent steep valley walls about 2.5 m below the bottom of the section. OSL samples were taken at 1.0 m (LUM-2942) and 0.7 m (LUM-2943) below surface.

Section E3 (38°47'33.01''N; 99°53'33.36''E; ~3030 m asl) is located on a hilltop position. It is around 600 m away from a seasonal tributary valley of Liyuan River and lies about 150 m above the valley base. The section has a thickness of 0.95 m, consisting of brownish silty loess. An OSL sample was taken at 0.75 m below surface (LUM-2944).

Section E4 (38°53'43.15''N, 99°35'16.21''E; ~2630 m asl) is located at the hilltop position on the watershed of two tributary valleys of Liyuan River. The loess deposits are more than 2.2 m thick and the bottom of the loess was not reached during the fieldwork. Loess is of yellowish to brownish colour. The upper 1.5 m consists of silty loess, followed by sandy loess from 1.5 m to 2.2 m. Four OSL samples were taken at 2.1 m (LUM-2948), 1.5 m (LUM-2949), 0.9 m (LUM-2950), and 0.4 m (LUM-2951) depths below surface.

Section E5 (38°57'53.97''N, 99°32'22.43''E; ~3010 m asl) is located close to the watershed of the Liyuan River catchment at a hilltop position. The yellow-brownish silty loess overlies the sediment of debris mixed with reworked loess (1.9- 1.7 m). Single gravels (<8 mm) are found up to 1.55 m. Loess is slightly compacted between 1.1 m and 0.4 m compared to neighboring parts. However no responsible matrix material was observed macroscopically. Three OSL samples were taken at depths of 1.5 m (LUM-2958), 0.9 cm (LUM-2959) and 0.4 m (LUM-2960).

Section E6 (38°48'36.68''N, 99°37'16.37''E; ~2460 m asl) is located on a river terrace of a tributary of Liyuan River close to Sunan village. The profile has a thickness of 1.40 m and the base of the silty loess deposit has not been reached. The loess is generally of yellowish to slightly brownish colour. Between 0.8 m and 0.35 m, the loess was relatively compacted. One OSL sample (LUM-2961) was taken at 1.1 m depth.

Section C1 (39°18'26.18''N, 98°55'03.96''E; ~2370 m asl) is located at hilltop position besides a steeply incised valley (Fig. 2.2d). The exposed deposits are 1.6 m thick and the bottom of the primary silty loess was reached at 1.18 m depth. A mixture of unstratified reworked loess and weathered debris from underlying granitic bedrock underlies the silty

loess below 1.18 m. The loess between 0.75 and 0.32 m depth is solidified and has a slightly brighter colour. Three OSL samples were taken at 1.05 m (LUM-2955), 0.62 m (LUM-2956) and 0.35 cm (LUM-2957) depths.

Section W1 (39°44'31.48''N, 97°41'31.48''E; ~2360 m asl) is located on a alluvial fan terrace (Fig. 2.2c). Braided seasonal river channels are immediately adjacent. This section is comprised of ~1.1 m homogenous silty loess overlying the reddish fluvial gravels. One sample (LUM-2935) at 0.95 m was collected.

Section W2 (39°46'02.69''N, 97°32'59.14E; ~2560 m asl) is located on the highest terrace of Shiyou River (cf. Küster et al., 2006). The profile is about one meter thick. The lower part of the profile (1-0.6 m) consists of reworked silty loess with slightly reddish-brownish colour. About 0.6 m sandy loess overlies the reworked loess. An OSL sample was taken at 0.47 m (LUM-2952) depth from the sandy loess.

Section W3 (39°35'16.61''N, 97°42'18.45''E; ~3310 m asl) is comprised of 0.67 m homogenous silty loess located on a mountain slope. The bedrock was reached at 0.7 m below surface. Two OSL samples were collected at 0.5 m (LUM-2953) and 0.3 m (LUM-2954).

Section W4 (39°36'42.76''N, 98°07'49.84''E; 2160 m asl) consists of 1.10 m thick homogenous yellowish loess covering the alluvial fans in the foreland. The loess cover has been intensively eroded by braided river channels originating from the mountains. One OSL samples was taken from this section at 0.95 m (LUM-2936) depth.

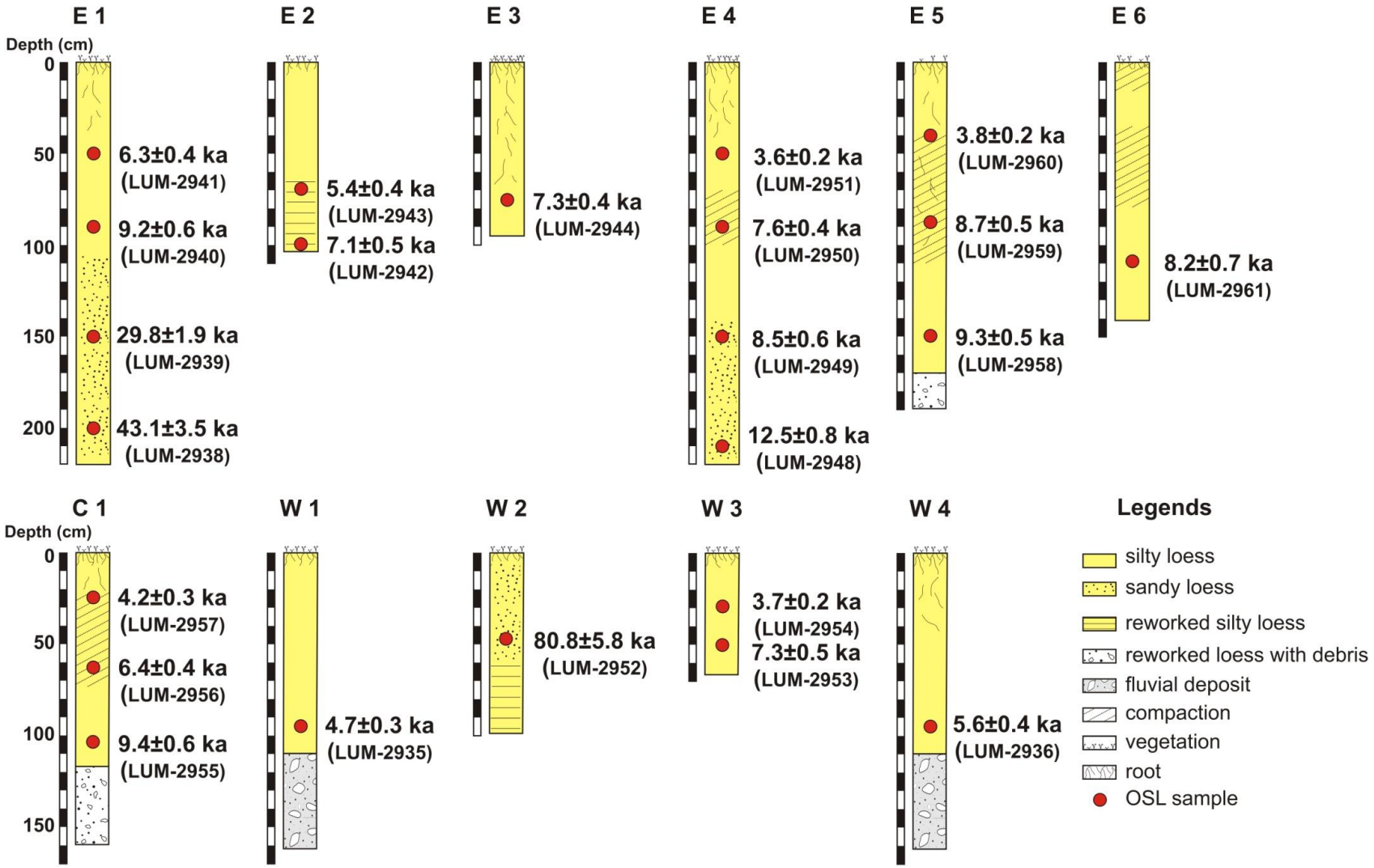

Fig. 2.3 Graphical logs of the loess sections. OSL ages of 23 loess samples are shown.

2.1.3 Luminescence dating

2.1.3.1 Sample preparation

All preparations were conducted under subdued red light conditions. The materials at each end of the sampling tubes that might have been exposed to light were removed. The chemical treatment with hydrochloric acid, sodium oxalate and hydrogen peroxide was employed to the remaining material to dissolve carbonate, aggregates, and organic matter, respectively. The fine-grained fraction (4-11 μm) of the samples was extracted following the description by Frechen et al. (1996). The separated 4-11 μm fraction was then etched using hydrofluorosilicic acid (H_2SiF_6) for 6 days to extract quartz fractions. The purity of quartz for each aliquot was checked using the IR depletion ratio (Duller, 2003) and no significant IR signal was observed, indicating that the isolation of quartz was successful. The quartz extracts were mounted on aluminum discs (diameter 9.7 mm) from a suspension in distilled water (2 mg quartz fine grains per disc) for luminescence measurement. For samples with very low OSL intensities (LUM-2935, LUM-2940 and LUM-2942), 5 mg quartz fine grains per disc were used for the D_e measurement. However, this did not help increase the OSL intensity.

2.1.3.2 OSL measurement

OSL measurements were carried out using an automated Risø TL/OSL DA15 reader equipped with a $^{90}Y/^{90}Sr$ beta source. Quartz OSL signals were stimulated with blue LEDs (470±30 nm) and detected through a Hoya U-340 (7.5 mm) filter. The single-aliquot regenerative-dose (SAR) protocol (Murray and Wintle, 2000) was applied for the D_e measurement. The dose response curves were fitted either with a single saturation exponential function or a saturating exponential plus linear function. The integral over the initial 0.8 s of the signal subtracted by an early background derived from the integral of 0.8-4.8 s was used for the D_e calculation, in order to isolate a signal that is dominated by the fast component (Ballarini et al., 2007). There are a number of internal checks which can be made on each aliquot measured using SAR protocol, such as the recuperation and recycling ratio. The recuperation has been suggested not to exceed 5% and the recycling ratio should be within 10% of unity (Murray and Wintle, 2000). Due to the high

uncertainty in the recycling ratio for samples with low OSL sensitivity, we lowered the rejection criteria for recycling ratios from 10% to 15% of unity for all samples.

In order to select a suitable thermal treatment for the SAR protocol, a set of routine tests (i.e. preheat plateau, dose recovery and thermal transfer tests) were applied to two representative samples (LUM-2940 and LUM-2944) prior to dating. For the preheat plateau test, a group of natural aliquots was measured with different preheat temperatures ranging from 160 °C to 280 °C at 20 °C increments with a cut-heat that tracks the preheat temperature by -20 °C, following the suggestion of Roberts (2006), except for the 160 °C preheat where the same cut-heat temperature was used. Dose recovery tests are considered to be essential for the applicability of any SAR protocol (Murray and Wintle, 2003). For the dose recovery test, natural aliquots were bleached using blue LED at room temperature for 300 s, followed by a >5000 s pause to allow for thermal decay of any phototransferred charge in the 110 °C TL trap and then were further bleached at room temperature for 300 s. A laboratory β-dose, approximately equal to the natural D_e, was then given to the bleached aliquots and measured using the same SAR protocol as the preheat plateau test. Three aliquots at each temperature point were measured for the preheat plateau and dose recovery tests. Based on the results of these tests (*see section 2.1.3.4*), a preheat temperature of 180 °C and a cut heat at 160 °C were selected. The dose recovery tests were then carried out for all samples under this condition. Owing to the averaging effect by many grains on one aliquot, the fine grain fraction is characterized by a low D_e scatter. Thus, precise D_e estimates are possible with a small number of aliquots. Accordingly, 8-20 aliquots for each sample were employed for the D_e measurement. The average D_e with 1σ standard error was applied for the age calculation.

2.1.3.3 Dose rate determination

Dose rates of the samples were derived by converting the radionuclide concentrations using the conversion factors from Guérin et al. (2011). High-resolution gamma spectrometry was applied to determine the radionuclide concentrations of U, Th and K in the samples. The samples were dried at 130 °C, homogenized, filled into 50 g air tight plastic containers and stored for at least one month to gain ^{226}Ra-^{222}Rn equilibrium condition before measurement (Murray et al., 1987). The beta attenuation factors of

Mejdahl (1979) were applied for dose rate calculation. An a-value of 0.04 ± 0.02 was adopted for fine grain quartz to allow for the lower efficiency of alpha radiation according to Rees-Jones and Tite (1997). Cosmic ray contributions were considered using the equations of Prescott and Hutton (1994). A water content of 5 ± 5% was assumed for the total dose rate calculation. As shown in Table 2.1, the dose rates do not vary significantly with sampling depth and between the different sites except sample LUM-2952 giving a total dose rate of 3.66 ± 0.2 Gy/ka, which is lower than that of the other samples ranging from 4.09 ± 0.24 Gy/ka to 4.59 ± 0.27 Gy/ka.

2.1.3.4 OSL characteristics

Fig. 2.4 shows the OSL decay and dose response curves for two representative samples (LUM-2940 and LUM-2944). Sample LUM-2940 has rather low OSL intensity with a natural signal is less than 200 counts/0.16 s. The OSL intensity of LUM-2940 generated by a test dose of 17.4 Gy (~100 counts/0.16 s) is significantly lower than that of LUM-2944 (~11.4×10^3 counts/0.16 s) to the same size of given dose. This indicates that the quartz OSL sensitivity of LUM- 2940 is much lower than LUM-2944.

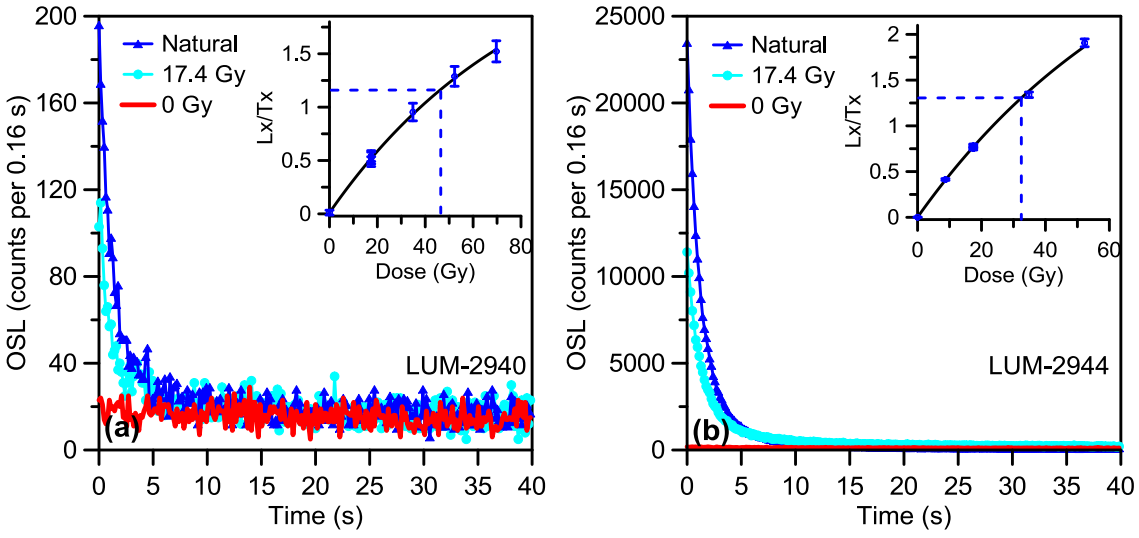

Fig. 2.4 OSL decay curves and dose-response curves for sample (a) LUM-2940 and (b) LUM-2944. These two representative samples show different luminescence characteristics.

Ten samples (LUM-2935, LUM-2936, LUM-2940, LUM-2942, LUM-2943, LUM-2949, LUM-2953, LUM-2955, LUM-2957 and LUM-2961) with low sensitivity

(<1000 count/0.16 s for test dose) are marked with asterisks (*) in Table 2.1. Previous studies suggest that the lower OSL sensitivity of unheated quartz grains is probably related to a short sedimentation history of the particles from the source region to depositional site (Li and Wintle, 1992; Preusser et al., 2006; Pietsch et al., 2008; Fitzsimmons et al., 2010). However, the variations of OSL sensitivity do not show any spatial and temporal pattern.

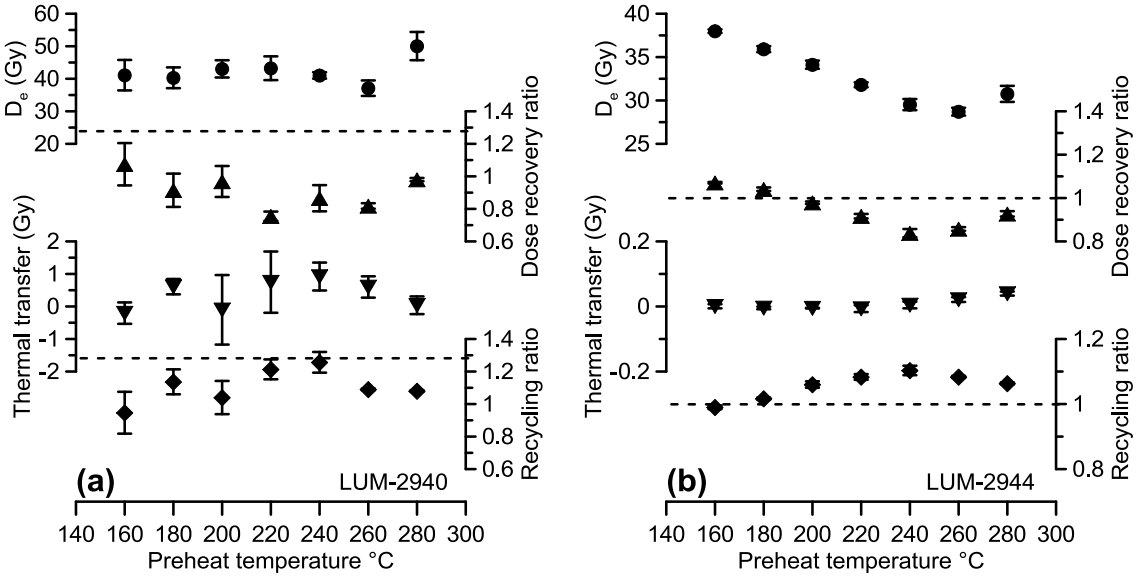

Fig. 2.5 Equivalent dose, dose recovery ratio, thermal transfer and recycling ratios as a function of preheat temperature for sample (a) LUM-2940 and (b) LUM-2944, respectively. A dashed line is drawn at 1 to highlight the ideal acceptance of unity for dose recovery ratio and recycling ratio. Each data point is the mean of three aliquots and 1s standard error was marked for the error ranges.

The results of the preheat plateau, dose recovery and thermal transfer tests for sample LUM-2940 and LUM-2944 are presented in Fig. 2.5a and 2.5b. For sample LUM-2940 (Fig. 2.5a), the mean D_es showed a wide plateau across the whole temperature range of 160-280 °C. The mean values of the dose recovery and recycling ratio are within 10% of unity except 220-260°C. The thermal transfer test yield doses ranging between – 0.2 ± 0.33 Gy and 0.92 ± 0.43 Gy. We attributed these relatively high values to extremely low signal/noise ratio rather than thermal transfer itself. The recycling ratios rather scatter

ranging between 0.95 ± 0.13 and 1.26 ± 0.06. It is noted that the OSL intensity was remarkably increased when the preheat temperature is above 220 °C. The high preheat temperature caused significant sensitivity increase in the quartz OSL signal for this sample. The recuperation was less than 5% for the whole temperature range. For sample LUM-2944 (Fig. 2.5b), the D_es are very sensitive to the temperature variation and no apparent D_e plateau was observed. The D_es decreased with increasing preheat temperature until 240 °C and thereafter increased again up to 280 °C. The dose recovery ratios show a similar trend as those of the preheat plateau test. Most of the dose recovery ratios were <10% of unity except at 240 and 260 °C. The thermal transfer is always smaller than 0.05 Gy which is negligible. The recuperation was consistently lower than 1% for the whole temperature range. The recycling ratios are generally above one but still within 15% of unity.

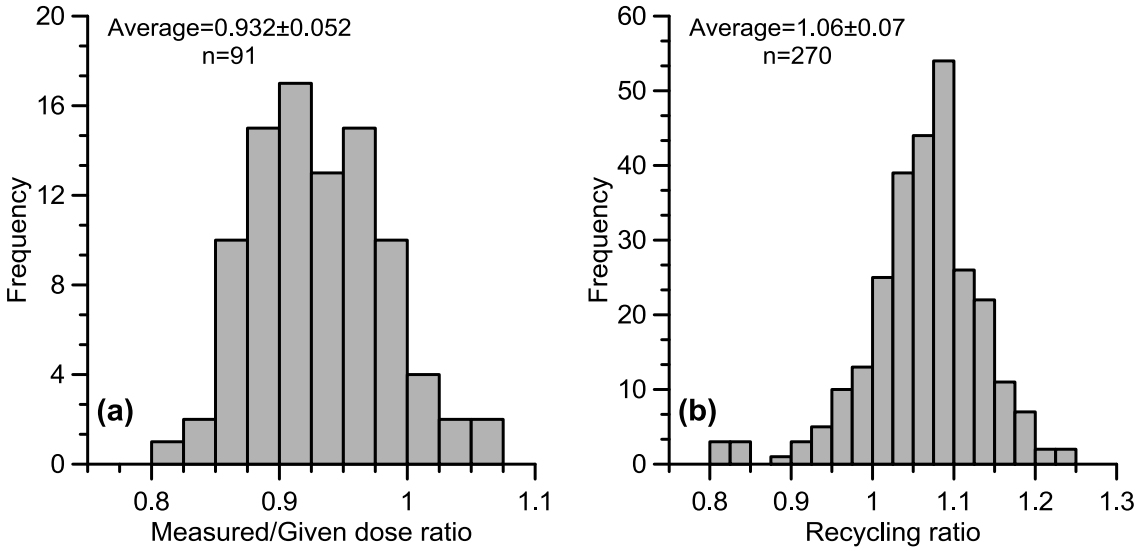

Fig. 2.6 (a) Measured to given doses ratio for the dose recovery test on all samples using preheat of 180 °C for 10 s followed by a cut-heat of 160 °C. Four to six aliquots were used for the dose recovery test per sample. (b) Recycling ratios of the D_e measurement for all samples. The aliquots whose recycling ratio fell out of the acceptance criteria (15% to the unity) have been rejected for the final De calculations.

Taking all the luminescence properties discussed above into consideration, such as the D_e plateau versus preheat temperature, dose recovery ratio, sensitivity change, etc., a preheat of 180 °C for 10 s followed by a cut-heat to 160 °C was selected for the measurement of

all samples in this study. The measured dose to given dose ratios for all samples under this condition are plotted in a histogram in Fig. 2.6a. The dose recovery ratios for most of the samples fall within the 15% of unity, except three aliquots yielding values lower than 85% of unity. The recycling ratios of the D_e measurement for all samples are shown in Fig. 2.6b.

2.1.3.5 Equivalent dose and OSL ages

The equivalent doses and the ages are summarized in Table 2.1. The D_es for all samples are ranging between 15.5 ± 0.4 Gy and 296 ± 13 Gy. The OSL ages are consistent with the stratigraphic order for each section and vary between 3.6 ± 0.2 ka and 80.8 ± 5.8 ka. The OSL ages against the sampling depth are presented in Fig. 2.3. 19 OSL ages from all sections except W2 correlate to the Holocene. Two samples below 1.5 m depth from E1 yielded ages of 43.1 ± 3.5 ka (LUM-2938) and 29.8 ± 1.9 ka (LUM-2939). The lowermost sample (LUM-2948) from E4 was dated to be 12.5 ± 0.8 ka. LUM-2952 from W2 sampled at 0.47 m depth has an age of 80.8 ± 5.8 ka.

Table 2.1 Summary of radionuclide concentrations, dose rates, Des and OSL ages for all samples.

Section No.	Elevation (m, a.s.l.)	Sample ID	Sampling depth (m)	Uranium (ppm)	Thorium (ppm)	K (%)	Environmental dose rate (Gy/ka)	Cosmic dose rate (Gy/ka)	Total dose rate (Gy/ka)	No. of aliquots[1]	D_e (Gy)	Age (ka)
E1	2030	LUM-2938	2	3.03±0.15	10.67±0.54	1.98±0.13	3.81±0.24	0.31±0.03	4.12±0.24	10 (10)	177.5±9.9	43.1±3.5
		LUM-2939	1.5	3.48±0.18	12.48±0.63	1.99±0.13	4.12±0.26	0.31±0.03	4.43±0.26	16 (13)	131.9±3.0	29.8±1.9
		LUM-2940*	0.9	3.32±0.17	11.84±0.60	1.97±0.12	3.99±0.25	0.32±0.03	4.31±0.25	13 (10)	39.8±1.4	9.2±0.6
		LUM-2941	0.5	3.39±0.17	11.67±0.59	2.03±0.13	4.05±0.25	0.32±0.03	4.37±0.26	10 (8)	27.5±1.0	6.3±0.4
E2	2020	LUM-2942*	1	2.78±0.14	10.90±0.56	2.06±0.13	3.84±0.24	0.31±0.03	4.15±0.24	12 (11)	29.3±1.5	7.1±0.5
		LUM-2943*	0.7	3.19±0.16	11.39±0.58	2.14±0.13	4.08±0.25	0.31±0.03	4.39±0.25	12 (9)	23.9±0.8	5.4±0.4
E3	3030	LUM-2944	0.75	3.56±0.18	12.37±0.63	2.06±0.12	4.20±0.26	0.39±0.04	4.59±0.27	11 (11)	33.5±0.3	7.3±0.4
E4	2630	LUM-2948	2	3.16±0.05	11.42±0.10	1.93±0.03	3.87±0.22	0.36±0.04	4.22±0.23	16 (12)	52.7±1.7	12.5±0.8
		LUM-2949*	1.5	3.31±0.03	11.39±0.06	2.00±0.02	3.97±0.23	0.36±0.04	4.33±0.23	12 (10)	36.8±1.5	8.5±0.6
		LUM-2950	0.9	3.26±0.06	11.15±0.10	1.94±0.03	3.88±0.23	0.36±0.04	4.24±0.23	12 (12)	32.2±0.5	7.6±0.4
		LUM-2951	0.4	3.33±0.03	11.60±0.07	1.93±0.02	3.93±0.23	0.36±0.04	4.29±0.23	12 (12)	15.5±0.4	3.6±0.2
E5	3010	LUM-2958	1.5	3.25±0.05	11.50±0.11	2.08±0.03	4.05±0.23	0.39±0.04	4.43±0.23	12 (12)	41.3±0.9	9.3±0.5
		LUM-2959	0.9	3.27±0.04	10.94±0.09	1.98±0.02	3.90±0.22	0.39±0.04	4.29±0.23	12 (12)	37.1±0.5	8.7±0.5
		LUM-2960	0.4	3.08±0.05	10.84±0.10	1.95±0.03	3.81±0.22	0.39±0.04	4.20±0.22	12 (12)	16.1±0.3	3.8±0.2
E6	2460	LUM-2961*	1.1	3.33±0.05	11.15±0.10	1.98±0.03	3.94±0.23	0.34±0.03	4.28±0.23	12 (7)	35.1±2.1	8.2±0.7
C1	2370	LUM-2955*	1.05	3.39±0.17	11.47±0.58	2.04±0.13	4.05±0.25	0.34±0.03	4.38±0.26	20 (14)	41.3±1.2	9.4±0.6
		LUM-2956	0.62	3.34±0.17	11.16±0.57	2.03±0.13	3.99±0.25	0.34±0.03	4.33±0.25	8 (8)	27.7±0.4	6.4±0.4
		LUM-2957*	0.35	3.04±0.15	11.46±0.58	1.97±0.13	3.87±0.25	0.34±0.03	4.21±0.25	8 (8)	17.8±0.5	4.2±0.3
W1	2360	LUM-2935*	0.95	3.06±0.15	10.51±0.53	1.93±0.12	3.75±0.24	0.34±0.03	4.09±0.24	16 (15)	19.2±0.7	4.7±0.3
W2	2560	LUM-2952	0.47	2.42±0.04	10.22±0.10	1.69±0.02	3.31±0.20	0.35±0.04	3.66±0.20	10 (10)	295.7±13.2	80.8±5.8
W3	3310	LUM-2953*	0.5	2.96±0.15	10.51±0.54	1.88±0.12	3.67±0.24	0.41±0.04	4.08±0.24	10 (8)	29.8±1.2	7.3±0.5
		LUM-2954	0.3	3.18±0.16	10.72±0.55	1.89±0.12	3.77±0.24	0.41±0.04	4.18±0.25	12 (12)	15.6±0.3	3.7±0.2
W4	2160	LUM-2936*	0.95	3.33±0.04	11.19±0.09	1.96±0.02	3.92±0.23	0.32±0.03	4.25±0.23	10 (9)	23.7±1.0	5.6±0.4

[1] the number of aliquots which were measured and the number of aliquots (inside the brackets) which were used for the final ages calculation after rejection.

* low luminescence intensity

2.1.4 Discussion

2.1.4.1 Dose response curve at high dose range and potential age underestimation

Dose response curves can be generally well fitted either with a linear or a single saturation exponential function. However, an additional linear or a second saturating exponential component with a larger saturation dose, has been often observed for the quartz dose response curve at high dose ranges (e.g. Roberts and Duller; 2004; Lai, 2009; Timar et al., 2010; Lowick et al., 2010a, 2010b; Schmidt et al., 2011; Timar-Gabor et al., 2012; Chapot et al., 2012). Despite some studies reported good agreements between ages derived from the linear growth part and independent age controls (e.g. Murray et al., 2008; Pawley et al., 2008), the additional component in the high dose region has been considered not reliable in producing accurate equivalent dose estimates and resulting in age underestimation. By investigating the performance of the SAR protocol for fine quartz and polyminerals, Wang et al. (2006) reported that fine-grained quartz from the well-known Luochuan site may able to provide reliable equivalent doses up to ~300 Gy. Lu et al. (2007) presented that SAR D_e values begin to underestimate the sensitivity-corrected multiple-aliquot regenerative D_e values from ~120 Gy. Buylaert et al. (2007, 2008) suggested that the application of the SAR-procedure to sand-sized quartz extracted from Chinese loess should be restricted to samples not exceeding ~40-50 ka with corresponding doses below ~120-150 Gy. They demonstrated that older age estimates should probably be regarded only as minimum ages. More recently, by investigation of Romanian loess, Timar et al. (2010) reported that above 200 Gy, despite their quartz characteristics apparently meet all the SAR performance criteria, the age underestimations have been also observed. By comparing the shape of natural and laboratory generated dose response curves for quartz OSL signals from Chinese Loess, Chapot et al. (2012) point out that the continued growth in the high dose range only occurs in the laboratory, not in nature and suggested that maximum limit of OSL dating at the Luochuan section using the SAR protocol on quartz grains is 150 Gy. So far, the underlying mechanisms of the additional linear growth which may relate to age underestimation still remain controversial.

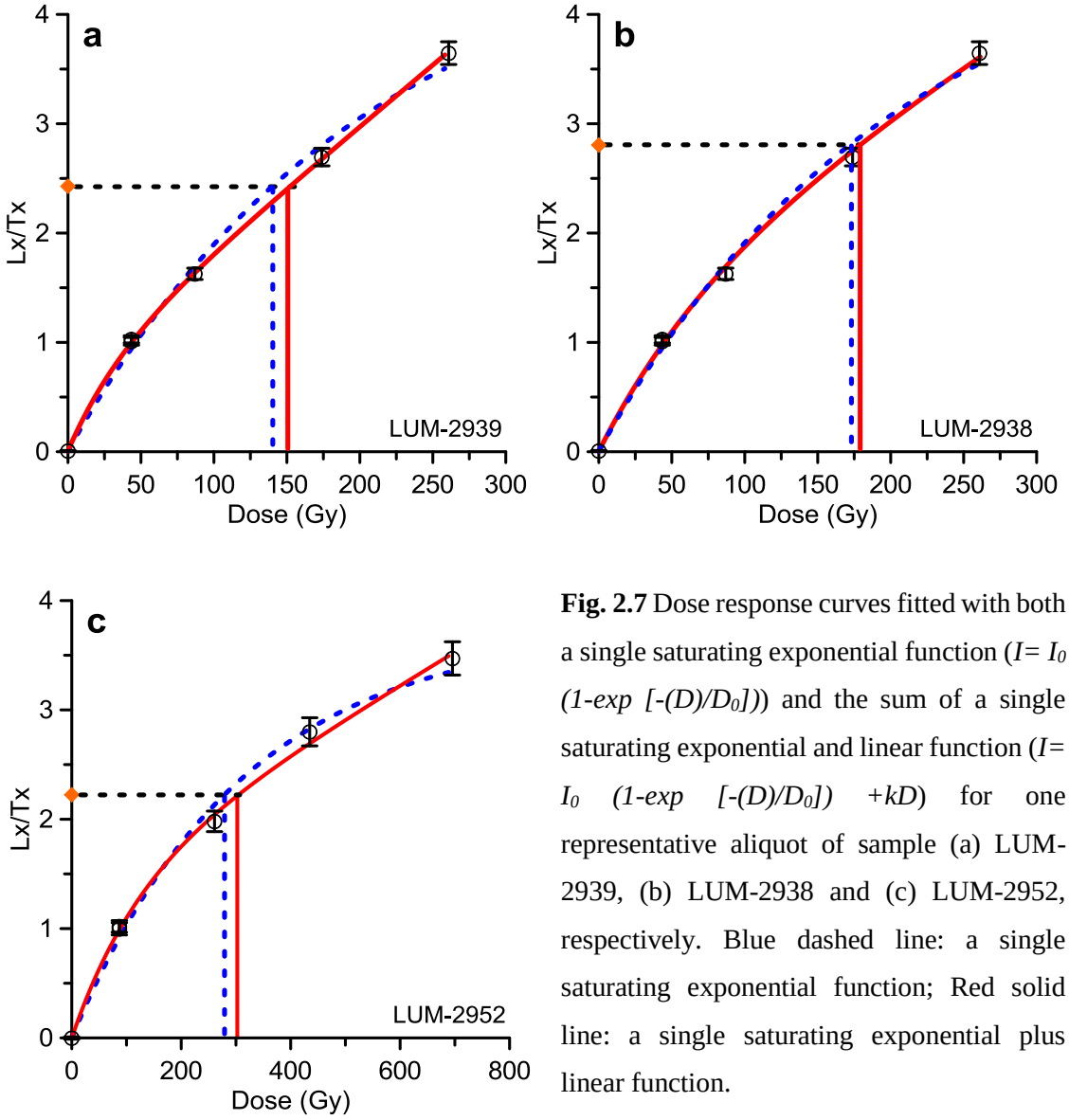

Fig. 2.7 Dose response curves fitted with both a single saturating exponential function ($I= I_0 (1-exp [-(D)/D_0])$) and the sum of a single saturating exponential and linear function ($I= I_0 (1-exp [-(D)/D_0]) +kD$) for one representative aliquot of sample (a) LUM-2939, (b) LUM-2938 and (c) LUM-2952, respectively. Blue dashed line: a single saturating exponential function; Red solid line: a single saturating exponential plus linear function.

In our study, three samples (LUM-2938, LUM-2939 and LUM-2952) yielded D_es above 120 Gy, reaching the critical dose range which is prone to underestimate the true ages according to the previous studies. The performances of the SAR protocol for these samples, such as the recycling ratio, recuperation and dose recovery test generally meet all the criteria set. The dose response curve can be fitted better with a single saturating exponential plus linear function than a single saturating exponential function (Fig. 2.7), especially for sample LUM-2952 when regenerative doses up to 700 Gy have been used. Wintle and Murray (2006) suggested $D_e<2D_0$ as a limit for reliable age estimates and the OSL signal should be about 15 % below the saturation value obtained in the laboratory dose response curve. The 2 D_0 from the exponential fitting part are ~89 Gy, ~108 Gy and ~286 Gy for sample LUM-2939, LUM-2938 and LUM-2952, respectively, which are all

lower than the corresponding natural D_es. This indicates that the natural doses of these samples are obtained by interpolating on a region of the dose response where the first exponential function is already in saturation, i.e. it derived from an additional linear component in the high dose region, which might cause an age underestimation according to the previous studies. Therefore, we should treat these ages cautiously for any further interpretation, especially for sample LUM-2952 which yielded an age of ~81 ka (D_e≈300 Gy). Further studies using feldspar infrared stimulated luminescence for these samples are currently conducted.

2.1.4.2 Timing of loess deposition in Qilian Shan and the adjacent area

Continental loess deposits provide one of the most important archives of climate fluctuations during the Quaternary. These loess-palaeosol sequences have been commonly correlated with the alternating glacial/interglacial climatic changes (Kukla, 1987; Rutter et al., 1991; Liu and Ding, 1993). Previous time-scale constructions of loess-palaeosol sequences mainly adopted proxy-based indirect methods, such as magnetic susceptibility and grain-size spectra, which allowed the investigation of the loess accumulation on the Chinese Loess Plateau throughout the last 2.4 Ma (e.g., Liu, 1985; Kukla, 1987; Kukla and An, 1989), and possibly back to 22 Ma (Guo et al., 2002). In the last decade, OSL dating has been intensively applied to date Chinese loess which has been proved to be a powerful approach to provide reliable and direct numerical chronologies for these loess records (e.g. Wang et al., 2006; Stevens et al. 2006, 2007, 2008; Lu et al. 2007; Buylaert et al., 2007, 2008; Kang et al., 2013). The researches on the OSL dating of Chinese loess have been mainly focused on the loess-palaeosol sequences from the Chinese Loess Plateau. Recently, more OSL ages have been reported concerning the loess accumulation outside the Chinese Loess Plateau in northwestern China (e.g. Stokes et al., 2003; Küster et al., 2006; Sun et al., 2007; Stauch et al., 2012; Chen et al., 2013; Pan et al., 2013; Lehmkuhl et al., 2014; Yang et al., 2014). Loess deposits are commonly observed but unevenly distributed in northwestern China. By reviewing the studies of aeolian sediments on the Tibetan Plateau, Stauch et al. (2012) pointed out that the onset of the loess deposition was restricted to the latest Pleistocene and/or early Holocene and loess sediments which are older than the Last Glacial

Maximum (LGM) have been presented only in few studies. Chen et al. (2013) examined loess sediments covering river banks and/or alluvial fans' surfaces located at the junction between the region of Gansu and Qinghai Provinces, near to the old Aksay town. All the loess sediment in their study are restricted to ages <8 ka as dated by OSL. Among these sites, the Qilian Shan, especially the Hexi Corridor in front of Qilian Shan, plays a very important role for loess deposition in northwestern China owing to its crucial geographic location. It serves not only as a main pathway for the dust transport from the source area to the more open landscape of the western Chinese Loess plateau but also an important source region of the silt deposits on the Chinese Loess Plateau (Derbyshire et al., 1998; Sun, 2002). In the eastern Qilian Shan, the variations of proxies such as the grain size and magnetic susceptibility of the 230 m thick loess-palaeosol sequences are comparable with those from the Chinese Loess Plateau for the past 0.8 Ma (Wu et al., 2005). The loess sediments up to ~35 m covering river terraces in the eastern Qilian Shan have been OSL dated by Pan et al. (2013) to constrain the formation ages of the underlying river terraces. The onset of the loess accumulation has been determined with different ages between 18 ka and 76 ka on seven river terraces. However, in the remote central and western Qilian Shan, the thickness of loess reduced significantly to only few meters (about 2 m in the current study). It is also noteworthy that no intercalated palaeosol layer has been recognized in the loess sequences. By studying loess deposits on a series of river terraces at a site located ~20 km SW of Zhangye City, Stokes et al. (2003) reported the presence of Holocene loess which has yielded OSL ages ranging from ca. 10 ka to the present. The two samples in their study collected from the river terrace sediment underlying the loess were dated to ~50 ka and ~34 ka, respectively, which demonstrated a hiatus between emplacement of the alluvial terrace sediments and the Holocene loess. Küster et al. (2006) investigated the loess sediment in another two river drainages further to the west called Shiyou He and Baiyong He, respectively. Non-reworked loess with a thickness of 0.4-1.5 m overlay the planar surfaces of river terraces. The sand-sized quartz OSL dating generated a series of loess ages ranging from 11.7 ± 1.2 to 4.1 ± 0.4 ka. Although the loess ages from Stokes et al. (2003) have been considered to be underestimated (Küster et al., 2006), both studies suggested that the loess deposits in the central and western Qilian Shan are restricted to the Holocene and/or latest Pleistocene. However, compared to the studies in eastern Qilian Shan as well as on the adjacent Chinese Loess Plateau, a question is therefore raised whether older loess (>~13 ka) exists in the central and western part of Qilian Shan. Our OSL ages show that the loess in the northern piedmont of central

and western Qilian Shan accumulated in the phases from at least ~81 ka till the present which indicate that the loess sedimentation occurred during both the interglacial (Holocene) and glacial period. The last glacial loess has been sporadically and episodically observed (in Section E1 and W2), which are located on alluvial fan terraces. No loess from the global LGM period was found. Since ~9 ka, the loess sediments are widespread till present. The loess ages do not show clear spatial patterns along the SE-NW transect. Unlike in the eastern Qilian Shan and on the Chinese Loess Plateau, post depositional pedogenesis during interglacial period (i.e. Holocene) was not observed indicated by the absence of intercalated palaeosol layers.

The general prerequisites for loess formation include the availability of dust, a wind system for dust transport, favorable conditions (e.g. vegetation cover acting as a dust trap) for dust deposition and the post depositional conservation (e.g. Tsoar and Pye, 1987; Smalley, 1995; Pye, 1995; Lehmkuhl, 1997; Lehmkuhl et al., 2000; Sun, 2002). The Qilian Shan area is strongly dominated by the East Asian Monsoon and the Westerlies. Loess deposition on the Chinese Loess Plateau demonstrates that dust has been transported continuously from northern China to the Chinese Loess Plateau during the entire Quaternary (Derbyshire, et al., 1998). Stokes et al. (2003) deduced that the climate conditions during glacial time were too harsh to favor dust deposition and loess preservation. The tundra grassland vegetation was replaced by desert resulting in insufficient dust trap conditions for the loess accumulation. They also pointed out that the availability of dust might be also reduced because of the presence of large terminal lakes to the north and northeast of the Qilian Shan during marine isotope stage 3 (60-25 ka), and less dust was available from the alluvial fans in the foothill of Qilian Shan during LGM. Küster et al. (2006) attributed the absence of pre-Holocene loess to the combination of low temperatures and high wind speeds which prevented the development of vegetation and resulted in dust bypassing the Qilian Shan through the Hexi Corridor. However, according to our OSL ages, the interpretations and deductions from Stokes et al. (2003) and Küster et al. (2006) suggesting no pre-Holocene loess, have to be questioned. The evidence for loess accumulation at least for the last ~81 ka demonstrates that environmental conditions (e.g. vegetation cover) in the central and western Qilian Shan should have enabled loess sedimentation not only during interglacial time (Holocene) as previously thought but also during the glacial period.

Loess sediment has been used to provide a minimum age control for the underlying fluvial/alluvial terraces (e.g. Chen et al., 2013; Pan et al., 2013). On the contrary, the timing of the underlying geomorphologic/geologic feature or sediment (such as fluvial terraces) constrains the onset of loess deposition. This may result in apparent asynchronous onsets of loess accumulation in comparison of different sections. For example, the bases of loess overlying the alluvial terraces yield different ages of 9.3 ± 0.5 ka, 4.7 ± 0.3 ka and 5.6 ± 0.4 ka from section E5, W1 and W4, respectively. These ages, however, do not necessarily reflect the beginning of a period with suitable conditions for dust trapping (and subsequent loess formation), but may represent the latest stabilization of the geomorphologic setting. In case of W1, loess accumulation was possible after the river incised into the alluvial fan, which reduced runoff on the terrace plains and concentrated in channels. Thus, runoff erosion of dust deposition on terrace surfaces was reduced and allowed constant dust preservation and loess formation. A similar phenomenon has been reported from the eastern Qilian Shan by Pan et al. (2013). In their study, the base of the loess from different terraces of the same river gave distinct OSL ages of 37.4 ± 4.7 ka (T2) and 71.0 ± 6.3 ka (T4) with a difference up to ~34 ka. These terraces have been considered to be formed during the incision of the river which was very likely triggered by the uplift of the Qilian Shan. The loess on the stream bed at the junction region of Gansu and Qinghai Provinces also has multiple onset ages ranging between ~0.8 ka and ~7.4 ka, which has been attributed to the fault slip of Altyn Tagh Fault (Chen et al., 2013). In these two studies, we can see that tectonic movements play crucial roles in the formation of fluvial terraces and consequently constrain the overlying loess accumulation. The discontinuity of the pre-Holocene loess sediments in the central and western Qilian Shan might be not only controlled by climate changes (e.g. vegetation cover, wind systems, etc), as previously debated, but also affected by non-climate factors such as tectonic activities in terms of reshaping the topography and subsequently changing the geomorphology.

2.1.5 Conclusions

Due to the scarcity of data, the understanding of the loess sedimentation in central and western Qilian Shan area has been previously restricted to the Holocene. By applying the

fine-grained quartz OSL dating, 23 loess samples from 11 sections have been dated in this study in order to further investigate the timing and processes of the loess accumulation in central and western Qilian Shan area. The OSL ages are consistent with the stratigraphic order for each section ranging between 3.6±0.2 ka and 80.8±5.8 ka (minimum age), which remarkably extend the chronology of the loess in the Qilian Shan area at least to the late Pleistocene. The Holocene loess is widespread along the northern piedmont of Qilian Shan. The loess sedimentation has been determined to be discontinuous during the late Pleistocene. The favorable environmental conditions could have been available for the loess accumulation during some phase of the glacial period.

Acknowledgements.–The authors would like to thank the Federal Ministry of Education and Research of Germany (BMBF) for funding the field work in the frame of the project "Supra-regional signal pathways and long-time archives: Quaternary monsoon dynamics at the northern margin of the Tibetan Plateau" (03G0814A) as part of the CAME-program. DAAD (Deutscher Akademischer Austauschdienst) is thanked for a PhD scholarship granted to Jingran Zhang. Gudrun Drewes, Sonja Riemenschneider, Sabine Mogwitz and Petra Posimowski (technicians of LIAG-Section S3) are thanked for their technical help during the preparation and measurement of OSL and gamma samples. The ASTER GDEM data used in this study is a product of METI and NASA.

References

An, Z.S., Kukla, G.J., Porter, S.C., Xiao, J.L., 1991. Magnetic Susceptibility Evidence of Monsoon Variation on the Loess Plateau of Central China during the Last 130,000 Years. Quaternary Research 36, 29-36.

Ballarini, M., Wallinga, J., Wintle, A.G., Bos, A.J.J., 2007. A modified SAR protocol for optical dating of individual grains from young quartz samples. Radiation Measurements 42, 360-369.

Banerjee, D., Murray, A.S., Bøtter-Jensen, L., Lang, A., 2001. Equivalent dose estimation using a single aliquot of polymineral fine grains. Radiation Measurements 33, 73-94.

Bourque, C.P.A., Mir, M.A., 2012. Seasonal snow cover in the Qilian Mountains of Northwest China: Its dependence on oasis seasonal evolution and lowland production of water vapour. Journal of Hydrology 454-455, 141-151.

Buylaert, J.P., Vandenberghe, D., Murray, A.S., Huot, S., De Corte, F., Van den haute, P., 2007. Luminescence dating of old (470 ka) Chinese loess: a comparison of single-aliquot OSL and IRSL techniques. Quaternary Geochronology 5, 9-14.

Buylaert, J.P., Murray, A.S., Vandenberghe, D., Vriend, M., De Corte, F., Van den haute, P., 2008. Optical dating of Chinese loess using sand-sized quartz: Establishing a time frame for Late Pleistocene climate changes in the western part of the Chinese Loess Plateau. Quaternary Geochronology 3, 99-113.

Chapot, M.S., Roberts, H.M., Duller, G.A.T., Lai, Z.P., 2012. A comparison of natural- and laboratory-generated dose response curves for quartz optically stimulated luminescence signals from Chinese Loess. Radiation Measurements 47, 1045-1052.

Chen, Y.W., Li, S-H, Sun, J.M., Fu, B.H., 2013. OSL dating of offset streams across the Altyn Tagh Fault: Channel deflection, loess deposition and implication for the slip rate. Tectonophysics 594, 182-194.

Derbyshire, E., Meng, X.M., Kemp, R.A., 1998. Provenance, transport and characteristics of modern aeolian dust in western Gansu Province, China, and interpretation of the Quaternary loess record. Journal of Arid Environments 39, 497-516.

Derbyshire, E., 2001. Characteristics, stratigraphy and chronology of loess and palaeosols, and their application to climatic reconstruction: a preface. Quaternary International 76/77, 1-5.

Duller, G.A.T., 2003. Distinguishing quartz and feldspar in single grain luminescence measurements. Radiation Measurements 37, 161-165.

Fitzsimmons, K.E., Rhodes, E.J., Barrows, T.T., 2010. OSL dating of southeast Australian quartz: a preliminary assessment of luminescence characteristics and behaviour. Quaternary Geochronology 5, 91-95.

Frechen, M., Schweitzer, U., Zander, A., 1996. Improvements in sample preparation for the fine grain technique. Ancient TL 14, 15-17.

Frechen, M., Zander, A., Cílek, V., Ložek, V., 1999. Loess chronology of the Last Interglacial/Glacial cycle in Bohemia and Moravia, Czech Republic. Quaternary Science Reviews 18, 1467-1493.

Guérin, G., Mercier, N., Adamiec, G., 2011. Dose-rate conversion factors: update. Ancient TL 29, 5-8.

Guo, Z.T., Ruddiman, W.F., Hao, Q.Z., Wu, H.B., Qiao, Y.S., Zhu, R.X., Peng, S.Z., Wei, J.J., Yuan, B.Y., Liu, T.S., 2002. Onset of Asian desertification by 22 Myr ago inferred from loess deposits in China. Nature 416, 159-162.

Kang, S. G., Wang, X. L., Lu, Y. C., 2013. Quartz OSL chronology and dust accumulation rate changes since the Last Glacial at Weinan on the southeastern Chinese Loess Plateau. Boreas 42, 815-829.

Kreutzer, S., Fuchs, M., Meszner, S., Faust, D., 2012. OSL chronostratigraphy of a loess-palaeosol sequence in Saxony/Germany using quartz of different grain sizes. Quaternary Geochronology 10, 102-109.

Kukla, G., 1987. Loess stratigraphy in Central China. Quaternary Science Reviews 6, 191-219.

Kukla, G., An, Z.S., 1989. Loess stratigraphy in Central China. Palaeogeography, Palaeoclimatology, Palaeoecology 72, 203-225.

Küster, Y., Hetzel, R., Krbetschek, M., Tao, M., 2006. Holocene loess sedimentation along the Qilian Shan (China): significance for under- standing the processes and timing of loess deposition. Quaternary Science Reviews 25, 114-125.

Lai, Z.P., 2009. Chronology and the upper dating limit for loess samples from Luochuan section in the Chinese Loess Plateau using quartz OSL SAR protocol. Journal of Asian Earth Science 37, 176-185.

Lehmkuhl, F., 1997. The spatial distribution of loess and loess-like sediments in the mountain areas of central and high Asia. Zeitschrift für Geomorphologie N.F. Suppl.-Bd 111, 97-116.

Lehmkuhl, F., Klinge, M., Rees-Jones, J., Rhodes, E. J., 2000. Late Quaternary aeolian sedimentation in central and south-eastern Tibet. Quaternary International 68-71, 117-132.

Lehmkuhl, F., Schulte, P., Zhao, H., Hülle, D., Protze, J., Stauch, G., 2014. Timing and spatial distribution of loess and loess-like sediments in the mountain areas of the northeastern Tibetan Plateau. Catena 117, 23-33.

Li, S.H., Wintle, A.G., 1992. A global view of the stability of luminescence signals from loess. Quaternary Science Reviews 11, 133-137.

Liu, T.S., 1985. Loess and the Environment. China Ocean Press, Beijing.

Liu, T.S., Ding, Z.L., 1993. Stepwise coupling of monsoon circulations to global ice volume variations during the late Cenozoic. Global and Planetary Change 7, 119-130.

Liu, T.S., Ding, Z., 1998. Chinese loess and the paleomonsoon. Annual Review of Earth and Planetary Sciences 26, 111-145.

Lowick, S.E., Preusser, F., Pini, R., Ravazzi, C., 2010a. Underestimation of fine grain quartz OSL dating towards the Eemian: comparison with palynostratigraphy from Azzano Decimo, northeastern Italy. Quaternary Geochronology 5, 583-590.

Lowick, S. E., Preusser, F., Wintle, A.G., 2010b. Investigating quartz optically stimulated luminescence dose-response curves at high doses. Radiation Measurements 45, 975-984.

Lu, Y.C., Wang, X.L., Wintle, A.G., 2007. A new OSL chronology for dust accumulation in the last 130,000 yr for the Chinese Loess Plateau. Quaternary Research 67, 152-160.

Marković, S.B., Timar-Gabor, A., Stevens, T., Hambach, U., Popov, D., Tomić, N., Obreht, I., Jovanović, M., Lehmkuhl, F., Kels, H., Marković, R., Gavrilov, M.B., 2014. Environmental dynamics and luminescence chronology from the Orlovat loess–

palaeosol sequence (Vojvodina, northern Serbia). Journal of Quaternary Science 29, 189-199.

Mejdahl, V., 1979. Thermoluminescence dating: beta attenuation in quartz grains. Achaeometry 21, 61-73.

Meyer, B., Tapponnier, P., Bourjot, L., Metivier, F., Gaudemer, Y., Peltzer, G., Shunmin, G., Zhitai,C., 1998. Crustal thickening in Gansu–Qinghai, lithospheric mantle subduction, and oblique, strike-slip controlled growth of the Tibet Plateau. Geophysical Journal International 135, 1-47.

Murray, A. S., Olley, J. M., 2002. Precision and accuracy in the optically stimulated luminescence dating of sedimentary quartz: a status review. Geochronometria 21, 1-16.

Murray, A. S., Marten, R., Johnston, A., Martin, P., 1987. Analysis for naturally occuring radionuclides at environmental concentrations by gamma spectrometry. Journal of Radioanalytical and Nuclear Chemistry 115, 263-288.

Murray, A.S., Wintle, A.G., 2000. Luminescence dating of quartz using an improved single-aliquot regenerative-dose protocol. Radiation Measurements 32, 57-73.

Murray, A.S., Wintle, A.G., 2003. The single aliquot regeneration dose protocol: potential for improvements in reliability. Radiation Measurements 37, 377-381.

Murray, A., Buylaert, J.P., Henriksen, M., Svendsen, J.I., Mangerud, J., 2008. Testing the reliability of quartz OSL ages beyond the Eemian. Radiation Measurements 43, 776-780.

Nottebaum, V., Lehmkuhl, F., Stauch, G., Hartmann, K., Wünnemann, B., Schimpf, S., Lu, H. 2014. Regional grain size variations in aeolian sediments along the transition between Tibetan highlands and north-western Chinese deserts– the influence of geomorphological settings on aeolian transport pathways. Earth Surfaces Processes and Landforms 39, 1960-1978.

Nottebaum, V., Stauch, G., Hartmann, K., Zhang, J.R., Lehmkuhl, F., 2015. Unmixed loess grain size populations along the northern Qilian Shan (China) – Relationships

between geomorphologic, sedimentologic and climatic controls. Quaternary International 372, 151-166.

Pan, B.T., Hu, X.F., Gao, H.S., Hu, Z.B., Cao, B., Geng, H.P., Li, Q,Y., 2013. Late Quaternary river incision rates and rock uplift pattern of the eastern Qilian Shan Mountain, China. Geomorphology 184, 84-97.

Pawley, S.M., Bailey, R.M., Rose, J., Moorlock, B.S.P., Hamblin, R.J.O., Booth, S.J., Lee, J.R., 2008. Age limits on Middle Pleistocene glacial sediments from OSL dating, north Norfolk, UK. Quaternary Science Reviews 27, 1363-1377.

Pietsch, T.J., Olley, J.M., Nanson, G.C., 2008. Fluvial transport as a natural luminscence sensitiser of quartz. Quaternary Geochronology 3, 365-376.

Prescott, J. R., Hutton, J. T., 1994. Cosmic ray contributions to dose rates for luminescence and ESR dating: large depths and long-term variations. Radiation Measurements 23, 497-500.

Preusser, F., Ramseyer, K., Schlüchter, C., 2006. Characterisation of low OSL intensity quartz from the New Zealand Alps. Radiation Measurements 41, 871-877.

Pye, K., 1995. The nature, origin and accumulation of loess. Quaternary Science Reviews 14, 653-667.

Rees-Jones, J., Tite, M.S., 1997. Optical dating results for British archaeological sediments. Archaeometry 36, 177-187.

Roberts, H.M., Wintle, A.G., 2001. Equivalent dose determinations for polymineralic fine-grains using the SAR protocol: application to a Holocene sequence of the Chinese Loess Plateau. Quaternary Science Reviews 20, 859-863.

Roberts, H.M., Duller, G.A.T., 2004. Standardised growth curves for optical dating of sediment using multiple-grain aliquots. Radiation Measurements 38, 241-252.

Roberts, H.M., 2006. Optical dating of coarse-silt sized quartz from loess: Evaluation of equivalent dose determinations and SAR procedural checks. Radiation Measurements 41, 923-929.

Rutter, N., Ding, Z.L., Evans, M.E., Liu, T.S., 1991. Baoji-type pedostratigraphic section, Loess Plateau, north-central China. Quaternary Science Reviews 10, 1-22.

Schatz, A.K., Buylaert, J.P., Murray, A., Stevens, T., Scholten, T., 2012. Establishing a luminescence chronology for a palaeosol-loess profile at Tokaj (Hungary): A comparison of quartz OSL and polymineral IRSL signals. Quaternary Geochronology 10, 68-74.

Schmidt, E.D., Frechen, M., Murray, A.S., Tsukamoto, S., Bittmann, F., 2011. Luminescence chronology of the loess record from the Tonchesberg section: a comparison of using quartz and feldspar as dosimeter to extend the age range beyond the Eemian. Quaternary International 234, 10-22.

Singhvi, A.K., Bluszcz, A., Bateman, P., Someshwar Rao, M., 2001. Luminescence dating of loess–palaeosol sequences and coversands: methodological aspects and palaeoclimatic implications. Earth Science Reviews 54, 193-211.

Smalley, I., 1995. Making the material: the formation of silt-sized primary mineral particles for loess deposits. Quaternary Science Reviews 14, 645-651.

Song, Y.G., Fang, X.M., King, J.W., Li, J.J., Naoto, I., An, Z.S., 2014. Magnetic parameter variations in the Chaona loess/paleosol sequences in the central Chinese Loess Plateau, and their significance for the middle Pleistocene climate transition. Quaternary Research 81, 433-444.

Stauch, G., IJmker, J., Pötsch, S., Zhai, H., Hilgers, A., Diekmann, B., Dietze, E., Hartmann, K., Opitz, S., Wünnemann, B., Lehmkuhl, F., 2012. Aeolian sediments on the north-eastern Tibetan Plateau. Quaternary Science Reviews 57, 71-84.

Stevens, T., Armitage, S.J., Lu, H.Y., Thomas, D.S.G., 2006. Sedimentation and diagenesis of Chinese loess: implications for the preservation of continuous, high-resolution climate records. Geology 34, 849-852.

Stevens, T., Thomas, D.S.G., Armitage, S.J., Lunn, H.R., Lu, H., 2007. Reinterpreting climate proxy records from late Quaternary Chinese loess: a detailed OSL investigation. Earth-Science Reviews 80, 111-136.

Stevens, T., Lu, H.Y., Thomas, D.S.G., Armitage, S.J., 2008. Optical dating of abrupt shifts in the late Pleistocene East Asian monsoon. Geology 36, 415-418.

Stokes, S., Hetzel, R., Bailey, R.M., Tao, M., 2003. Combined IRSL-OSL single aliquot regeneration (SAR) equivalent dose (D_e) estimates from source proximal Chinese loess. Quaternary Science Reviews 22, 975-983.

Sun, J.M., 2002. Provenance of loess material and formation of loess deposits on the Chinese Loess Plateau. Earth and Planetary Science Letters 203, 845-859.

Sun, J.M., Li, S.H., Muhs, D.R., Li, B., 2007. Loess sedimentation in Tibet: provenance, processes, and link with Quaternary glaciations. Quaternary Science Reviews 26, 2265-2280.

Ta, W., Xiao, H., Qu, J., Xiao, Z., Yang, G., Wang, T., Zhang, X., 2004. Measurements of dust deposition in Gansu Province, China, 1986-2000. Geomorphology 57, 41-51.

Tsoar, H., Pye, K., 1987. Dust transport and the question of desert loess formation. Sedimentology 34, 139-153.

Thiel, C., Buylaert, J. P., Murray, A., Terhorst, B., Hofer, I., Tsukamoto, S., Frechen, M. 2011. Luminescence dating of the Stratzing loess profile (Austria)-Testing the potential of an elevated temperature post-IR IRSL protocol. Quaternary International 234, 23-31.

Timar, A., Vandenberghe, D., Panaiotu, E.C., Panaiotu, C.G., Necula, C., Cosma, C., van den haute, P., 2010. Optical dating of Romanian loess using fine-grained quartz. Quaternary Geochronology 5, 143-148.

Timar-Gabor, A., Vasiliniuc, S., Vandenberghe, D.A.G., Cosma, C., Wintle, A.G., 2012. Investigations into the reliability of SAR-OSL equivalent doses obtained for quartz samples displaying dose response curves with more than one component. Radiation Measurements 47, 740-745.

Wang, X.L., Lu, Y.C., Zhao, H., 2006. On the performances of the single- aliquot regenerative-dose (SAR) protocol for Chinese loess: fine quartz and polymineral grains. Radiation Measurements 41, 1-8.

Wang, Z., 1981. Glacier Inventory of China: Qilian Mountains. Lanzhou Institute of Glaciaology and Geocryology, Chinese Academy of Sciences, 78-79.

Wintle, A.G., Murray, A.S., 2006. A review of quartz optically stimulated luminescence characteristics and their relevance in single-aliquot regeneraton dating protocols. Radiation Measurements 41, 369-391.

Wu, G.J., Pan, B.T., Li, J.J., Guan, Q.Y., Liu, Z.G., 2001. Tectonic-climatic events in eastern Qilian Mountains over the past 0.83 Ma. Science in China (Series D) 44, 251-260.

Wu, G.J., Pan, B.T., Guan, Q.Y., Liu, Z.G., Li, J.J., 2002. Loess record of climatic changes during MIS5 in the Hexi Corridor, northwest China. Quaternary International 97/98, 167-172.

Wu, G.J., Pan, B.T., Guan, Q.Y., Xia, D.S., 2005. Terminations and their correlation with solar insolation in the Northern Hemisphere: a record from a loess section in Northwest China. Palaeogeography, Palaeoclimatology, Palaeoecology 216, 267-277.

Yang, S.L., Forman, S.L., Song, Y.G., Pierson, J., Mazzocco, J., Li, X.X., Shi, Z.T., Fang, X.M., 2014. Evaluating OSL-SAR protocols for dating quartz grains from the loess in Ili Basin, Central Asia. Quaternary Geochronology 20, 78-88.

Zhou, L.P., Dodonov, A.E., Shackleton, N.J., 1995. Thermoluminescence dating of the Orkutsay loess section in Tashkent region, Uzbekistan, Central Asia. Quaternary Science Reviews 14, 721-730.

Chapter 3 Late Quaternary sedimentary processes in German North Sea coast

3.1 OSL and ^{14}C chronologies of a Holocene sedimentary record (Garding-2 core) from the German North Sea coast

Jingran Zhang[1], Sumiko Tsukamoto[1], Alf Grube[2], Manfred Frechen[1]

[1] Leibniz Institute for Applied Geophysics (LIAG), S3: Geochronology and Isotope Hydrology, Stilleweg 2, 30655 Hannover, Germany

[2] State Agency for Agriculture, Environment and Rural Areas (LLUR) of the Federal State Schleswig-Holstein, Geological survey, Hamburger Chaussee 25, 24220 Flintbeck, Germany

Boreas, Vol. 43, pp. 856–868.

DOI: http://onlinelibrary.wiley.com/doi/10.1111/bor.12071/abstract

Abstract

The history of sea level change and sediment accumulation since the last deglaciation along the German North Sea coast is still controversial due to a limitation in quantity and quality of chronological data. In the current study, the chronology of a 16 ka coastal sedimentary record from the Garding-2 core, retrieved from the Eiderstedt Peninsula in Schleswig-Holstein northern Germany, is established using OSL and AMS ^{14}C dating techniques. The robust chronology using 14 radiocarbon and 25 OSL dates from Garding-2 core is the first long-term record which covers the Holocene as well as the last deglaciation period in one succession in the German North Sea area. It provides a new insight into understanding the Holocene transgression and coastal accumulation histories. The combined evidence from the sedimentology and chronology investigations indicates that an estuarine environment dominated in Eiderstedt Peninsula from 16 ka to 13 ka, followed by a depositional hiatus between 13 ka and 8.3 ka, attributed to erosion caused by the Holocene transgression; the onset of the Holocene transgression at the core site occurred at around 8.3 ka. The sea level continued to rise with a decelerated rate until around 3 ka. Since 3 ka, the shoreline has begun to prograde. Foreshore (tidal flat)

sediments have been deposited at the drilling site with a very high sedimentation rate of about 10 m ka^{-1}. At around 2 ka, a sandy beach deposit accumulated in the sedimentary succession, indicating that the coastline shifted landward, which may represent a small scale transgression in the late Holocene. At around 1.5 ka, terrestrial clastic sediment started to accumulate, indicating a retreat of the relative sea level in this area, which may be related to local diking activities undertook since the 11th century.

Key word: German North Sea, OSL dating, ^{14}C dating, Coastal sedimentology, Holocene transgression

3.1.1 Introduction

Since the last century, numerous studies have been carried out in the North Sea coastal area to reconstruct past sedimentary processes, palaeoclimatic conditions, and eustatic and glacio-isostatic movement histories (e.g. Dittmer 1952; Cameron et al. 1993; Denys & Baeteman 1995; Roe 1999; Shennan et al. 2000; Kiden et al. 2002; Behre 2003, 2007; Hoffman 2004; Streif 2004; Gehrels et al. 2006; Vink et al. 2007; Bungenstock & Weerts 2010; Alappat et al. 2010; Baeteman et al. 2011). The German sector of North Sea coastline has long been regarded as isostatically stable and hence ideal for studies on eustatic sea-level curves (Behre 2003, 2007). Based on this assumption, Behre (2003, 2007) reconstructed two sea level curves for the entire German North Sea coast using the published data available at the time, which show strong fluctuations in the sea level change especially during the late Holocene. Some recent studies show that the whole of northwest Europe may have been influenced by post-glacial isostatic movements associated with the melting of the northern European ice sheets (Vink et al. 2007 and the references therein). By comparing sea level curves from other areas in the southern North Sea, e.g. Belgium and the Netherlands, it has been demonstrated that relevant isostatic movements along the German coast existed (Kiden et al. 2002; Vink et al. 2007; Bungenstock & Weerts 2010). Therefore, debates and discussions persist about the pattern of the Holocene sea level changes in the German sector of the North Sea. The histories of the Holocene sea level change and the sediment accumulation along the German North Sea coast are currently still controversial due to the scarcity of field data. The chronologies that have been used in the existing studies for the coastal sediment

succession and sea level curve reconstruction in the German North Sea area were mainly based on conventional ^{14}C dating of bulk samples (e.g. peat), mostly derived from the coastal hinterland for the purpose of geological mapping and archaeological investigation (Streif 2004; Baeteman et al. 2011). It is considered that peat layers are widespread in the German North Sea basin, and these have also been used as an indicator of sea-level changes. However, due to the transgression and intensive tidal erosion, peat layers are often absent or reworked. The relationships between the peat formation and the sea-level change are complex and still open to alternative interpretations (Vink et al. 2007; Baeteman et al. 2011). Furthermore, conventional ^{14}C dating of peat using bulk samples was often problematic and lacked precision, because of contamination by older carbon (Törnqvist et al. 1998), the erosion and reworking of peat layer (Waller et al. 2006), etc. Thus, new dating technique and more dates are needed for setting up reliable and robust chronologies in the North Sea area, especially for reconstructing long continuous sedimentary records.

In the last few decades, optically stimulated luminescence (OSL) dating has been successfully applied to coastal deposits in numerous studies (e.g. Murray-Wallace et al. 2002; Madsen et al. 2005; Nielsen et al. 2006; Boomer & Horton 2006; Lopez & Rink 2007; Roberts & Plater 2007; Jacobs 2008; Mauz et al. 2010; Alappat et al. 2010; Reimann et al. 2012) and has been proven to be a powerful and reliable dating technique. OSL dating has the potential to provide numerical dates of the depositional event itself, with uncertainties of ~5-10%, and can date back up to ~100-200 ka (Murray & Olley 2002), far beyond the upper limit of ^{14}C dating. Furthermore, in contrast to the ^{14}C technique, the main material used for OSL dating is quartz, which is dominant in coastal deposits. Recently, OSL dating using quartz has been successfully applied to coastal sediments from the North Sea area. Madsen et al. (2005, 2007a, b, 2010, 2011) presented a series of OSL ages from the Danish sector of the North Sea, with most of the results generated from young Wadden Sea sediments and/or estuarine deposits along the Danish sector of North Sea coast. Mauz & Bungenstock (2007) showed that OSL dating of tidal flat deposits can be used to reconstruct the late Holocene relative sea level changes. Mauz et al. (2010) further tested the bleaching status and the reliability of OSL dating of tidal sediments from the North Sea coast. The authors demonstrated that more than 85% of their samples yielded accurate ages, although partial-bleaching existed in the tidal deposits. Alappat et al. (2010) applied OSL dating to the Late Weichselian and early

Holocene sediments from seven cores which were derived from the shallow continental shelf in the southern North Sea area. Although all samples from their study showed significant heterogeneous bleaching from the glaciofluvial origin, it was possible to establish a reliable OSL chronology, which was in agreement with the independent age control when the minimum age model (MAM) (Galbraith et al. 1999) was employed. More recently, Reimann et al. (2012) and Costas et al. (2012) successfully dated young coastal sediments from the southern North Sea island of Sylt in northern Germany. To obtain a comprehensive record of the Quaternary sediment succession, a drilling project was carried out in 2011 and retrieved a 240 m long deep terrestrial sediment core (Garding-2 core) from the Eiderstedt Peninsula in Schleswig-Holstein, northern Germany. The aim of the present study is to reconstruct the sediment accumulation processes and Holocene transgression history in the coastal area of the German North Sea since the last deglaciation employing high-resolution OSL and Accelerator Mass Spectrometry (AMS) ^{14}C dating techniques.

3.1.2 Geological setting and core description

The general outline of the North Sea Basin was formed at the end of the (Miocene) Tertiary, when the sea began to retreat from the European mainland and two main river systems developed (Streif 2004). The North Sea is bounded by the Orkney Islands to the north, east coasts of England and Scotland to the west and the northern and central European mainland to the east and south, including Norway, Denmark, Germany, the Netherlands, Belgium, and France. The German North Sea sector (Fig. 3.1) extends between 53° and 56°N, and 3° and 9°E. For most of the Quaternary period, the German North Sea sector and its coastal areas were above sea level.

The local present-day landscape and coastline are controlled by the relief of the surface which was formed during different periods of the Pleistocene and the Holocene sea level variations in addition to the anthropogenic influences (e.g. diking, drainage of marshes, peat cutting) (Hoffmann 2004). The sedimentary record along the German North Sea coast is characterized by a Holocene wedge-like sediment body resting on top of Pleistocene sediments. The Holocene standard sediments consist of a basal peat bed covered by fine-grained sandy, silty and clayey brackish and marine deposits with

intercalated peat beds. Due to subsequent phases of erosion and re-deposition of the original sedimentary successions, only a fragmentary sedimentary record is preserved (Streif 2004).

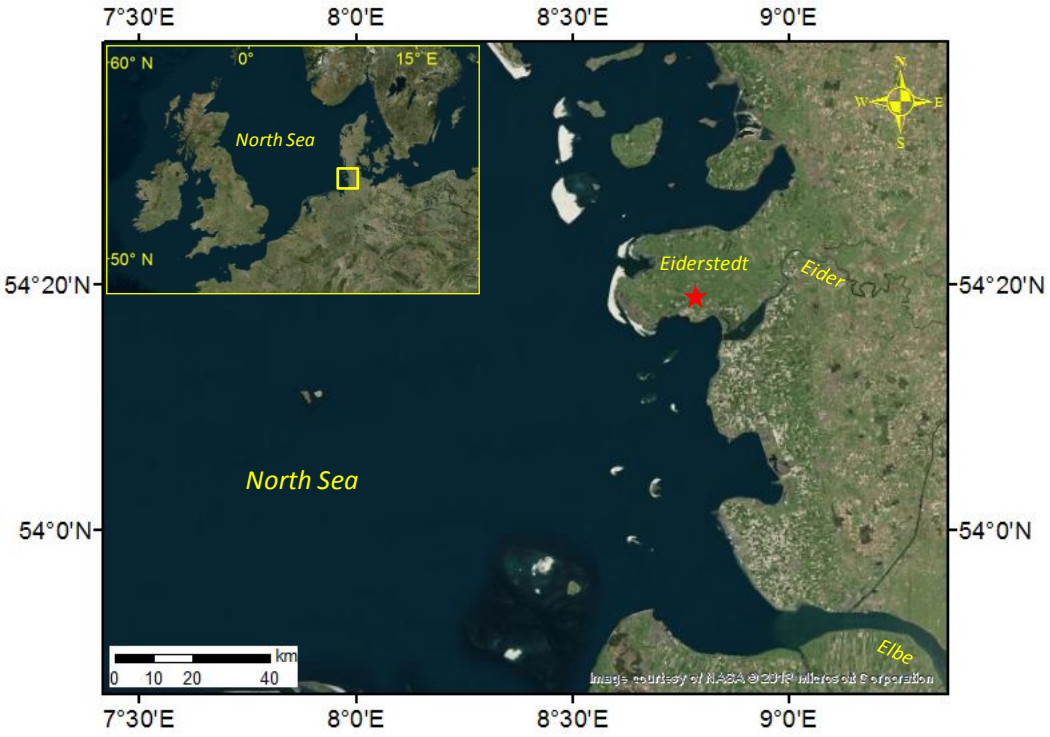

Fig. 3.1 A satellite image of the North Sea area (Google Earth). The red star shows the location of the Garding-2 borehole.

The Garding-2 core (54°18’13.74”N, 08°46’35.22”E) was taken from the southern part of the Eiderstedt Peninsula in Schleswig-Holstein, which is ~4 km inland from the present-day coastline and ~7 km northwest of the River Eider estuary. The elevation of the borehole position is close to the modern sea level and the tidal range is ~3.8 m. The uppermost 26 m of the Garding-2 core sediments show several sedimentary facies (Fig. 3.2) and can be divided into six main units. The subdivision of the coastal sedimentary facies refers to the “foreshore-shoreface-offshore” model of Walker and Plint (1992). The basal peat and other peat layers or fossil vegetation horizons are absent in the investigated sedimentary succession. The uppermost 1 m of the core was missing in Fig. 3.2 as it was abandoned due to contamination and exposure to sunlight. From 1 to 2 m the sediment core consists of brownish terrestrial clastic deposit (Unit 1) and between 2 and 6 m (Unit 2) there is shoreface deposit consisting of grayish fine to medium sand. At the depth from

4.5 to 4.9 m there is a ~0.4 m thick grey silty sand layer with abundant whole mollusk shells. These well preserved shells indicate a slack water environment, which may be considered as tidal creek/channel sediment. From 6 to 16 m, shell-bearing greyish silt alternating with sand layers was found (Unit 3). The deposit of this unit is stratified into fine laminae, which is considered as a typical tidal flat deposit. Dark coloured organic-rich lenses are often found in the sediment from 10 to 15 m, which can also be found in the modern tidal flat sediments. Between 16 and 19.30 m, offshore sediment deposits exist, consisting of grey to brown clayish silt (Unit 4). From 19.30 to 19.85 m (Unit 5), a mollusk shell-rich, fine sand forms an unconformity overlying the lower sand deposits. Most of the mollusk shells were broken into fragments indicating a strong water energy environment. From 19.85 to 26 m, the sediment is composed of well-sorted light greyish medium to coarse grained sand indicating an estuarine sedimentary environment (Unit 6).

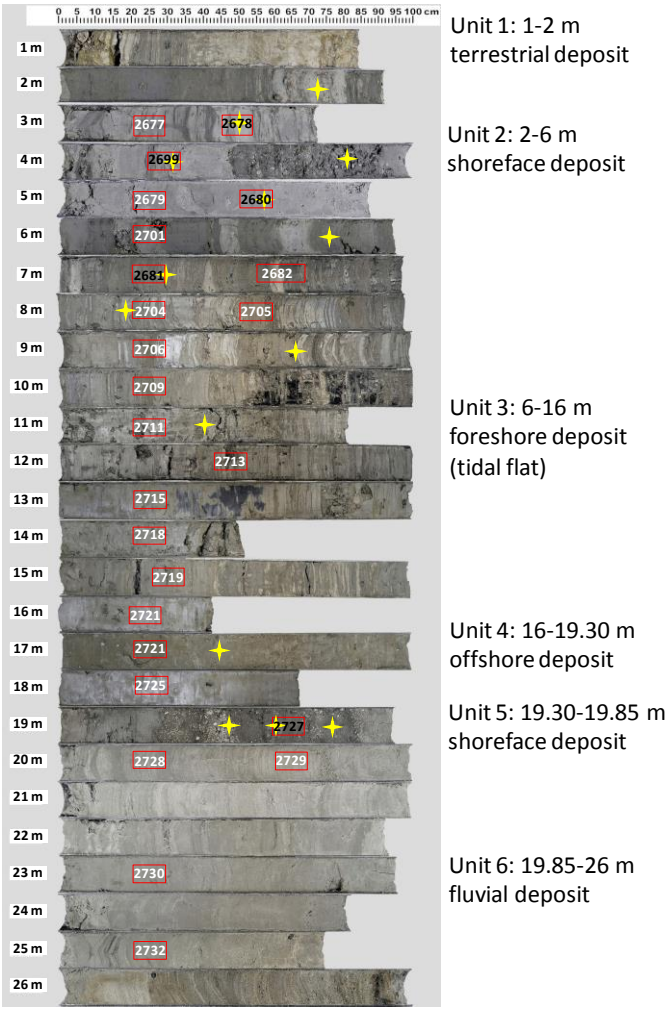

Fig. 3.2 A photograph of the core with the locations of the sedimentary units. The red boxes and yellow stars show the sampling sites for OSL and radiocarbon dating, respectively.

3.1.3 Methods

3.1.3.1 Sampling

The core samples were split lengthwise into two parts, and one half was immediately packed in opaque black plastic bags. The sampling for OSL dating was conducted under subdued red light laboratory conditions. For OSL sampling, ~2 cm from the cutting surface and the ~1 cm close to the inner wall of the tube were removed to avoid possible contamination of bleached grains and/or disturbances during drilling and transportation. 25 OSL samples and 14 radiocarbon samples were collected from the uppermost 26 m of the Garding-2 sediment core. No OSL samples were taken from the uppermost 3 m of the core due to a light exposure after cutting. The depths of the OSL (including laboratory codes) and ^{14}C samples are shown in Fig. 3.2.

3.1.3.2 OSL sample preparation

The materials were first dry-sieved to extract grains of either 100−150 μm or 150−200 μm in diameter. The extracted fractions were treated with 10% hydrochloric acid (HCl) and 30% hydrogen peroxide (H_2O_2) to remove the carbonate and the organic matter, respectively. Sodium oxalate ($Na_2C_2O_4$) was used to disperse aggregates. The quartz-rich fraction (2.62−2.70 g cm^{-3}) was separated using heavy liquid density separation with sodium polytungstate solution. The quartz fraction was then treated with 40% hydrofluoric acid (HF) for ~60 min to remove feldspar contamination and the outer layer of the quartz grains i.e. to dissolve the alpha-irradiated surface. After the HF etching, the quartz grains were sieved again with 100 μm or 150 μm mesh to remove smaller grains. Several aliquots for each sample were used to check feldspar contamination in the quartz fraction, and no obvious IRSL signals were observed for any of the samples. The quartz grains were then mounted on stainless steel discs as a monolayer using silicon spray.

3.1.3.3 Dose rate determination

High-resolution gamma spectrometry was used to measure the radioactivity of ^{40}K, U, Th and their daughter nuclides and to calculate the dose rates of the samples in this study. The samples were dried at 130°C, homogenized and filled into 50 g plastic containers for gamma spectrometry measurements. The prepared samples were sealed air tight and stored for at least one month to gain ^{226}Ra-^{222}Rn equilibrium condition before measuring on the high-resolution gamma spectrometer (Murray et al. 1987). Each sample was measured for 3−4 days.

The activities of ^{234}Th, ^{214}Pb, ^{214}Bi and ^{210}Pb from the U-series decay chain, and ^{228}Ac, ^{212}Pb and ^{208}Tl for Th-series, and ^{40}K have been determined. The dose rate conversion factors of Guérin et al. (2011) and beta attenuation factors of Mejdahl (1979) were applied for dose rate calculation. The contribution of alpha radiation was not taken into account because the outer layer of the coarse-grained quartz has been removed by HF etching. The cosmic dose rate was derived from the altitude and latitude of the sampling site, the burial depth and the density of the overlying sediment (Prescott and Stephan 1982; Prescott and Hutton 1994).

3.1.3.4 Equivalent dose measurements

An automated Risø TL/OSL DA15 reader with attached ^{90}Sr/^{90}Y beta source was used for the OSL measurements. The quartz OSL signal was stimulated with blue light emitting diodes (LED) of 470 ± 30 nm and a Hoya U-340 (7.5 mm) filter was used for detection. The OSL measurements were conducted either using medium-sized (6 mm) aliquots containing ~1000 grains or small-sized (2.5 mm) aliquots with ~80-150 grains. The single aliquot regenerative dose (SAR) protocol (Murray and Wintle 2000; Wintle and Murray 2006) was applied for equivalent dose (D_e) measurements. In order to select a suitable preheat temperature for the SAR protocol, a set of tests (i.e. preheat plateau, dose recovery and thermal transfer tests) were applied to two representative samples prior to dating (LUM-2679 and LUM-2728). For thermal transfer tests, a group of 24 medium-sized aliquots were bleached twice with 300 s blue stimulation at room temperature (a pause of >5000 s in between), before measuring with different temperature preheats ranging

from 160°C to 260°C at 20°C increments with a fixed low temperature cut heat at 160°C. For dose recovery tests, aliquots were first bleached in the same manner as in the thermal transfer tests. Then a known laboratory beta dose, which was approximately equal to the natural dose, was given to all bleached aliquots. The SAR measurements were subsequently applied to the laboratory irradiated aliquots using the same six different preheat temperatures as above. For preheat plateau tests, the natural D_e was measured from a suite of 24 fresh aliquots using an identical SAR protocol at the six different preheat temperatures with a cutheat of 160°C. Four aliquots at each preheat temperature were analyzed for the tests mentioned above.

D_e values were obtained from between 18 and 50 medium-sized aliquots for each sample. The acceptance criteria of the D_e by Alappat et al. (2010) were adopted in this study. The distribution of D_e values using both medium-sized aliquots (6 mm) and small-sized aliquots (2.5 mm) for two representative samples were compared to check whether the OSL signals had been well-bleached at deposition.

3.1.3.5 AMS ^{14}C dating

Fourteen radiocarbon samples (13 mollusk shells and one wood fragment) were extracted from the core sediments. The measurements were performed by AMS ^{14}C dating at the Leibniz Laboratory of Kiel University. The samples were first checked under a microscope and an appropriate amount of material was selected for dating. To remove adhering dust and detrital carbonate as well as organic surface coating, the mollusk shell samples were first cleaned with 30% H_2O_2 in an ultrasonic bath, followed by a second cleaning step of 15% H_2O_2, also in an ultrasonic bath. The sample CO_2 was liberated from each sample with 100% phosphoric acid at 90°C and was then reduced with H_2 over about 2 mg of Fe powder as a catalyst, and the resulting carbon/iron mixture was pressed into a pellet in the target holder. For the wood sample (14C-07), the selected material was extracted with 1% HCl, 1% NaOH, each at 60°C, and again 1% HCl to remove any alkaline residue. The combustion to CO_2 was performed in a closed quartz tube together with CuO and silver wool at 900°C. The measured ^{14}C ages were calibrated with the Marine09 calibration curve (Reimer et al. 2009) using the CALIB Radiocarbon Calibration Program 6.1.0 (Stuiver and Reimer 1993). After calibration, all ages were

converted to the format of thousand years before 2012 (ka) in order to directly compare them with the OSL ages.

3.1.4 Results

3.1.4.1 OSL characteristics

Fig. 3.3 shows the results obtained from the tests performed for LUM-2679 and LUM-2728 from the depths of 5.2−5.3 m and 20.2−20.3 m, respectively. Each data point is the mean obtained from four medium-sized aliquots (6 mm) and the given uncertainty is based on 1σ standard error. For LUM-2679, the result of the preheat plateau test (Fig. 3.3a) suggests that the dose measurement is insensitive to preheat temperature. The dose recovery ratios are close to unity at all preheat temperatures. No thermal transfer is detected for preheats between 160 and 220 °C. However, the thermal transfer slightly increased for the preheats of 240 and 260 °C, but remained less than 0.1 Gy, which is less than 5% of the D_e value for this sample. Although the mean dose recovery ratio at all temperatures are within 10% from the unity for sample LUM-2728 (Fig. 3.3b), the measured dose/given dose ratios decrease towards higher preheat temperatures. Also, the thermal transfer is close to zero for all preheat temperatures; thus, based on these results, a combination of 200 °C preheat (10 s) and a 160 °C cutheat was chosen for all SAR measurements in this study. For each sample six to eight aliquots were used for dose recovery test using the selected preheat and cut heat condition. Fig. 3.3c presents a summary histogram of all the dose recovery ratios (measured/given dose) with a mean of 1.02 ± 0.01, which is within the range of acceptability of 0.9−1.1 suggested by (Wintle and Murray 2006). The mean recycling ratio generated from each sample's D_e measurements (inset) is 1.008 ± 0.003.

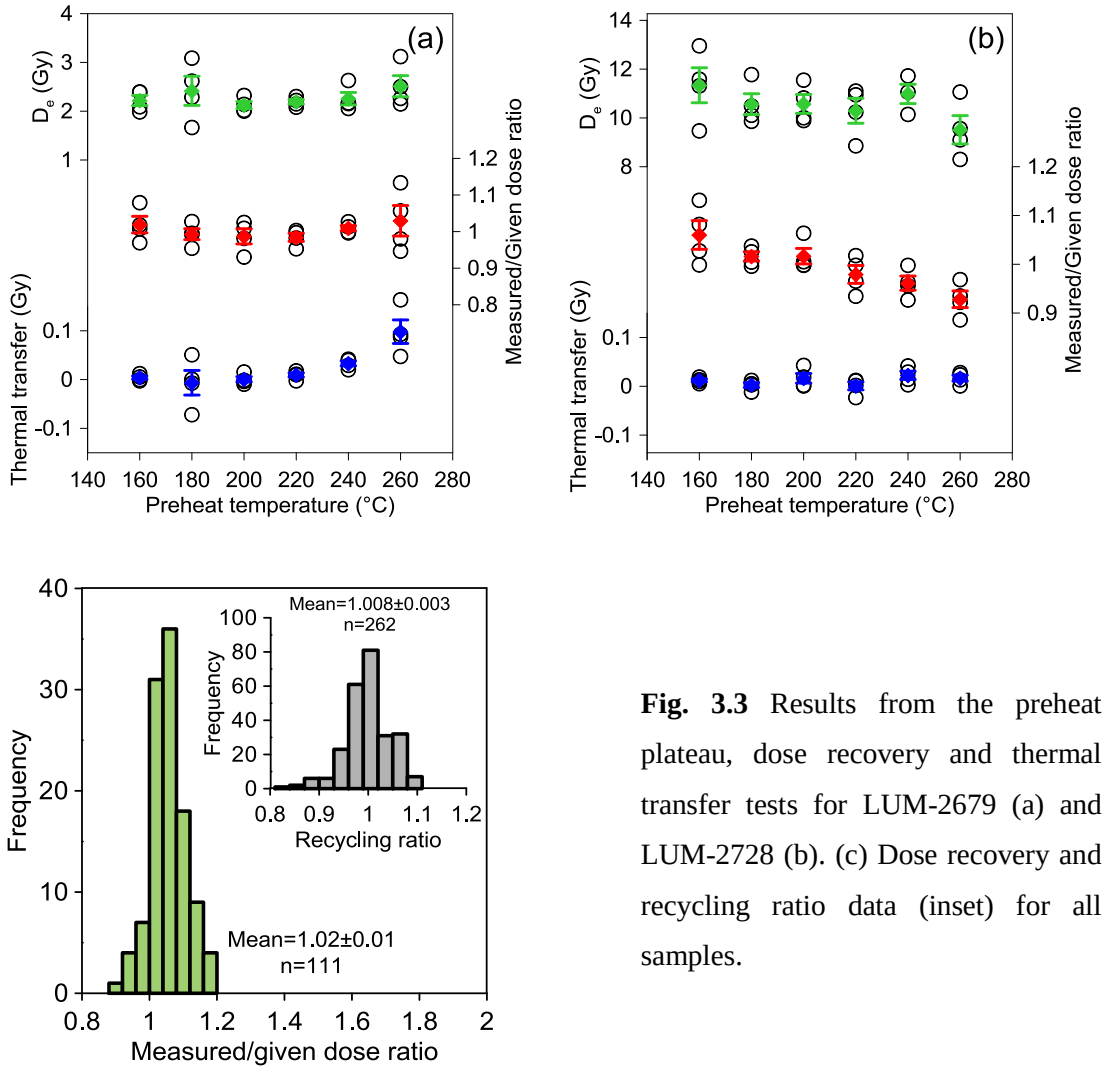

Fig. 3.3 Results from the preheat plateau, dose recovery and thermal transfer tests for LUM-2679 (a) and LUM-2728 (b). (c) Dose recovery and recycling ratio data (inset) for all samples.

Based on the fact that insufficiently bleached sediment contains a mixture of grains with differential bleaching (Duller 1994), the scatter of the D_e derived from single aliquot measurements has the potential to detect incomplete bleaching (Li 1994; Clarke 1996). Small aliquots contain fewer grains than medium aliquots so they are less influenced by averaging effects, therefore small aliquots are better to identify sediments which contain grains that were not well-bleached before burial (Olley et al. 1999). In order to check if our samples have problems with partial bleaching, samples LUM-2678 and LUM-2728 were measured using both medium aliquot and small aliquots (the latter contains 80-150 grains on each aliquot). The D_e distributions of both medium and small aliquots for the two samples are shown as histograms in Fig. 3.4.

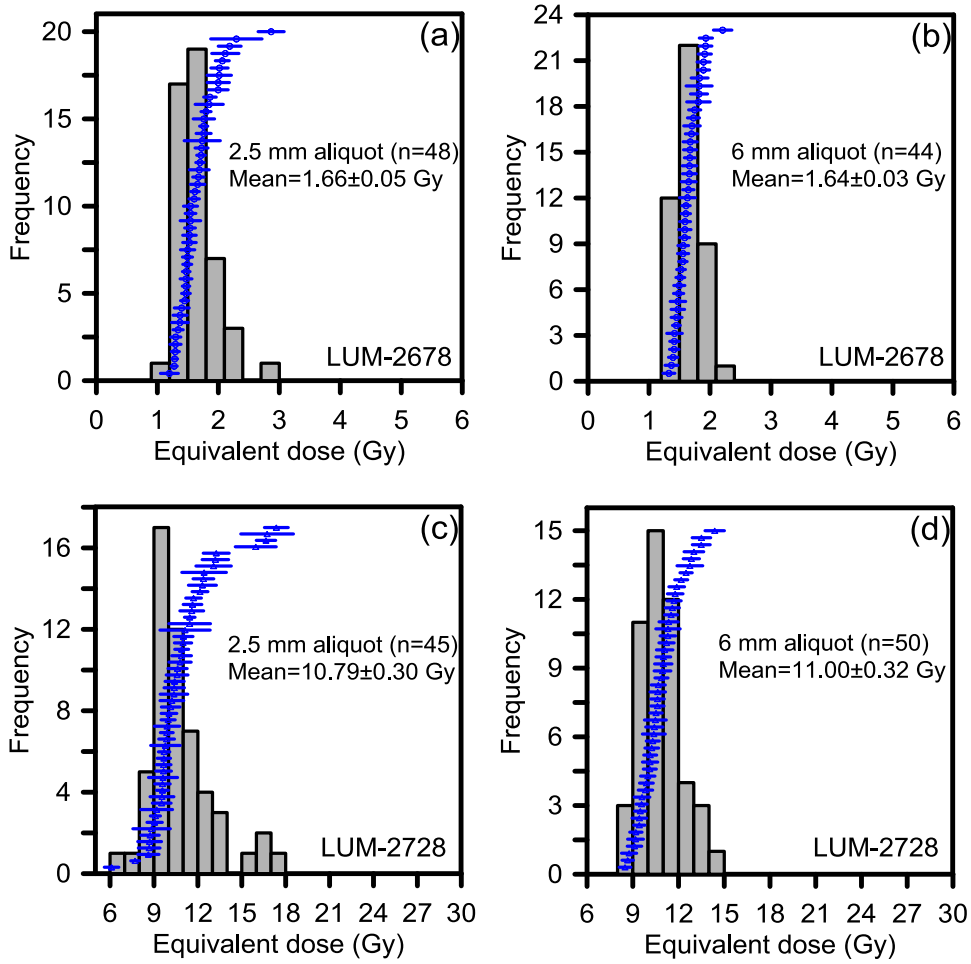

Fig. 3.4 The D_e distributions for medium and small aliquots of samples (a) LUM-2678 and (b) LUM-2728.

The D_e values show tight normal Gaussian distributions for both aliquot sizes, which also yielded nearly the same D_e values within the uncertainties. This suggests that the sediment was sufficiently bleached prior to deposition (e.g. Olley et al. 1998; Fuchs and Wagner 2003) and both medium and small aliquots were capable to derive reliable burial ages of the sediment. However, the signals from the small-sized aliquots are rather dim, thus all samples were measured with 6 mm diameter medium aliquots. The D_e values were calculated by the mean and the uncertainty was given by 1σ standard error.

3.1.4.2 Dosimetry

The activities of ^{226}Ra (from ^{214}Pb and ^{214}Bi from ^{238}U series), ^{232}Th, ^{40}K and the dose rate data for all samples are plotted in Fig. 3.5, together with the observed water contents and the D_e values. The variation in absolute concentrations of ^{226}Ra and ^{232}Th are very similar to one another as well as those of ^{40}K, with no systematic trends apparent with depth. The ratios of ^{226}Ra/^{232}Th and ^{40}K/^{232}Th show that there is no systematic decrease with depth, suggesting there is no ^{230}Th excess (Sugisaki et al. 2012). The ^{226}Ra and ^{232}Th activities and the water content are relatively high from 10 to 16 m depth, i.e. the tidal flat deposit.

The dose rate is affected by the water content of the sediments owing to the dose absorption by water (Aitken 1985). As water content of coastal sediments could be variable through time because of dewatering and compaction, it is difficult to accurately evaluate the water content. Recently, Sugisaki et al. (2012) compared ages derived from observed water contents and modeled water contents, considering the dewatering effects to assess the water content variability with time for OSL age calculation. Their ages calculated with the observed water content lie closest to the independent ages, rather than those from the modelled water content. Therefore, the measured in-situ water content with ±10% uncertainty was used for the dose rate calculation in the current study. The total dose rates vary between 0.82 ± 0.15 and 1.73 ± 0.14 Gy ka^{-1} throughout the core and are plotted in Fig. 3.5 and also listed in Table 3.1.

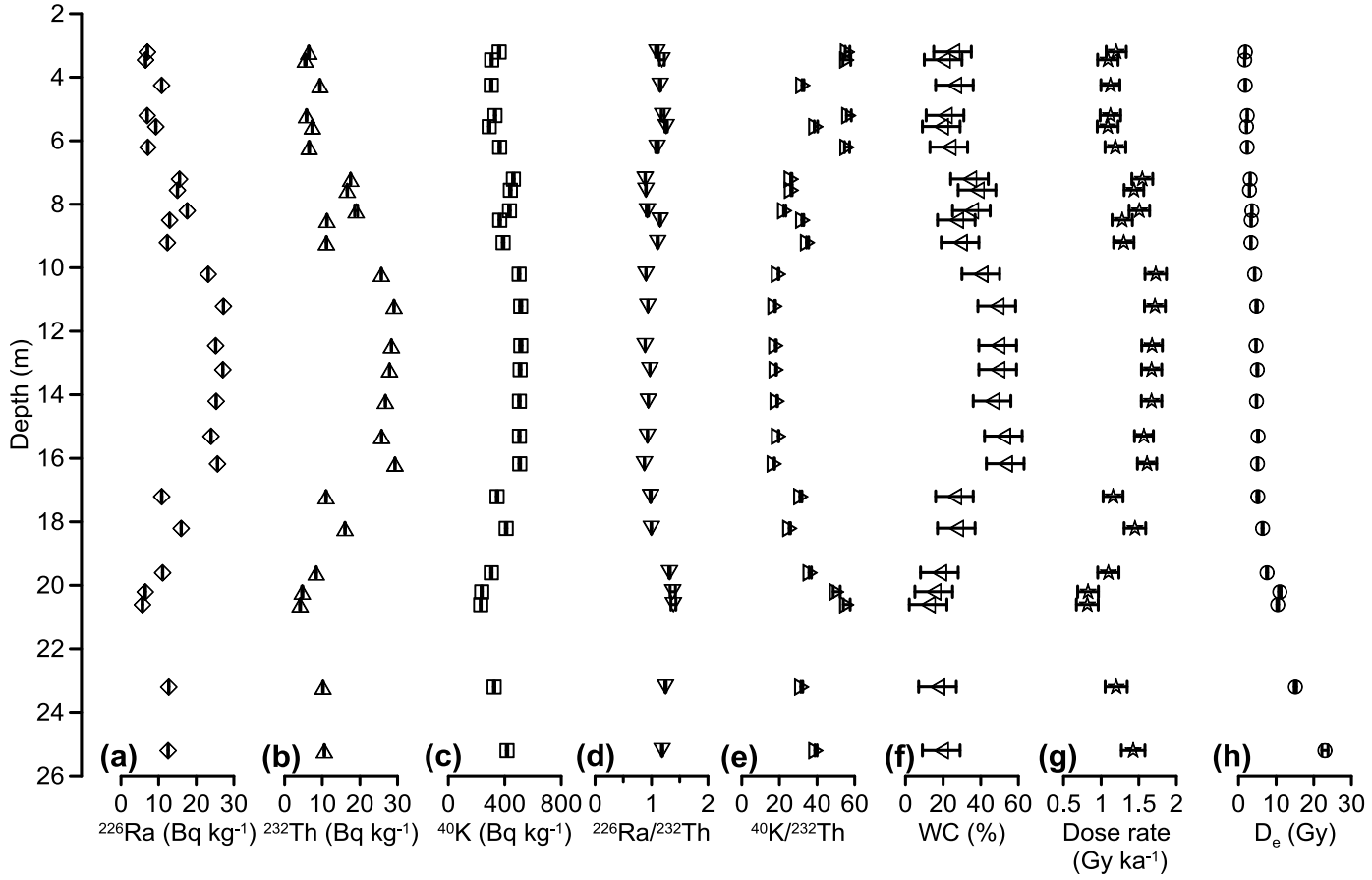

Fig. 3.5 The summary of the dose rate data. (a-c) the radionuclide activities; (d)&(e) radionuclide activity ratios, (f) water contents, (g) total dose rate for age calculation, (h) equivalent doses of all samples.

3.1.4.3 D_e estimation and OSL ages

All the D_e values and the resulting 25 OSL ages are summarized in Table 3.1. The obtained D_e values gradually increased with depth ranging from 1.64 ± 0.03 Gy to 23.0 ± 0.81 Gy. The OSL ages ranging from 16.1 ± 1.9 to1.50 ± 0.17 ka, are consistent with the stratigraphic order and increase with depth (Fig. 3.6).

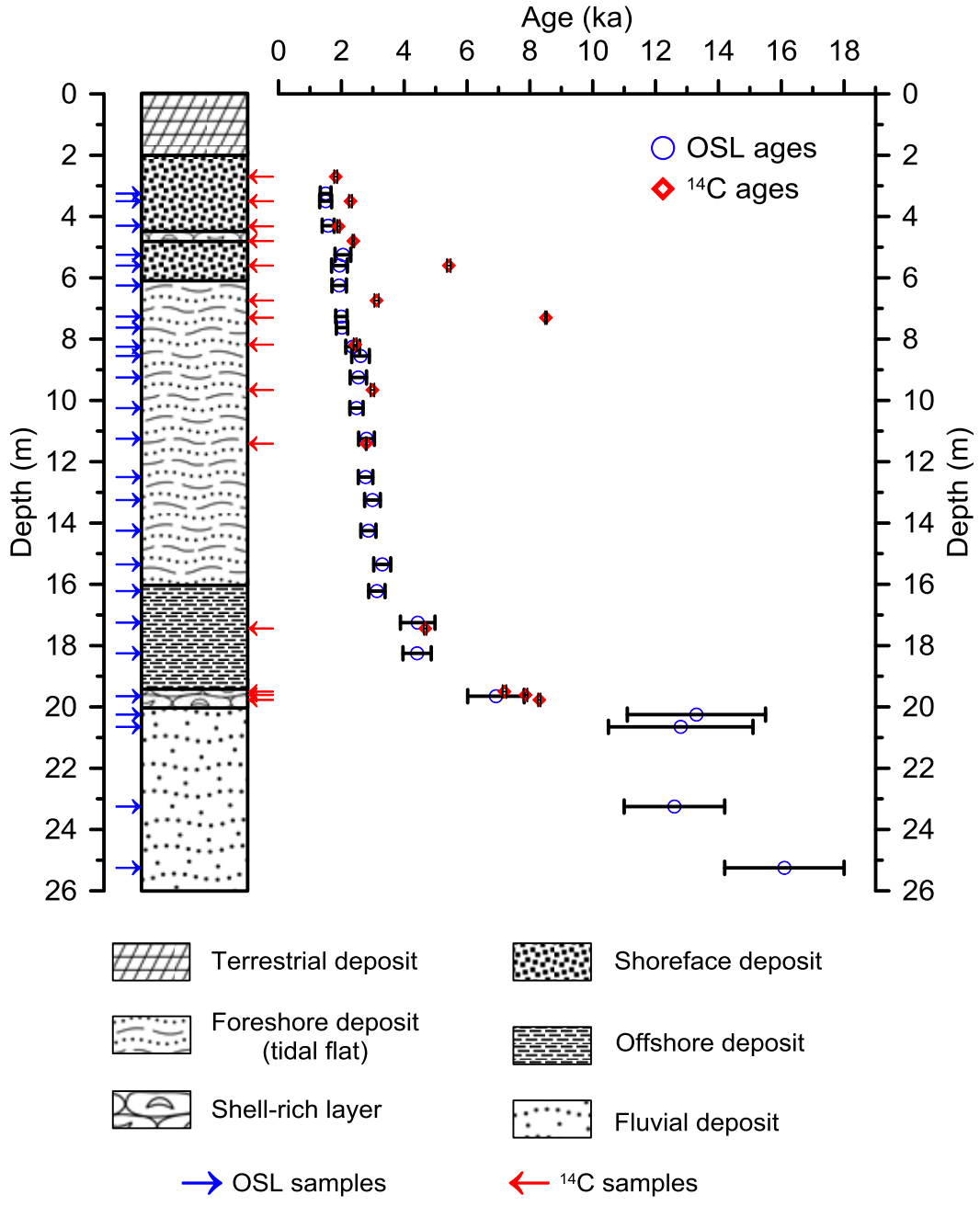

Fig. 3.6 Lithology and chronology of the Garding-2 core.

Table 3.1 Summary of the U, Th and K contents, observed water contents, dose rates, D_e values and OSL ages for the Garding-2 core.

Sample ID	Grain size (μm)	Depth (m)	Water content (%)	Uranium (ppm)	Thorium (ppm)	K (%)	Environmental dose rate (Gy ka^{-1})	Cosmic dose rate (Gy ka^{-1})	Total dose rate (Gy ka^{-1})	No. of aliquots[1]	D_e (Gy)	Age (ka)
2677	150-200	3.20-3.30	25±10	0.57±0.03	1.58±0.11	1.16±0.07	1.06±0.13	0.14±0.01	1.20±0.13	24 (24)	1.8±0.05	1.50±0.17
2678	150-200	3.45-3.55	20±10	0.52±0.03	1.36±0.11	0.99±0.06	0.96±0.14	0.13±0.01	1.09±0.14	48 (48)	1.6±0.03	1.50±0.19
2699	150-200	4.25-4.35	26±10	0.87±0.05	2.31±0.14	0.98±0.06	1.00±0.13	0.12±0.01	1.12±0.13	26 (26)	1.8±0.06	1.58±0.19
2679	150-200	5.20-5.30	21±10	0.56±0.03	1.43±0.10	1.06±0.07	1.02±0.14	0.11±0.01	1.12±0.14	24 (24)	2.3±0.04	2.05±0.25
2680	150-200	5.55-5.65	19±10	0.75±0.04	1.81±0.12	0.93±0.06	0.98±0.14	0.10±0.01	1.09±0.14	24 (24)	2.1±0.04	1.94±0.25
2701	150-200	6.20-6.30	23±10	0.57±0.04	1.60±0.11	1.17±0.07	1.09±0.14	0.09±0.01	1.19±0.14	39 (39)	2.3±0.06	1.93±0.23
2681	100-150	7.20-7.33	34±10	1.25±0.07	4.32±0.23	1.48±0.09	1.46±0.14	0.08±0.01	1.55±0.14	28 (28)	3.1±0.04	2.00±0.18
2682	100-150	7.55-7.70	38±10	1.21±0.06	4.10±0.22	1.41±0.09	1.35±0.13	0.08±0.01	1.44±0.13	28 (28)	2.9±0.03	2.02±0.18
2704	100-150	8.20-8.30	35±10	1.42±0.07	4.68±0.33	1.39±0.09	1.43±0.14	0.08±0.01	1.51±0.14	26 (25)	3.6±0.04	2.36±0.22
2705	100-150	8.50-8.60	27±10	1.04±0.06	2.77±0.16	1.17±0.08	1.21±0.13	0.07±0.01	1.28±0.13	22 (22)	3.3±0.06	2.61±0.28
2706	100-150	9.20-9.30	29±10	0.99±0.05	2.74±0.16	1.25±0.08	1.23±0.13	0.07±0.01	1.30±0.13	26 (26)	3.3±0.05	2.54±0.26
2709	100-150	10.20-10.30	40±10	1.86±0.10	6.33±0.33	1.61±0.10	1.66±0.14	0.06±0.01	1.73±0.14	20 (19)	4.3±0.07	2.48±0.21
2711	100-150	11.20-11.30	49±10	2.19±0.11	7.16±0.37	1.65±0.11	1.66±0.14	0.06±0.01	1.71±0.14	22 (22)	4.8±0.19	2.80±0.25
2713	100-150	12.45-12.55	49±10	2.02±0.10	6.99±0.36	1.65±0.11	1.63±0.14	0.05±0.01	1.68±0.14	24 (24)	4.6±0.04	2.77±0.23
2715	100-150	13.20-13.30	49±10	2.18±0.11	6.87±0.35	1.64±0.10	1.62±0.13	0.05±0.00	1.67±0.13	22 (18)	5.0±0.14	2.99±0.25
2718	100-150	14.20-14.30	46±10	2.03±0.10	6.60±0.34	1.62±0.10	1.63±0.14	0.04±0.00	1.67±0.14	24 (24)	4.8±0.07	2.86±0.24
2719	100-150	15.30-15.40	52±10	1.92±0.10	6.35±0.33	1.62±0.10	1.53±0.13	0.04±0.00	1.57±0.13	21 (19)	5.2±0.11	3.30±0.27
2721	100-150	16.17-16.27	53±10	2.06±0.11	7.22±0.37	1.63±0.10	1.57±0.13	0.04±0.00	1.61±0.13	20 (20)	5.0±0.09	3.13±0.26
2722	150-200	17.20-17.30	26±10	0.87±0.05	2.71±0.16	1.11±0.07	1.12±0.13	0.03±0.00	1.16±0.13	23 (22)	5.1±0.26	4.43±0.55
2725	100-150	18.20-18.30	27±10	1.29±0.07	3.95±0.22	1.32±0.08	1.42±0.14	0.03±0.00	1.45±0.14	24 (24)	6.4±0.15	4.41±0.45
2727	150-200	19.60-19.70	18±10	0.89±0.05	2.07±0.12	0.98±0.06	1.07±0.14	0.03±0.00	1.10±0.14	20 (20)	7.6±0.16	6.92±0.90
2728	150-200	20.20-20.30	15±10	0.52±0.03	1.15±0.10	0.76±0.05	0.80±0.14	0.03±0.00	0.83±0.14	50 (50)	11.0±0.32	13.3±2.2
2729	150-200	20.60-20.70	12±10	0.46±0.03	1.01±0.08	0.74±0.05	0.79±0.15	0.03±0.00	0.82±0.15	22 (22)	10.4±0.22	12.8±2.3
2730	150-200	23.20-23.30	17±10	1.02±0.05	2.51±0.15	1.04±0.07	1.18±0.15	0.02±0.00	1.20±0.15	24 (24)	15.1±0.30	12.6±1.6
2732	150-200	25.20-25.30	19±10	1.01±0.05	2.60±0.15	1.34±0.08	1.40±0.16	0.02±0.00	1.43±0.16	18 (17)	23.0±0.81	16.1±1.9

[1] the number of aliquots which were measured and the number of aliquots (inside the brackets)which were used for the final ages caculation after rejection.

3.1.4.4 AMS ^{14}C ages

All samples yielded enough carbon and produced sufficient ion beam during the AMS measurement to calculate ^{14}C ages. The δ^{13}C values are in the normal range to the extent that the ages are reliable. The sample information and the ages are listed in Table 3.2 as well as in Fig. 3.6. The final ^{14}C dates, ranging from 8.51 ± 0.03 to 1.82 ± 0.05 ka, were generally in stratigraphic order, except three ages at the depth from 5.6 to 7.3 m, which were severely inversed.

Table 3.2 Sample data and ^{14}C ages for the Garding-2 core.

Lab Code	Sample ID	Depth (m)	Material	^{13}C (‰)	Conventional age (a BP)	Calibrated age (a BP, 1σ)	Age (ka, before 2012)
KIA48060	14C-01	2.70	Shell	0.82±0.11	2165±25	1759±46	1.82±0.05
KIA48666	14C-02	3.50	Shell	0.18±0.15	2545±30	2228±54	2.29±0.05
KIA48667	14C-03	4.32	Shell	0.45 ±0.28	2245±30	1850±42	1.91±0.04
KIA48668	14C-04	4.80	Shell	-1.72±0.19	2640±30	2321±31	2.38±0.03
KIA48669	14C-05	5.60	Shell	0.46±0.21	5005±45	5361±57	5.42±0.06
KIA48061	14C-06	6.74	Shell	-0.88±0.48	3235±35	3058±71	3.12±0.07
KIA48670	14C-07	7.30	Wood	-30.10±0.09	7675±40	8447±33	8.51±0.03
KIA48671	14C-08	8.18	Shell	-2.04 ± 0.12	2685±35	2374±50	2.44±0.05
KIA48672	14C-09	9.66	Shell	-0.54 ± 0.50	2825±45	2927±61	2.99±0.06
KIA48062	14C-10	11.41	Shell	1.66 ±0.07	2945±25	2724±24	2.79±0.02
KIA48674	14C-11	17.44	Shell	-2.71 ± 0.16	4115±35	4608±40	4.67±0.04
KIA48063	14C-12	19.50	Shell	-0.32±0.10	6600±40	7129±64	7.19±0.06
KIA48675	14C-13	19.61	Shell	-0.85 ± 0.21	6975±45	7799±55	7.86±0.06
KIA48676	14C-14	19.77	Shell	-1.30 ± 0.41	7445±60	8235±35	8.30±0.04

3.1.5 Comparison between OSL and ^{14}C chronologies

The OSL ages and laboratory tests of luminescence characteristics were used to assess the precision of this method, but could not test the accuracy of the ages. Consequently, the results must be validated by independent age control (Murray & Olley 2002; Madsen et al. 2010), and so the obtained OSL chronology (Table 3.1, Fig. 3.6) was compared with 14 independent ^{14}C ages (Table 3.2, Fig. 3.6) to evaluate the accuracy of the ages in the current study.

Ages of Unit 6 (19.85−26 m) were obtained only from four OSL dates. No ^{14}C age is available due to the lack of dating material. The OSL dating yielded ages ranging from 16.1 ± 1.9 to 12.6 ± 1.6 ka. Unit 5 (19.30−19.85 m) was characterized by shoreface

deposits. An OSL age of 6.92 ± 0.90 ka was obtained for this unit. Three ^{14}C samples of complete mollusk shells were collected from this layer and gave ages of 8.30 ± 0.04, 7.86 ± 0.06 and 7.19 ± 0.06 ka, which are consistent with the stratigraphical order. The OSL age is in good agreement with these three ^{14}C ages within the uncertainty. Unit 4 (16−19.30 m) is composed of an offshore deposit. Three OSL ages ranging from 3.13 ± 0.26 ka to 4.41 ± 0.45 ka were obtained for this unit, in addition to a ^{14}C sample collected at the depth of 17.44 m, which yielded a calibrated age of 4.67 ± 0.04 ka consistent with the OSL chronology. Unit 3 (6−16 m) is a 10 m thick foreshore (tidal flat) sediment unit. Fragments of mollusk shell and remnants of wood were occasionally found in the sediment. Ten OSL ages range from 3.30 ± 0.27 to 1.93 ± 0.23 ka, overall consistent with the stratigraphic order. Some adjacent samples even yield nearly the same ages (within uncertainties) due to a high sedimentation rate. In contrast, the ^{14}C dating yields five ages falling into the time period from 8.51 ± 0.03 to 2.44 ± 0.05 ka, which are much older than the OSL ages. Unit 2 (2−6 m) consists of a 4 m-thick shoreface deposit, interrupted by a ~0.4 m thick shell-rich tidal channel deposit. The high-resolution OSL ages ranging from 1.94 ± 0.25 to 1.50 ± 0.17 ka are consistent with the stratigraphic order. Meanwhile, the five ^{14}C samples gave ages ranging from 5.42 ± 0.06 to 1.82 ± 0.05 ka.

Comparing the OSL and AMS ^{14}C dating results, the two chronologies are generally consistent with each other and the stratigraphical order, except three outliers (sample 14C-7, 14C-6 and 14C-05) from the AMS ^{14}C dating. Sample 14C-7 is a small piece of wood fragment collected from the tidal flat deposit at a depth of 7.3 m and yields an age of 8.51 ± 0.03 ka. Samples 14C-6 and 14C-05, which are both single shells found in the sediment, gave ages of 3.12 ± 0.07 and 5.42 ± 0.06 ka, respectively. The ages of these three samples are severely inversed with depth and inconsistent with the OSL chronology as well as the over/underlying ^{14}C ages. We assume that the single shell and the fragment of wood might have been reworked from the older strata into younger sediment. Therefore, these three ages should be excluded for the chronology construction.

In conclusion, the OSL chronology is consistent with the stratigraphic order and also has good agreement with ^{14}C ages, except with those ages which are considered to be derived from reworked material. The comparison between ^{14}C and OSL ages demonstrates that the OSL technique is able to provide reliable depositional ages, especially when ^{14}C age shows limitations due to reworking of sediment and/or lacking of dating material. Hence,

the combination of OSL and ^{14}C dating provides a better high-resolution age control of the Garding-2 core for the past 16 ka.

3.1.6 Transgression and sediment accumulation history during the past 16 ka

By the start of the last deglaciation, ocean volume had been increasing (e.g. Chappell and Shackleton 1986). Consequently, a rapid rise of sea level up to ~60 m took place worldwide during the early Holocene (11.6−7 ka BP) which was largely driven by meltwater release from decaying ice masses and the breakup of coastal ice streams, followed by a deceleration in the rate of both ocean volume and sea level rising after 7 ka BP (Smith et al. 2011 and the references therein). It has been reported that since the last deglaciation the transgression of the North Sea started at about 18 ka and has continued until today (Jelgersma 1979; Cameron et al. 1993). The progress of marine transgression and land inundation can be divided into three phases based on ^{14}C dating, from 18.0 to 10.3 ka BP, from 10.3 to 7.1 ka BP and from 7.5 ka BP until today (Streif 2004). The sea level rose from the lowstand of about 130 m to about 72 m below the present-day sea level within the first phase of the transgression. In the course of the second phase, the sea level rose from about 72 to 25 m below the present sea level and the tidal-flat sedimentation became widespread in the southern North Sea basin between 9 and 8 ka BP. The last phase continued until present and is characterized by a 25 m rise of the sea level to its current level, which resulted in the formation of the present-day coastlines and the local landscapes.

In the Garding-2 core, the presence of fluvial deposits from 26 m to 19.85 m (Unit 6) indicates that the core locality was dominated by estuary environment and not influenced by the sea before c. 13 ka. It was reported that the sea level fell to ~110−130 m below the present sea level during the Last Glacial Maximum, and consequently, the coastline retreated from present position about 600 km to the north (Jelgersma 1979). The rivers Ems, Weser, Elbe, and Eider had been joined to flow through a 30−40 km wide valley to the central North Sea and the North Atlantic (Figge 1980). We assume that this deposit was the estuarine deposit of the Eider River system, which is only about ~7 km away from the core location.

Generally, fragments of limnic muds and peat as well as a shell rich layer are found at the base of the Holocene sequences in the North Sea area, which have been considered to be the beginning of the Holocene transgression (Behre 2003, 2007). A shell-rich layer was also found in the Garding-2 core at depth of 19.30−19.85 m (Unit 5). The OSL and ^{14}C ages of the shell-rich layer indicate that the Holocene transgression started at around 8.3 ka and the marine sediments began to accumulate in the drilling site. It is widely known that the Holocene transgression was accompanied by an erosion of the pre-existing surface deposits. According to the chronology and the sediment facies of the Garding-2 core, a depositional hiatus is also present between ~8.3 and ~13 ka in the sediment succession. This shell rich layer is covered by 3.3 m-thick offshore deposit (Unit 4), which dated back to the time span between 6.92 ± 0.90 and 3.13 ± 0.26 ka. Combined with the stratigraphic analysis, we conclude that after the first Holocene transgression, the sea level rose rapidly and the borehole area was soon inundated by relatively deep sea water indicated by the offshore deposits. Concerning the compaction and the dewatering of the fine sediment, we assume that the original thickness of this offshore deposit unit might have been thicker in the actual sedimentation process, which means the accretion rate might have been even higher. After about 3 ka, foreshore (tidal flat) deposits prevailed until around 2 ka. Within this millennium, the sedimentation rate was up to about 10 m ka^{-1} which was much higher than the other periods during the last 16 ka. In the German North Sea area, it has been reported that at the early stage of the Holocene transgression (from 9 to 7 ka), the rate of sea level rise was about 12.5 m ka^{-1} which is much higher than 1.4 m ka^{-1} from 7 ka to 3 ka and 1.1 m ka^{-1} from 3 ka to the present (Behre 2007). In the Garding-2 core, the sediment facies changed from fluvial deposit (Unit 6), shoreface deposit (Unit 5), and then to offshore deposit (Unit 4), which represents a sedimentary tract in a transgressive phase from 8.3 to 3 ka. Subsequently, the sediment facies changed from the offshore (Unit 4) to foreshore deposit (Unit 3), which suggests that the sea level rise decelerated by c. 3 ka. Consequently, the sediment supply exceeded the available accommodation space in the depositional area. The coast line started to prograde and shift seawards from 3 to 2 ka. A high sedimentation rate of c. 10 m ka^{-1} was recorded for this time interval.

After 2 ka, the sandy beach deposits dominated the sedimentary succession indicating that the coastline shifted landwards. It has been reported that a west-east direction spit system was formed on the Eiderstedt Peninsula from c. 2000 BC (Menke 1988). The

source of sands for the spit system is considered to be the erosion of old morainic material which was located northwest of the Eiderstedt Peninsula in the present offshore area (Dittmer 1952). The sand layer at depths between 3 and 6 m might have originated from this spit system. On the other hand, it is also possible that a small scale transgression existed during the late Holocene. The sea level curve for the German Bight shows several sea level fluctuations during the late Holocene (Behre 2007), which were later considered to be generated from data-artefacts or local effects (Bungenstock and Schäfer 2009; Baeteman et al. 2011). The strong fluctuations of sea level change in term of frequency and magnitude are also not confirmed by our current results.

Terrestrial clastic deposits formed an unconformity on top of the shoreface deposits after c. 1.5 ka. As the uppermost 3 m core had been exposed to light before sampling, there is no age control after 1.5 ka. Hence, the accurate timing of when the terrestrial clastic deposits started to accumulate is not available from the present chronology. However, archaeological and historical evidence suggests that at around the 11th century the local people started to build dikes along the coastline of the German sector of North Sea (e.g. Kühn and Panten 1989). We deduce that the terrestrial clastic deposits accumulated as a result of the diking activity, which prevented further marine sedimentation in the borehole area; the OSL chronology presented here generally fits with the historical record.

Since the last century, many studies have contributed to reconstruct the sea level change and sedimentary process in the southern North Sea coast area. Several sea level curves were also generated for the German Bight (Schütte 1939; Behre 2003, 2007; Vink et al. 2007; Bungenstock and Schäfer 2009; Bungenstock and Weerts 2010). However, debates concerning the reliability and accuracy of the sea level change reconstruction in German North Sea area still persist. The main limitation of the existing studies is the scarcity of data. The robust chronology from Garding-2 core is the first long-term age framework that covers the Holocene as well as the last deglaciation period in one succession. It provides a new insight to understand the coastal evolution in the German North Sea. Recently, the southern North Sea coast was considered to have been influenced by the post-glacial isostatic movement instead of the traditional opinion that this area has been isostatic-free since the deglaciation. This makes the comparison of sea level change from different places difficult and complex. Furthermore, the local scale processes such as past variations in tidal range, the local water table and sediment compaction can also influence

the reconstruction of sea level changes registered in the sedimentary record (Vink et al. 2007 and the references therein). Due to these reasons, we should be cautious in comparing our apparent chronologies with previous studies in the southern North Sea area. For example, the distance between the study sites and the methods employed for the chronology should be considered in order to minimize the influence from the potential isostatic movement and the local effects.

One short core from the near-shore region off the island of Sylt, NW OF the Eiderstedt Peninsula was dated by both OSL and ^{14}C techniques and presented a similar sedimentology and chronology as in our study (Alappat et al. 2010). The lowermost Pleistocene glaciofluvial sand yielded an OSL age of 14.7 ± 2.1 ka at a depth of 22.19 m below sea level. The Holocene basal peat layer was found in their core (06VC) overlying the glaciofluvial sand and yielded a calibrated radiocarbon age of 8.4−8.2 ka BP. Besides, they found a wood sample from the fluvial deposit at 0.26 m below the basal peat layer giving a radiocarbon age of 9.1−8.7 ka BP. In Garding-2 core, the base of the shell-rich layer above the fluvial deposit was dated to 8.30±0.04 ka, which is nearly synchronous with the ages presented in Alappat et al. (2010). Further to the north, a 7 ka sedimentary record was established by Clemmensen et al. (2006) based on OSL and AMS ^{14}C techniques in western Jutland in Denmark to investigate the sea level change in the North Sea. Their study site is about 150 km away from Garding-2 core location. However, their chronology indicates that the onset of the Holocene transgression started at around 7.1 ka (5100 BC), which is around 1 ka later than in Garding-2 core. By comparing sea level data from different places along southern North Sea coast, Kiden et al. (2002) mentioned that smaller areas in the coastal regions of the southern North Sea potentially have their own neotectonic and glacio-isostatic histories. They therefore recommend choosing areas not larger than about 50 km across to compile data for reliable sea-level curves. Following this recommendation, Bungenstock and Schäfer (2009) divided the German North Sea coast into five sections and built up individual sea level curves for each sector, based on the same dataset as the "Behre curve" (Behre 2003, 2007) for the entire German North Sea coast. They found that the five curves all differ from the original "Behre curve" and from each other and the strong fluctuations in the sea level change of the later curve were not detected. The authors attributed this difference to data-artefacts or local effects. The deviation in the onset of the Holocene transgression between our study and that of Clemmensen et al. (2006) might be also related to the local effects due to the relatively

long distance (>50 km) between the two study areas. Thus, sea level changes and sedimentary processes generated from the sediment record along the German North Sea area probably consist of not only regional and/or global but also local signals.

3.1.7 Conclusions

In this study, we have shown that the OSL dating of quartz is a powerful tool for dating coastal sediments. The OSL signal was sufficiently bleached prior to the deposition, and the ages obtained are reliable and consistent with the stratigraphic order as well as with the ^{14}C chronology. Based on the internal evaluation and external cross-checking of these two chronologies, we conclude that the combination of OSL and ^{14}C dating techniques provides the most reliable and robust chronology for the Garding-2 core. The Holocene transgression history is generally consistent with the former investigations in the southern North Sea area but shows inconsistencies in detail.

An estuarine environment dominated in Eiderstedt Peninsula between 16 and ~13 ka. Probably due to erosion during the transgression, there is a depositional hiatus between ~13 and 8.3 ka. The Holocene transgression started at about 8.3 ka and the sea level rose rapidly until 3 ka. During this period, the offshore sediments accumulated at the drilling site. From 3 to 2 ka, the sea level was stabilized and the foreshore (tidal flat) deposits characterized by a very high sedimentation rate prevailed at the drilling location in Eiderstedt Peninsula. After 2 ka, the sandy beach deposit accumulated in the sediment succession, and the terrestrial clastic sediment started to accumulate after 1.5 ka. This sea regression was probably affected by local diking activities which started at around 11th century.

Acknowledgements. – This research has been supported by a DAAD scholarship, funded by the German Academic Exchange Service (DAAD) and the Leibniz Institute for Applied Geophysics (LIAG), Hannover. The authors are grateful to Dr. Annemiek Vink (Bundesanstalt für Geowissenschaften und Rohstoffe) and Dr. Michael Naumann (Landesamt für Bergbau, Energie und Geologie) for the helpful discussions and comments on the core description and interpretation. The constructive comments from the anonymous reviewer are appreciated. We thank Rachel

Smedley (Aberystwyth University) for careful language corrections. Sonja Riemenschneider, Sabine Mogwitz and Petra Posimowski (technicians of LIAG-Section S3) are thanked for are thanked for their technical help during the preparation and measurement of OSL and gamma samples. We thank the crew at the Kiel Leibniz Laboratory for the radiocarbon dating and S. Pietrzok for photographic work.

References

Aitken, M. 1985: Thermoluminescence Dating. 359 pp. Academic Press, London.

Alappat, L, Vink, A., Tsukamoto, S., Frechen, M. 2010. Establishing the Late Pleistocene-Holocene sedimentation boundary in the southern North Sea using OSL dating of shallow continental shelf sediments. Proceedings of the Geologists' Association 121, 43-54.

Baeteman, C., Waller, M., Kiden, P., 2011. Reconstructing middle to late Holocene sea-level change: A methodological review with particular reference to 'A new Holocene sea-level curve for the southern North Sea' presented by K.-E. Behre. Boreas 40, 557-572.

Behre, K. E., 2003. Eine neue Meeresspiegelkurve für die südliche Nordsee - Transgressionen und Regressionen in den letzten 10.000 Jahren. Probleme der Küstenforschung im südlichen Nordseegebiet 28, 9-63.

Behre, K. E., 2007. A new Holocene sea-level curve for the southern North Sea. Boreas 36, 82-102.

Boomer, I., Horton, B. P., 2006. Holocene relative sea-level movements along the North Norfolk Coast, UK. Palaeogeography, Palaeoclimatology, Palaeoecology 230, 32-51.

Bungenstock, F., Schäfer, A., 2009. The Holocene relative sea-level curve for the tidal basin of the barrier island Langeoog, German Bight, Southern North Sea. Global and Planetary Change 66, 34-51.

Bungenstock, F., Weerts, H. J. T., 2010. The high-resolution Holocene sea-level curve for Northwest Germany: global signals, local effects or data-artefacts? International Journal of Earth Sciences 99, 1687-1706.

Cameron, D., van Doorn, D., Laban, C., Streif, H., 1993. Geology of the southern North Sea basin. In Hillen, R. & Verhagen, H. (eds.): Coastlines of the southern North Sea, 14-26. American Society of Civil Engineers, New York.

Chappell, J., Shackleton, N.J., 1986. Oxygen isotopes and sea level. Nature 324, 137-140.

Clarke, M. L. 1996: IRSL dating of sands: bleaching characteristics at deposition inferred from the use of single aliquots. Radiation Measurements 26, 611-620.

Clemmensen, L. B., Pedersen, K., Murray, A., Heinemeier, J., 2006. A 7000-year record of coastal evolution, Vejers, SW Jutland, Denmark. Bulletin of Geological Society of Denmark 53, 1-22.

Costas, I., Reimann, T., Tsukamoto, S., Ludwig, J., Lindhorst, S., Frechen, M., Hass, C., Betzler, C., 2012. Comparison of OSL ages from young dune sediments with a high-resolution independent age model. Quaternary Geochronology 10, 16-23.

Denys, L., Baeteman, C., 1995. Holocene evolution of relative sea level and local mean high water spring tides in Belgium-a first assessment. Marine Geology 124, 1-19.

Dittmer, E., 1952. Die nacheiszeitliche Entwicklung der schleswig-holsteinischen Westküste. Meyniana 1, 138-168.

Duller, G.A.T., 1994. Luminescence dating of poorly bleached sediments from Scotland. Quaternary Geochronology 13, 521-524.

Figge, K., 1980. Das Elbe-Urstromtal im Bereich der Deutschen Bucht (Nordsee). Eiszeitalter und Gegenwart 30, 203-211.

Fuchs, M., Wagner, G. A., 2003. Recognition of insufficient bleaching by small aliquots of quartz for reconstructing soil erosion in Greece. Quaternary Science Reviews 22, 1161-1167.

Galbraith, R. F., Roberts, R. G., Laslett, G. M., Yoshida, H., Olley, J. M., 1999. Optical dating of single and multiple grains of quartz from Jinmium rock shelter, Northern Australia: part 1, experimental details and statistical models. Archaeometry 41, 339-364.

Gehrels, W. R., Szkornik, K., Bartholdy, J., Kirby, J. R., Bradley, S. L., Marshall, W. A., Heinemeier, J., Pedersen, J. B. T., 2006. Late Holocene sea-level changes and isostasy in western Denmark. Quaternary Research 66, 288-302.

Guérin, G., Mercier, N., Adamiec, G., 2011. Dose-rate conversion factors: update. Ancient TL 29, 5-8.

Hoffmann, D., 2004. Holocene landscape development in the marshes of the West Coast of Schleswig-Holstein, Germany. Quaternary International 112, 29-36.

Jacobs, Z., 2008. Luminescence chronologies for coastal and marine sediments. Boreas 37, 508-535.

Jelgersma, S., 1979. Sea-level changes in the North Sea basin. In Oele, E., Schüttenhelm, R. T. E. & Wiggers, A. J. (eds.): The Quaternary History of the North Sea, 233-248. Acta Universitatis Upsaliensis, Symposium Universitatis Upsaliensis Annum Quingentesimum Celebrantis, University of Uppsala, Uppsala.

Kiden, P., Denys, L., Johnston, P., 2002. Late Quaternary sea-level change and isostatic and tectonic land movements along the Belgian-Dutch North Sea coast: geological data and model results. Journal of Quaternary Science 17, 535-546.

Kühn, H.J., Panten, A., 1989. Der frühe Deichbau in Nordfriesland: Archäologisch-historische Untersuchungen, 127 pp. Neumann, Bredstedt.

Li, S-H., 1994. Optical dating: insufficiently bleached sediments. Radiation Measurements 23, 563-568.

Lopez, G. I., Rink, W. J., 2007. Characteristics of the burial environment related to quartz SAR-OSL dating at St. Vincent Island, NW Florida, USA. Quaternary Geochronology 2, 65-70.

Madsen, A. T., Murray, A. S., Andersen, T. J., Pejrup, M., Breuning-Madsen, H., 2005. Optically stimulated luminescence dating of young estuarine sediments: a comparison with ^{210}Pb and ^{137}Cs dating. Marine Geology 214, 251-268.

Madsen, A. T., Murray, A. S., Andersen, T. J., 2007a. Optical dating of dune ridges on Rømø, a barrier island in the Wadden Sea, Denmark. Journal of Coastal Research 23, 1259-1269.

Madsen, A. T., Murray, A. S., Andersen, T. J., Pejrup, M., 2007b. Optical dating of young tidal sediments in the Danish Wadden Sea. Quaternary Geochronology 2, 89-94.

Madsen, A. T., Murray, A. S., Andersen, T. J., Pejrup, M., 2010. Luminescence dating of Holocene sedimentary deposits on Rømø, a barrier island in the Wadden Sea, Denmark. The Holocene 20, 1247-1256.

Madsen, A. T., Murray, A. S., Jain, M., Andersen, T. J., Pejrup, M., 2011. A new method for measuring bioturbation rates in sandy tidal flat sediments based on luminescence dating. Estuarine, Coastal and Shelf Science 92, 464-471.

Mauz, B., Bungenstock, F., 2007. How to reconstruct trends of late Holocene relative sea level: A new approach using tidal flat clastic sediments and optical dating. Marine Geology 237, 225-237.

Mauz, B., Baeteman, C., Bungenstock, F., Plater, A. J., 2010. Optical dating of tidal sediments: potential and limits inferred from the North Sea coast. Quaternary Geochronology 5, 667-678.

Mejdahl, V., 1979. Thermoluminescence dating: beta attenuation in quartz grains. Achaeometry 21, 61-73.

Menke, B., 1988. Die holozäne Nordseetransgression im Küstenbereich der südöstlichen Deutschen Bucht. In Haffner, A. & Müller-Wille, M. (eds.): Norderhever-Projekt 1. Landschaftsentwicklung und Siedlungsgeschichte im Einzugsgebiet der Norderhever (Nordfriesland), Offa-Bücher 66, 117- 137. Karl Wachholtz Verlag, Neumünster.

Murray, A. S., Marten, R., Johnston, A., Martin, P., 1987. Analysis for naturally occuring radionuclides at environmental concentrations by gamma spectrometry. Journal of Radioanalytical and Nuclear Chemistry 115, 263-288.

Murray, A. S., Wintle, A. G., 2000. Luminescence dating of quartz using an improved single-aliquot regenerative-dose protocol. Radiation Measurements 32, 57-73.

Murray, A. S., Olley, J. M., 2002. Precision and accuracy in the optically stimulated luminescence dating of sedimentary quartz: a status review. Geochronometria 21, 1-16.

Murray-Wallace, C. V., Banerjee, D., Rourman, R. P., Olley, J. M., Brooke, B. P., 2002. Optically stimulated luminescence dating of Holocene relict foredunes, Guichen Bay, South Australia. Quaternary Science Reviews 21, 1077-1086.

Nielsen, A., Murray, A. S., Pejrup, M., Elberling, B., 2006. Optically stimulated luminescence dating of a Holocene beach ridge plain in Northern Jutland, Denmark. Quaternary Geochronology 1, 305-312.

Olley, J., Caitcheon, G., Murray, A., 1998. The distribution of apparent dose as determined by optical stimulated luminescence in small aliquots of fluvial quartz: implications for dating young sediments. Quaternary Science Reviews 17, 1033-1040.

Olley, J. M., Caitcheon, G. G., Roberts, R. G., 1999. The origin of dose distributions in fluvial sediments, and the prospect of dating single grains from fluvial deposits using optically stimulated luminescence. Radiation Measurements 30, 207-217.

Prescott, J. R., Stephan, L. G., 1982. The contribution of cosmic radiation to the environmental dose for thermoluminescent dating- Latitude, altitude and depth dependences. PACT 6, 17-25.

Prescott, J. R., Hutton, J. T., 1994. Cosmic ray distributions to dose rates for luminescence and ESR dating: large depths and long-term variations. Radiation Measurements 23, 497-500.

Reimann, T., Lindhorst, S., Thomsen, K. J., Murray, A. S., Frechen, M., 2012. OSL dating of mixed coastal sediment (Sylt, German Bight, North Sea). Quaternary Geochronology 11, 52-67.

Reimer, P. J., Baillie, M. G. L., Bard, E., Bayliss, A., Beck, J. W., Blackwell, P. G., Bronk Ramsey, C., Buck, C. E., Burr, G. S., Edwards, R. L., Friedrich, M., Grootes, P. M., Guilderson, T. P., Hajdas, I., Heaton, T. J., Hogg, A. G., Hughen, K. A., Kaiser, K. F., Kromer, B., McCormac, F. G., Manning, S. W., Reimer, R.W., Richards, D. A., Southon, J. R., Talamo, S., Turney, C. S. M., van der Plicht, J., Weyhenmeyer C. E., 2009. IntCal09 and Marine09 radiocarbon age calibration curves, 0-50,000 years cal BP. Radiocarbon 51, 1111-1150.

Roberts, H. M., Plater, A. J., 2007. Reconstruction of Holocene foreland progradation using optically stimulated luminescence (OSL) dating: An example from Dungeness, UK. The Holocene 17, 495-505.

Roe, H. M., 1999. Late Middle Pleistocene sea-level change in the southern North Sea: the record from eastern Essex, UK. Quaternary International 55, 115-128.

Shennan, I., Horton, B., Innes, J., Gehrels, R., Lloyd, J., McArthur, J., Rutherford, M., 2000. Late Quaternary sea-level changes, crustal movements and coastal evolution in Northumberland, UK. Journal of Quaternary Science 15, 215-237.

Schütte, H.. 1939. Sinkendes Land an der Nordsee? Zur Küstengeschichte Nordwestdeutschlands. Schriften des Deutschen Naturkundevereins Neue Folge 9,144 pp. Öhringen.

Streif, H., 2004. Sedimentary record of Pleistocene and Holocene marine inundations along the North Sea coast of Lower Saxony, Germany. Quaternary International 112, 3-28.

Stuiver, M., Reimer, P. J., 1993. Extended 14C data base and revised CALIB 3.0 14C age calibration program. Radiocarbon 35, 215-230.

Sugisaki, S., Buylaert, J. P., Murray, A. S., Harada, N., Kimoto, K., Okazaki, Y., Sakamoto, T., Iijima, K., Tsukamoto, S., Miura, H., Nogi, Y., 2012. High resolution

optically stimulated luminescence dating of a sediment core from the southwestern Sea of Okhotsk. Geochemistry Geophysics Geosystems 13, 1-20.

Törnqvist, T. E., van Ree, M. H. M., van 't Veer, R., van Geel, B., 1998. Improving methodology for high-resolution reconstruction of sea-level rise and neotectonics by paleoecological analysis and AMS ^{14}C dating of basal peats. Quaternary Research 49, 72-85.

Vink, A., Steffen, H., Reinhardt, L., Kaufmann, G., 2007. Holocene relative sea-level change, isostatic subsidence and the radial viscosity structure of the mantle of northwest Europe (Belgium, the Netherlands, Germany, southern North Sea). Quaternary Science Reviews 26, 3249-3275.

Walker, R. G., Plint, A. G., 1992. Wave- and storm-dominated shallow marine systems. In Walker, R. G. & James, N. P. (eds.): Facies models: response to sea-level change. 219-238: Geological Association of Canada. St. John's.

Waller, M. P., Long, A. J., Schofield, J. E., 2006. Interpretation of radiocarbon dates from the upper surface of late-Holocene peat layers in coastal lowlands. The Holocene 16, 51-61.

Wintle, A. G., Murray, A. S., 2006. A review of quartz optically stimulated luminescence characteristics and their relevance in single-aliquot regeneration dating protocols. Radiation Measurements 41, 369-391.

Chapter 4 Late Quaternary lake evolution of Huangqihai in northern China

4.1 Lake level reconstruction of Huangqihai Lake in northern China since MIS 3 based on pulsed optically stimulated luminescence dating

Jingran Zhang[1], Sumiko Tsukamoto[1], Yulian Jia[2], Manfred Frechen[1]

[1] Leibniz Institute for Applied Geophysics (LIAG), Stilleweg 2, 30655 Hannover, Germany

[2] Key laboratory of Poyang Lake Wetland and Watershed Research, Ministry of Education, School of Geography and Environment of Jiangxi Normal University, 330022 Nanchang, China

Journal of Quaternary Science, Vol. 31, pp. 225-238;

http://dx.doi.org/10.1002/jqs.2861

Due to copyrights this manuscript is not included in the online version.

Chapter 5 Post-IR IRSL dating of K-rich feldspar and polymineral fine grains

5.1 Application of the post-IR IRSL dating in the Garding-2 core sediment from the German North Sea coast

Jingran Zhang[1], Sumiko Tsukamoto[1], Manfred Frechen[1]

[1]Leibniz Institute for Applied Geophysics (LIAG), S3: Geochronology and Isotope Hydrology, 30655 Hannover, Germany

Preparing for submission to a peer-review journal

Abstract

The infrared stimulated luminescence (IRSL) signal of feldspars saturates at much higher doses compared with that of the quartz optically stimulated luminescence (OSL), having a great potential for extending the age range of luminescence dating. However, the application of feldspar IRSL signal for dating has long been hampered by the anomalous fading effect. The development of post-IR IRSL (pIRIR) protocols provides the possibility for overcoming this disadvantage. In this study, pIRIR protocols using different combinations of preheat and stimulation temperatures ($pIRIR_{150}$, $pIRIR_{225}$ and $pIRIR_{290}$) have been tested on a group of samples with various ages. The behaviour of different pIRIR signals and the corresponding IR_{50} signals, in term of residual, fading rate and dose recovery ratio, has been systematically examined. The residual dose increases from ~0.3 Gy up to ~40 Gy for both pIRIR and IR_{50} signals with increasing preheat and stimulation temperatures. No obvious temperature dependence in the fading rate for the pIRIR signals has been observed. However when these protocols are applied to an infinitely old sample, the natural pIRIR signal is in saturation only for the $pIRIR_{290}$ signal, whereas the saturation levels are 73% and 83% for the $pIRIR_{150}$ and $pIRIR_{225}$ signals, respectively. Finally the uncorrected ages obtained by $pIRIR_{150}$, $pIRIR_{225}$ and $pIRIR_{290}$ protocols have been compared with independent quartz OSL ages. The results demonstrate that for the Holocene samples $pIRIR_{150}$ ages without fading correction have the best agreements with the independent age control.

Key words: post-IR IRSL dating; temperature dependency; residual; fading rate; field saturation.

5.1.1 Introduction

Feldspar luminescence signals are commonly affected by anomalous fading, which has been explained as a result of quantum mechanical tunneling (Aitken, 1985; Visocekas, 1985; Visocekas et al., 1994). Anomalous fading is responsible for significant age underestimations in luminescence dating using feldspar, typically 30−50% over the entire dating range of this mineral (Lamothe and Auclair, 1999; Balescu et al., 2003; Huntley and Lamothe, 2001; Wallinga et al., 2001) and therefore fading rates should be systematically investigated. In recent years, many efforts have been done to overcome the problem. These include methods to correct for fading (Huntley and Lamothe, 2001; Kars et al., 2008) and to extract non-fading or less fading signals (e.g. Tsukamoto et al., 2006; Thomsen et al., 2008; Buylaert et al., 2009; Thiel et al., 2011a, 2011b; Li and Li, 2011) . Thomsen et al. (2008) observed for the first time that the post-IR IRSL (pIRIR) signals of feldspar at elevated temperature gives lower fading rate than conventional IRSL signals measured at a low stimulation temperature, e.g. 50 °C (IR_{50}). Since then, the pIRIR signal stimulated at 225 °C ($pIRIR_{225}$) with a preheat at 250 °C has been applied to date both sand-sized K-rich feldspar (Buylaert et al., 2009; Thiel et al., 2010; Alappat et al., 2010) and polymineral fine grains (Wacha and Frechen, 2011; Vasiliniuc, et al., 2012). Murray et al. (2009) have argued that there is no a priori reason that the preheat temperature should not be higher than 250 °C which has been commonly used, because the IRSL signal from K-feldspar is associated with a TL peak at about 410 °C and that no significant IRSL is derived from lower temperature traps. Thus, the combination of higher preheat and stimulation temperatures ($pIRIR_{290}$ with a preheat temperature at 320 °C) was first tested using polymineral fine grains to date loess sediment (Thiel et al. 2011a). They observed that the natural signal of a sample from below the Brunhes/Matuyama (B/M) boundary (~780 ka) was in saturation on the laboratory regenerated dose response curve, which implies that there is no evidence for anomalous fading of the $pIRIR_{290}$ signal. Based on a comprehensive study of the pIRIR signal, Buylaert et al. (2012) showed that $pIRIR_{290}$ ages without fading correction agree very well with independent age control of samples from all over the world. The pIRIR signals measured at elevated temperature can minimize the fading rate compared to the conventional IR_{50} signal, however, they have

also been found to be more difficult to bleach (Li and Li 2011; Buylaert et al., 2012).A range of residual doses from a few Gy up to hundred Gy has been reported for $pIRIR_{225}$ and $pIRIR_{290}$ signals from different studies (Li et al, 2014 and the references therein), which might cause significant age overestimation especially for young samples (e.g. Holocene). Reimann et al. (2011) showed that the pIRIR residual dose can be reduced significantly by lowering preheat and pIRIR stimulation temperatures without losing its major advantage of reducing the anomalous fading rate. Thus, modified pIRIR protocols using lower preheat and pIRIR stimulation temperatures have been successfully tested and applied to Holocene sediments (Reimann et al., 2011; Madsen et al., 2011; Reimann and Tsukamoto, 2012; Fu and Li, 2013).

However, there is so far still no consensus on how to select a suitable preheat and/or stimulation temperature in the pIRIR protocols when dating samples with different dose (age) ranges. Systematic investigation of performances (e.g. residual, fading rate, dose recovery test, etc.) of pIRIR signals using samples with independent age control is therefore mandatory to understand how the preheat and stimulation temperatures affect pIRIR D_e measurements. In order to investigate the temperature and/or dose dependences of the feldspar pIRIR signal, a series of investigation including fading rate, residual dose and dose recovery test have been performed using pIRIR signals at different preheat and pIRIR stimulation temperatures. The commonly applied stimulation temperatures, i.e. 150 °C ($pIRIR_{150}$), 225 °C ($pIRIR_{225}$) and 290 °C ($pIRIR_{290}$) were applied with a preheat temperature (PH) at 180 °C, 250 °C and 320 °C, respectively. The main focus of this study is to compare the performance of the pIRIR signals which is obtained with different preheat and stimulation temperatures.

5.1.2 Samples and experimental details

5.1.2.1 Samples and preparation

Six samples (Table 5.1) were collected from a 240 m long core (Garding-2 core, 54°18.229'N, 08°46.587'E) which was taken from the southern part of the Eiderstedt Peninsula in Schleswig-Holstein, Germany (Zhang et al., 2014). The chronology of the uppermost 26 m sediment of the core has been well established by quartz OSL and ^{14}C dating techniques (Zhang et al., 2014). Sample LUM-2699 (4.25−4.35 m) and LUM-2727

(19.6−19.7 m) are shoreface (beach) deposits with OSL ages of 1.58±0.19 ka and 6.92 ± 0.90 ka, respectively. Sample LUM-2719 (15.3−15.4 m) is foreshore (tidal channel) deposits yielding an OSL age of 3.30 ± 0.27 ka. Sample LUM-2728 (20.2−20.3 m) has an OSL age of 13.3 ± 2.2 ka which was collected from the fluvial deposit. Sample LUM-2746, taken at 77.2−77.3 m depth, consists of offshore (shallow marine) deposit. The natural quartz OSL signal of this sample is in saturation and yielded a minimum age of ~190 ka (unpublished data). The stratigraphical analysis of the Garding-2 core suggested that below 200 m the age of the sediment should beyond Quaternary. The IRSL and pIRIR signals of sample LUM-2761 from 200.2−200.3 m depth should thus have reached the field saturation. There is no reliable independent age control for these two older samples.

Table 5.1 Summary of the U, Th and K contents and the dose rates.

Sample ID	Grain size (μm)	Depth (m)	Water content (%)	Uranium (ppm)	Thorium (ppm)	K (%)	Cosmic dose rate (Gy ka^{-1})	Total dose rate (Gy ka^{-1})
2699	150−200	4.3−4.4	26 ± 10	0.87 ± 0.05	2.31 ± 0.14	0.98 ± 0.06	0.12 ± 0.01	1.84 ± 0.16
2719	4−11	15.3−15.4	52 ± 10	1.92 ± 0.10	6.35 ± 0.33	1.62 ± 0.10	0.04 ± 0.00	1.99 ± 0.13
2727	150−200	19.6−19.7	18 ± 10	0.89 ± 0.05	2.07 ± 0.12	0.98 ± 0.06	0.03 ± 0.00	1.82 ± 0.18
2728	150−200	20.2−20.3	15 ± 10	0.52 ± 0.03	1.15 ± 0.10	0.76 ± 0.05	0.03 ± 0.00	1.54 ± 0.19
2746	150−200	77.2−77.3	12 ± 10	1.51 ± 0.08	3.54 ± 0.19	1.65 ± 0.10	0.003 ± 0.000	2.67 ± 0.21
2761	150−200	200.2−200.3	19 ± 10	1.08 ± 0.06	3.30 ± 0.19	0.83 ± 0.06	0.0003 ± 0.0000	1.77 ± 0.18

All preparations were conducted under subdued red light conditions. The chemical treatment with hydrochloric acid, sodium oxalate, and hydrogen peroxide were employed to dissolve carbonate, aggregates, and organic matter, respectively. The extracts of either sand-sized K-feldspar (LUM-2699, LUM-2727, LUM-2746 and LUM-2761) or 4−11 μm polymineral fine grains (LUM-2719) were used for the pIRIR measurement. The sand-sized K-feldspar (K- <2.58 g/cm^3) were density separated from other minerals by heavy liquid (sodium polytungstate). The obtained K-feldspar grains were then mounted on stainless steel discs as a monolayer using silicon spray. The polymineral fine grains were deposited onto aluminum discs from a suspension in distilled water (2 mg/disc).

5.1.2.2 Dose rate determination

High-resolution gamma spectrometry was applied to determine the U, Th and K content for the dose rate calculation of the samples. The samples were dried at 130 °C, homogenized, filled into 50 g air tight plastic containers and stored for at least one month to gain ^{226}Ra-^{222}Rn equilibrium condition before measuring on the high-resolution gamma spectrometer (Murray et al., 1987). Each sample was measured for 3-4 days. The dose rate conversion factors of Guérin et al. (2011) and beta attenuation factors of Mejdahl (1979) were applied for dose rate calculation. An a-value of 0.09 ± 0.02 was used according to Balescu et al. (2007) for external alpha dose rate calculation of the non-etched feldspar grains. For the internal β-dose rate a K concentration of 12.5 ± 0.5 % (Huntley and Baril, 1997) and Rb content of 400 ± 50 μg/g (following Huntley and Hancock, 2001) was assumed. The cosmic dose rate was derived from the altitude and latitude of the sampling site, the burial depth and the density of the overburden (Prescott and Hutton, 1994). The "*in situ*" water content of the samples was measured for the total dose rate calculation (Aitken, 1985). The dosimetric data including U, Th and K content and dose rates are listed in Table 5.1. The dose rate data of sample LUM-2699, LUM-2719, LUM-2727 and LUM-2728 has been previously reported in (Zhang et al., 2014) for the quartz age calculation.

5.1.2.3 IRSL measurements

An automated Risø TL/OSL DA-15 reader with a ^{90}Sr/^{90}Y beta source was used for the luminescence measurements. The feldspar luminescence signal was stimulated with infrared diodes emitting at 870 nm, and the luminescence was detected in the blue-violet region through a Schott BG-39/Corning 7-59 filter combination. The single-aliquot regenerative-dose (SAR) protocol (Murray and Wintle, 2000) was applied for the pIRIR measurement (Table 5.2).

Table 5.2 The pIRIR single-aliquot-regenerative-dose (SAR) protocols used in this study.

Step	Treatment	Observed
1	Given dose, D_i (i=0,1,2,3…)	
2	Preheat, 180 / 250 /320 ^oC, 60 s	
3	IR stimulation, 120 s at 50 ^oC	L_x (IR_{50})
4	IR stimulation, 240 s at 150 / 225 / 290 ^oC	L_x ($pIRIR_{150/225/290}$)
5	Given dose, D_T	
6	Cutheat, 180 / 250 /320 ^oC, 60 s	
7	IR stimulation, 120 s at 50 ^oC	L_x (IR_{50})
8	IR stimulation, 240 s at 150 / 225 / 290 ^oC	T_x ($pIRIR_{150/225/290}$)
9	Return to step 1	

The same thermal treatment was employed prior to both the dose and test dose measurements (Huot and Lamothe, 2003; Blair et al., 2005). After dosing and preheating, the first IR stimulation was carried out at 50 °C for 120 s (IR_{50}), followed by the second stimulation for 240 s with an elevated temperature (pIRIR). At the start and the end of each IRSL measurement, discs were held at the stimulation temperature without stimulating with IR (10 s for IR_{50} and 20 s for pIRIR) to monitor and minimize any thermally stimulated signal. The integrated signal intensity over the initial 20 s of the pIRIR signal minus a background of the last 40 s was used while the initial 10 s signal minus a background of the last 30 s was used for the IR_{50}.

5.1.3 Equivalent doses

The protocol shown in Table 5.2 was applied to all samples for the D_e measurement. The IR_{50} and pIRIR D_es and ages were summarized in Table 5.3. All the D_es were obtained from the mean of 6−14 aliquots. As shown in Fig. 5.1 the D_es increase as a function of preheat and stimulation temperatures for both IR_{50} and pIRIR signals. The D_es obtained by IR_{50} are systematically smaller than those of the corresponding pIRIR signals. Besides, the pIRIR D_es increase more significantly than those of the IR_{50} D_es as a function of temperature. On average, the $pIRIR_{290}$ D_es are about 120% larger than the corresponding IR_{50} D_es. The D_es of $pIRIR_{150}$ and $pIRIR_{225}$ are about 50% larger than the corresponding IR_{50} D_es.

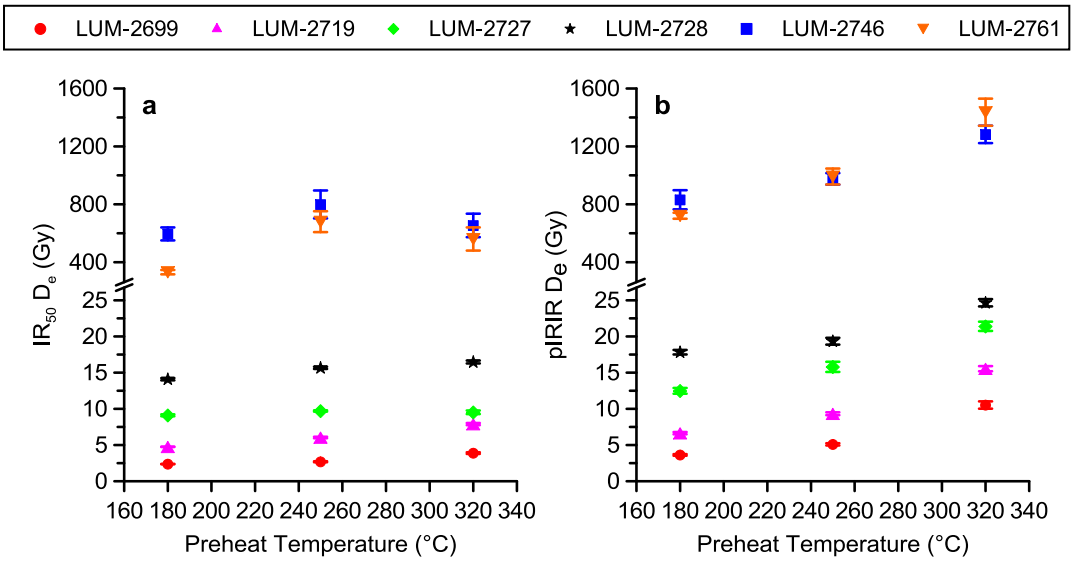

Fig. 5.1 The D_es for (a) IR_{50} and (b) pIRIR signals obtained from different preheat/stimulation temperatures.

5.1.4 Bleachability and residual dose

It is known that the feldspar luminescence signal is reset by daylight (bleaches) more slowly than the OSL from quartz (Godfrey-Smith et al., 1988). Poolton et al. (2002) first suggested that elevated-temperature IRSL bleaches more slowly than IRSL stimulated at low temperatures. Thomsen et al. (2008) have shown that there is no obvious difference in bleachability between the IR_{50} signal and the signal measured at 225 °C. However, residual doses of three modern samples for IR_{50} were ~0.5 Gy and up to 2 Gy when stimulated at 225 °C, indicating that the higher temperature IR signal is probably less bleachable in nature. Buylaert et al. (2012) observed the different bleaching rates for IR_{50} and $pIRIR_{290}$ derived from the $pIRIR_{290}$ protocol and found that the $pIRIR_{290}$ signal bleaches significantly more slowly than the IR_{50} signal and both of them bleach more slowly than the quartz OSL signal. A solar bleaching experiments reported by Li and Li (2011) confirmed this observation that the higher the stimulation temperatures, the more resistant of the IRSL signal to sunlight bleaching. More recently, Kars et al. (2014) showed that both IR and pIRIR signals continuously decrease with exposure times of up to 11 days in a solar simulator without reaching a plateau and pIRIR signals measured at increasingly higher stimulation temperatures are harder to bleach.

Table 5.3 D_es and ages of $pIRIR_{150}$, $pIRIR_{225}$ and $pIRIR_{190}$ for all the samples. The quartz ages were used as the independent age control.

Sample ID	De (Gy)						Age (ka)						Quartz age (ka)
	PH180		PH250		PH320		PH180		PH250		PH320		
	IR_{50}	$pIRIR_{150}$	IR_{50}	$pIRIR_{225}$	IR_{50}	$pIRIR_{290}$	IR_{50}	$pIRIR_{150}$	IR_{50}	$pIRIR_{225}$	IR_{50}	$pIRIR_{290}$	
2699	2.4 ± 0.03	3.6 ± 0.11	2.7 ± 0.1	5.1 ± 0.2	3.9 ± 0.1	10.5 ± 0.5	1.3 ± 0.1	2.0 ± 0.2	1.5 ± 0.1	2.8 ± 0.3	2.1 ± 0.2	5.7 ± 0.6	1.9 ± 0.2
2719	4.8 ± 0.03	6.6 ± 0.2	6.0 ± 0.1	9.3 ± 0.2	7.9 ± 0.1	15.5 ± 0.4	2.4 ± 0.2	3.3 ± 0.2	3.0 ± 0.2	4.7 ± 0.3	4.0 ± 0.3	7.8 ± 0.5	3.3 ± 0.3
2727	9.1 ± 0.1	12.5 ± 0.4	9.7 ± 0.1	15.8 ± 0.7	9.5 ± 0.2	21.4 ± 0.6	5.0 ± 0.5	6.8 ± 0.7	5.3 ± 0.5	8.7 ± 0.9	5.2 ± 0.5	11.7 ± 1.2	6.9 ± 0.9
2728	14.1 ± 0.2	17.8 ± 0.3	15.7 ± 0.2	19.3 ± 0.5	16.5 ± 0.2	24.7 ± 0.5	9.1 ± 1.1	11.5 ± 1.4	10.1 ± 1.2	12.5 ± 1.5	10.6 ± 1.3	15.9 ± 1.9	13.3 ± 2.2
2746	595 ± 45	831 ± 66	799 ± 96	976 ± 40	654 ± 81	1283 ± 60	223 ± 24	311 ± 35	299 ± 43	365 ± 32	245 ± 36	480 ± 43	>192 ± 25
2761	331 ± 15	721 ± 21	680 ± 72	992 ± 55	560 ± 80	1436 ± 94	188 ± 21	408 ± 43	385 ± 56	562 ± 64	317 ± 55	>814 ± 97	-

To investigate the bleachability of pIRIR signals, the residual doses have been measured at different temperatures using pIRIR protocols, as described in Table 5.2. The residual dose refers to the dose remaining after laboratory bleaching, as described by Kars et al. (2014). Natural aliquots (4 discs for each temperature step) were bleached with a Hönle SOL2 solar simulator for 4 h prior to the measurement. The residual doses of the IR_{50} and $pIRIR_{150}$, $pIRIR_{225}$, $pIRIR_{290}$ are shown in Fig. 5.2, upper panels.

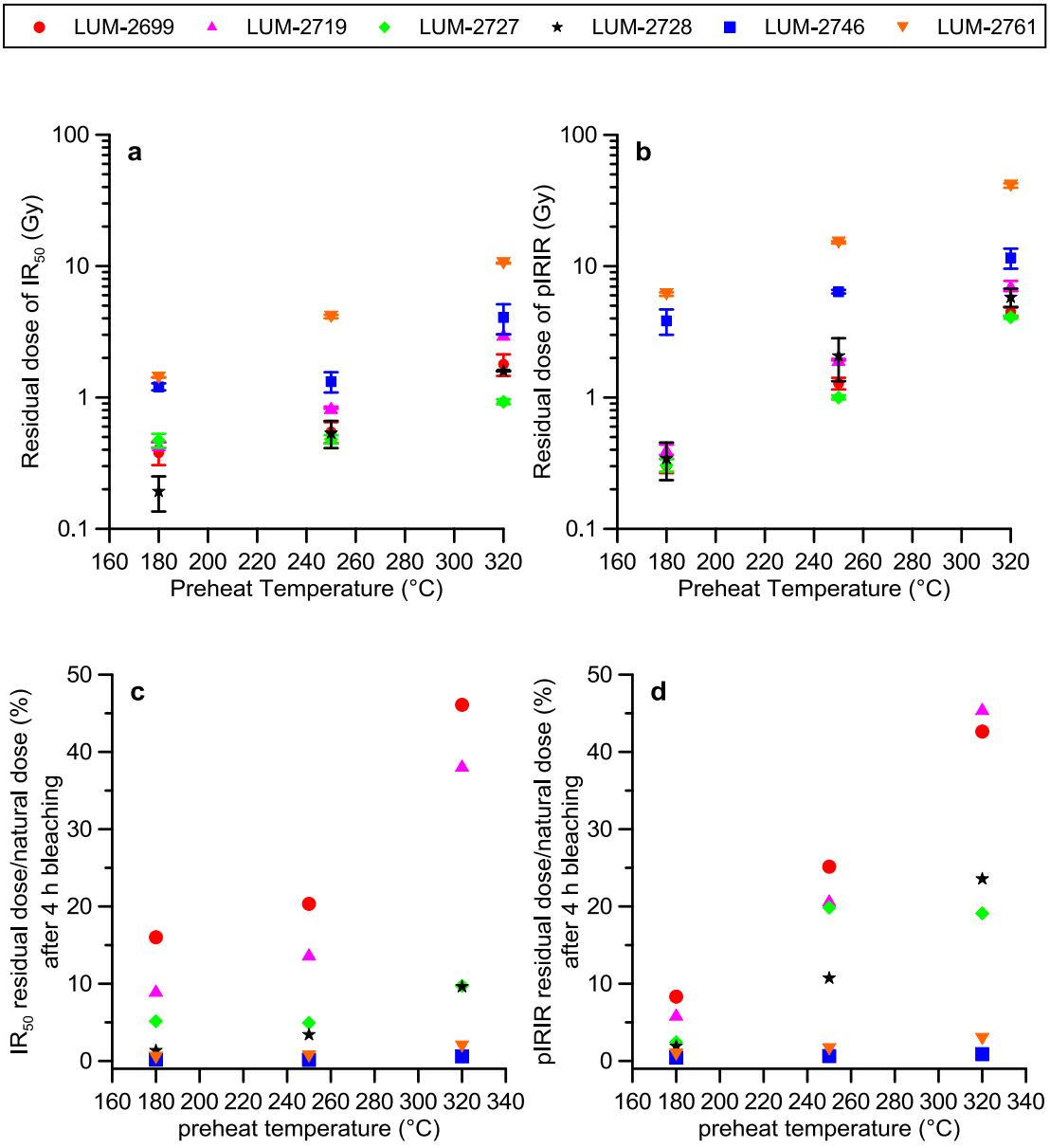

Fig. 5.2 Residual doses of the IR_{50} and pIRIR signals. (a) Residual doses of IR_{50} signals. (b) Residual doses of pIRIR signals. (c) Residual/natural dose ratio of IR_{50}. (d) Residual/natural dose ratio of pIRIR.

The residual doses of pIRIR signals consistently increase with temperature and are generally higher than that of the IR_{50} signals. The increase in the preheat temperature also induced a rising in the residual dose of the IR_{50} signals. Similar to the previous observations (e.g. Reimann et al., 2011), the signals of $pIRIR_{290}$ yielded the largest residual doses suggested that the $pIRIR_{290}$ signals are most difficult to bleach. Surprisingly, the smallest residual doses were obtained from the $pIRIR_{150}$ signal instead of the corresponding IR_{50} signals for sample LUM-2699, LUM-2719 and LUM-2727. The oldest sample (LUM-2761) yielded consistently the highest residual doses up to 41.17 ± 1.58 Gy at all temperatures for both IR_{50} and pIRIR signals among all the investigated samples (Fig. 5.2 a and b).

The proportions of the residual doses to natural doses as a function of preheat temperatures are shown in Fig. 5.2 c and d. The proportion of residual dose relative to the natural D_e generally increases as a function of preheat (stimulation) temperatures for both IR_{50} and pIRIR signals of all samples, but decreases with increasing natural D_e. After 4 h bleaching, the residual doses of both IR_{50} and pIRIR signals could still be as high as up to ~46% of the natural D_e value for young samples (LUM-2699 and LUM-2719), although the residual doses are less than ~5 Gy. In contrast, for the old samples, a residual dose to D_e ratio less than ~3% were consistently observed for both IR_{50} and pIRIR signals, although much higher residual doses (up to 41.17 ± 1.58 Gy) have been obtained compared to the young samples. The results indicate that the pIRIR signal is more bleachable at lower stimulation temperatures, consistent with recent work of Kars et al. (2014). The residual dose dramatically increased up to a higher level when more stringent preheat and stimulation temperatures were applied, which can cause significant overestimation for young samples. However, the relatively high residual dose is still insignificant when dating older sediment. We conclude that the residual dose is highly dependent on the preheat and stimulation temperatures. In several previous studies, a residual dose subtraction has been applied for the age calculation (e.g. Buylaert et al., 2013; Li et al., 2013). However, as Kars et al. (2014) suggested the residual dose should not be subtracted from the D_e as it is not a reliable measure for the remnant dose in nature.

5.1.5 Dose recovery test

A dose recovery test for feldspars was first proposed by Wallinga et al., (2000). In the previous studies, dose recovery tests were carried out either by bleaching the natural aliquots in a solar simulator (Thiel et al., 2011a, 2011b) or by natural sunlight (Stevens et al., 2011; Thiel et al., 2012) prior to beta dose irradiation and measurement or giving a dose directly in addition to the natural doses (which should be subtracted from the dose recovery ratio calculation) (Buylaert et al., 2009). In this study, the dose recovery test has been carried out after bleaching the natural aliquots in the solar simulator for 4 h. A dose close to the expected natural dose of each sample (6.7 Gy for LUM-2699; 21.6 Gy for LUM-2719, LUM-2727 and LUM-2728; 1078 Gy for LUM-2746 and LUM-2761) was given to the bleached aliquots (four aliquots per sample per protocol); this dose was then measured in the usual manner using the pIRIR protocol at different temperatures. The ratio of the measured dose to the known dose was calculated. If the SAR protocol is able to recover the known dose correctly, this ratio will be close to unity (Wintle and Murray, 2006). The respective residual doses obtained from the residual test of each sample (Fig. 5.2 a and b) were subtracted from the measured doses. The dose recovery ratios of IR_{50} and pIRIR are shown in Fig. 5.3 a and b.

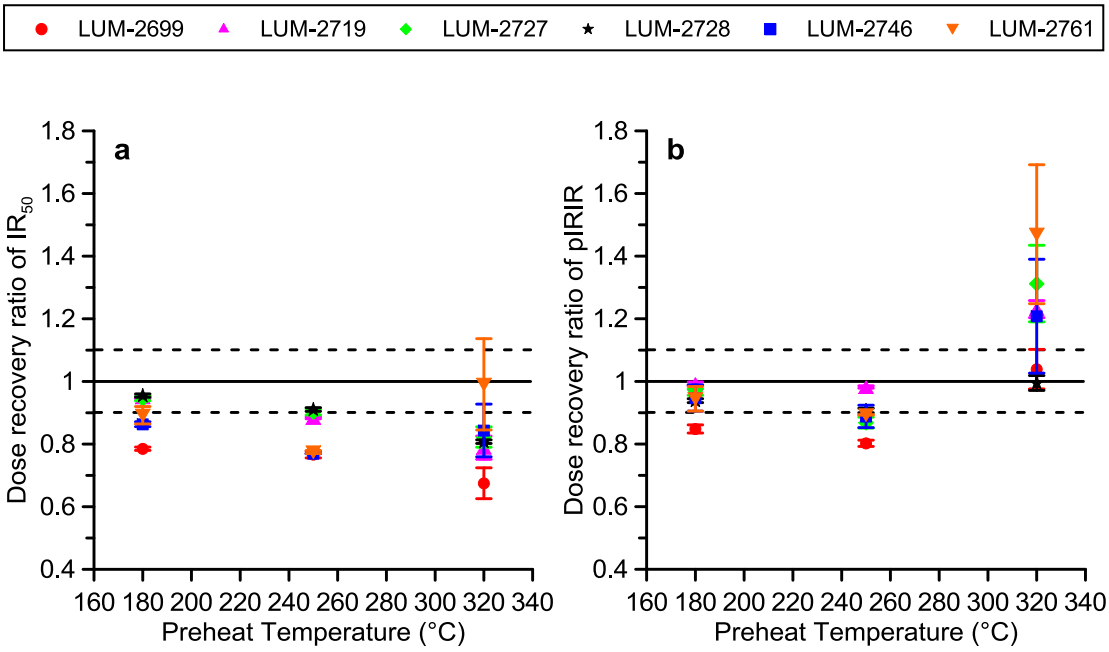

Fig. 5.3 The dose recovery ratio for (a) IR_{50} and (b) pIRIR signals obtained from different preheat/stimulation temperatures.

For all samples, the dose recovery ratios range from 0.80 ± 0.01 to 1.47 ± 0.22 for the pIRIR signals and from 0.67 ± 0.05 to 0.99 ± 0.15 for the corresponding IR_{50} signals. The uncertainties on these ratios of $pIRIR_{290}$ are relatively high due to a high inter-aliquot scatter among aliquots. For the IR_{50} signals, the dose recovery ratio is less satisfactory and most of the ratios were smaller than 0.9 which fall out of the normal range of acceptability of 0.9−1.1 for dose recovery ratios (Wintle and Murray, 2006), some even out of 20% from unity. For $pIRIR_{150}$ and $pIRIR_{225}$, the dose recovery ratios are generally within the range of acceptability of 0.9−1.1 with 1σ uncertainty except the youngest sample LUM-2699. For $pIRIR_{290}$, the dose recovery ratios of sample LUM-2699 and LUM-2728 are 1.04 ± 0.06 and 1.03 ± 0.02, respectively. The other four samples, LUM-2719, LUM-2827, LUM-2746 and LUM-2761, yield much higher dose recovery ratios of 1.23 ± 0.03, 1.31 ± 0.12 and 1.47 ± 0.22, respectively, indicating that the selected measurement condition may not be able to recover the given dose accurately at high temperatures. In previous studies, poor dose recovery ratios for the $pIRIR_{290}$ signal have been reported (e.g. Stevens et al., 2011; Thiel et al., 2011b; Buylaert et al., 2012). However, the poor dose recovery ratio does not necessary predict inaccurate D_e estimation as Buylaert et al. (2012) suggested. The dose recovery ratio might not always reflect whether the pIRIR protocol is suitable or not, although we do not have a satisfactory explanation at this stage.

5.1.6 Fading test

Anomalous fading rate is defined as *g*-value and can be measured in terms of the percentage loss of signal intensity per decade of time (Aitken, 1985; Huntley and Lamothe, 2001; Auclair et al., 2003). Huntley and Lamothe (2001) proposed a method to correct for anomalous fading based on *g* values, which has been widely used for IRSL dating. However, this fading correction method is theoretically only applicable for the young samples when the D_e is within the linear range of the dose response curve. The dose dependence of the fading rate has been also reported in few studies. Huntley and Lian (2006) observed an increase in fading rate with absorbed dose from 3.1%/decade at 175 Gy to 6.0%/decade at ~350 Gy, suggesting that the fading rate might be dependent on the size of the regenerative dose. Li and Li (2008) also reported that the fading rate increases with regenerative dose, from ~3%/decades at small doses (~30 Gy) to ~6% at

high doses (>1000 Gy). More recently, Morthekai et al. (2013) investigated the dose dependence of fading rates in feldspars and found out that the fading rate is strongly dose dependent, i.e. the higher the dose, the higher the fading rate. Jain and Ankjaergaard (2011) suggested that the pIRIR signal is dominated by the emissions from thermally assisted recombination through the band tail states and the stability of the pIRIR signal does increase with the preheat and stimulation temperatures. Thus, the higher the preheat and stimulation temperatures in the pIRIR protocol, the lower fading rate can be expected.

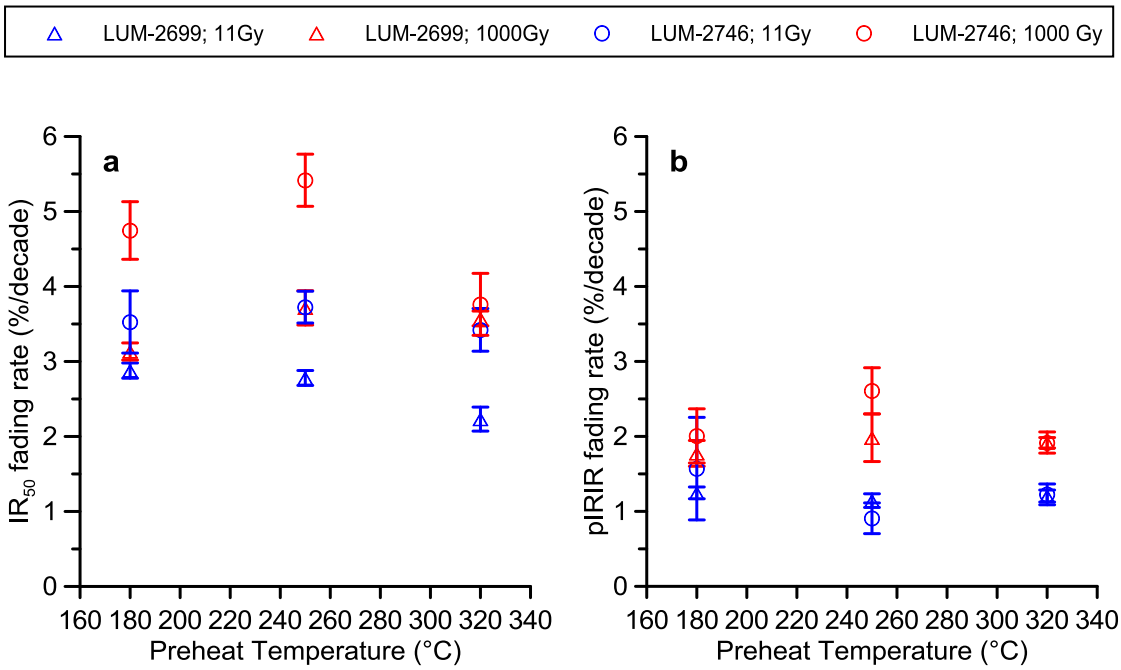

Fig. 5.4 Laboratory fading tests of (a) IR_{50} and (b) pIRIR signals obtained at different preheat/stimulation temperatures.

In order to test the preheat and stimulation temperature dependence of the fading rate, fading tests were carried out with pIRIR protocols at three different temperature combinations, i.e. $pIRIR_{150}$ with 180 °C preheat, $pIRIR_{225}$ with 250 °C preheat and $pIRIR_{290}$ with 320 °C preheat. Furthermore, two different magnitudes of irradiated dose (11 Gy and 1000 Gy) were applied to investigate whether the size of dose affects the fading rate. Two samples (LUM-2699 and LUM-2746) were selected to investigate g-values with different measurement conditions. Six natural aliquots of each sample were bleached with solar simulator for 4 h. Subsequently, the doses (11 Gy and 1000 Gy) were given to each aliquot and then measured using the pIRIR protocols following various time

delays varying from 0.09 h to 117 h. The summary of the fading test is presented in Fig. 5.4. The obtained fading rates (average of six aliquots) range from 2.2 ± 0.2 %/decade to 5.4 ± 0.4 %/decade with an average of 3.58 ± 0.25 %/decade for the IR_{50} and from 0.9 ± 0.2 %/decade to 2.6 ± 0.3 %/decade with an average of 1.63 ± 0.14 %/decade for the pIRIR. The *g*-values for the pIRIR signals are consistently lower compared to that of the IR_{50} signals. These data suggest that pIRIR fades by ~55% less than IR_{50}.

However, we have observed large variations of the fading rates among aliquots of same samples measured with the same protocol. For example, the fading rates of $pIRIR_{150}$ for sample LUM-2746 with 11 Gy given dose varied between -0.06±-1.07 %/decade and 4.37 ± 1.29 %/decade with an average of 1.57 ± 0.68 %/decade. Lamothe and Auclair (1999) found that individual grains of a sample can have a very wide range of fading rates. Such variability was also inferred earlier by Huntley (1997) and Huntley and Lian (2006). The L_x/T_x plots as a function of delay time for a representative aliquot of sample LUM-2699 are shown in Fig. 5.5. When a given dose of 11 Gy was applied, the $pIRIR_{150}$, $pIRIR_{225}$ and $pIRIR_{290}$ signals yield fading rates of 0.93 ± 0.86 %/decade, 0.90 ± 0.86 %/decade and 1.14 ± 0.87 %/decade, respectively. No clear relationship was observed between the fading rate of pIRIR signals and the preheat and stimulation temperatures. The corresponding IR_{50} signals gave fading rates of 2.75 ± 0.80 %/decade, 2.66 ± 0.80 %/decade and 2.11 ± 0.80 %/decade, which are slightly smaller as the preheat temperature increased. When the given dose was raised to 1000 Gy, the pIRIR signals yield fading rates between 1.30 ± 0.86 %/decade and 1.78 ± 0.86 %/decade. The corresponding IR_{50} signals yield fading rates between 2.66 ± 0.85 %/decade and 3.51 ± 0.86 %/decade. Neither IR_{50} nor pIRIR signals show clear decreasing trends in fading rate as a function of increasing preheat and stimulation temperatures. General increases have been observed in the fading rates for both IR_{50} and pIRIR signals when the given dose rose from 11 Gy to 1000 Gy. Our result confirms the observation by Huntley and Lian (2006) and Li and Li (2008) that for both IR_{50} and pIRIR signals, the larger is the given dose, the higher is the fading rate. However, the increments of the fading rate were not as significant as in the previous studies.

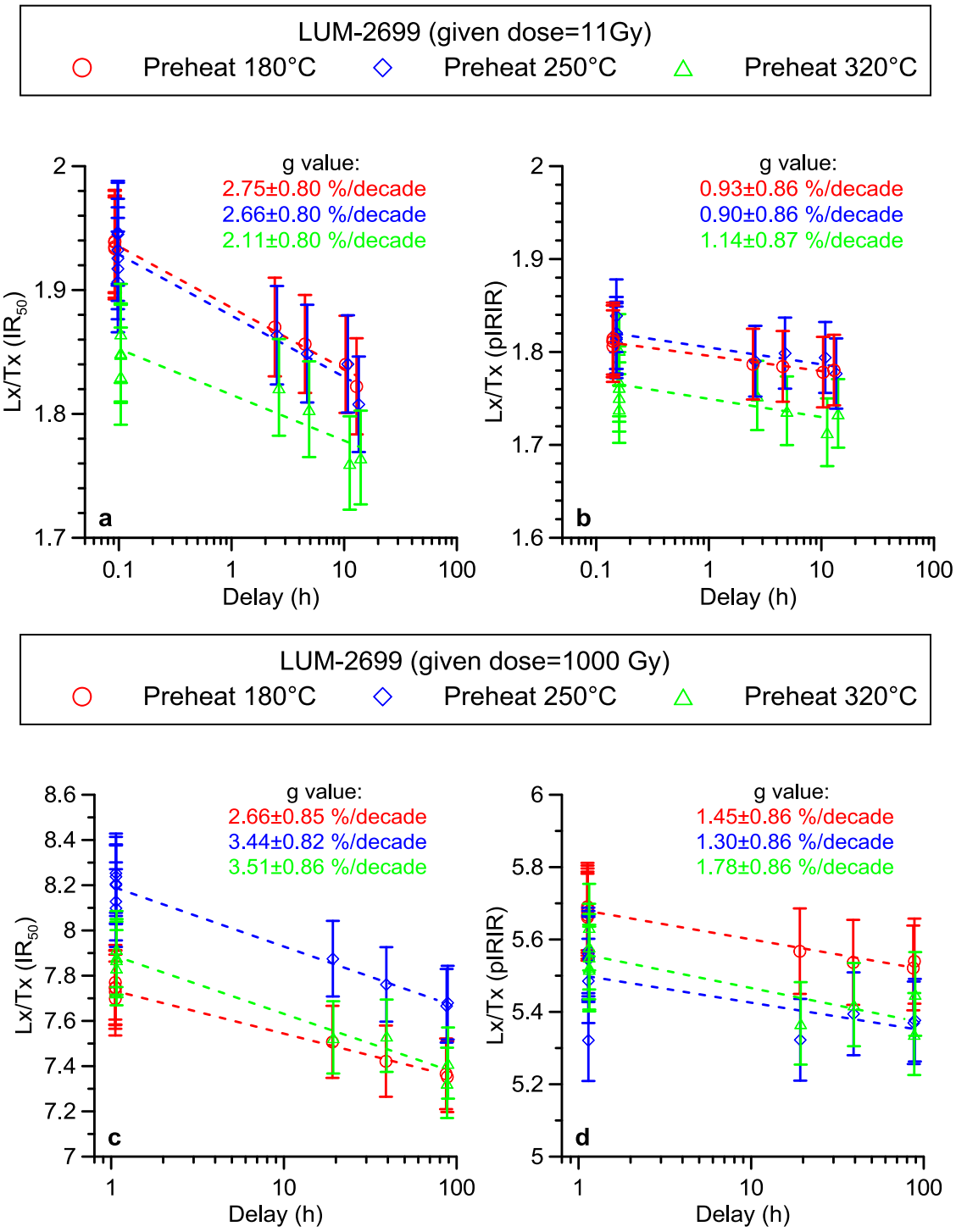

Fig. 5.5 Fading rate (*g*-value) determination of a representative aliquot of sample LUM-2699. (a) *g*-values of IR_{50} signals with 11 Gy given dose. (b) *g*-values of pIRIR signals with 11 Gy given dose. (c) g-values of IR_{50} signals with 1000 Gy given dose. (d) *g*-values of pIRIR signals with 1000 Gy given dose.

A sample in field saturation was considered to be in a state of dynamic equilibrium between electron filling and escaping (Lamothe et al., 2003; Huntley and Lian, 2006; Li and Li, 2008). For the conventional IRSL signals, the field saturation is typically found to be 50−70 % of laboratory saturation and a higher fading rate can be expected for a field saturated sample (Huntley and Lian, 2006). The field saturation of pIRIR signal which is equal to the laboratory saturation has been first observed by Thiel et al. (2011a) by applying the $pIRIR_{290}$ protocol to the polymineral fine grains from loess. They concluded therefore that the $pIRIR_{290}$ signals do not fade in nature. They also argued that the fading rates (~1 %/decade) measured in the laboratory using a pIRIR protocol may be a laboratory artefact and thus do not represent the natural process. This observation has been later confirmed by other studies (e.g. Thomsen et al., 2011; Buylaert et al., 2012; Murray et al., 2014). Buylaert et al. (2012) showed that fading uncorrected $pIRIR_{290}$ ages agree very well with independent age control for a world-wide set of samples, although fading rates of ~1−1.5 %/decade were observed by the laboratory fading experiments.

The sand-sized K-feldspar fractions of sample LUM-2761 were measured with the $pIRIR_{150}$, $pIRIR_{225}$ and $pIRIR_{290}$ protocols up to the maximum regeneration dose of 3330 Gy to build up dose response curves to the saturation level. The natural intensity of this sample should be consistent with the laboratory saturation level if there is no fading in nature and the signals are thermally stable. The test dose of ~56 Gy was used. The dose response curves have been fitted with a single saturating exponential function (Fig. 5.6). Wintle and Murray (2006) suggested $D_e<2D_0$ as a limit for reliable age estimates and the OSL signal should be about 15% below the saturation value obtained in the laboratory dose response curve. The saturation ratios for the IR_{50} signals were all below 74% of the laboratory saturation level, for example the IR_{50} signal with 180 °C preheat only showed 3% of saturation, confirming that this signal fades significantly in nature. The natural D_es for $pIRIR_{150}$, $pIRIR_{225}$ and $pIRIR_{290}$ are 754 ± 32 Gy, 1046 ± 61 Gy and 1632 ± 187 Gy, whose corresponding $2D_0$ values are 1235 Gy, 1133 Gy and 1093 Gy, respectively. The saturation rate of the $pIRIR_{290}$ natural signal is 96% (Fig. 5.6) whereas the natural signal of $pIRIR_{225}$ and $pIRIR_{150}$ signals are 83% and 73% of saturation, respectively. These data suggest that for $pIRIR_{290}$ signals the field saturation is close to the laboratory saturation (e.g. Murray et al., 2014; Schmidt et al., 2014) and therefore the $pIRIR_{290}$ signals suffer negligible anomalous fading in nature. However, this contradicts with the measured fading rate of pIRIR signals of ~1−2 %/decade. Furthermore, the $pIRIR_{150}$ and $pIRIR_{225}$

signals showed a much lower saturation rate than that of $pIRIR_{290}$, although all pIRIR fading rates are very similar. This observation confirmed that the laboratory measured fading rates may not represent the fading rates in nature. Therefore, the fading correction based on the measured fading rate may be problematic.

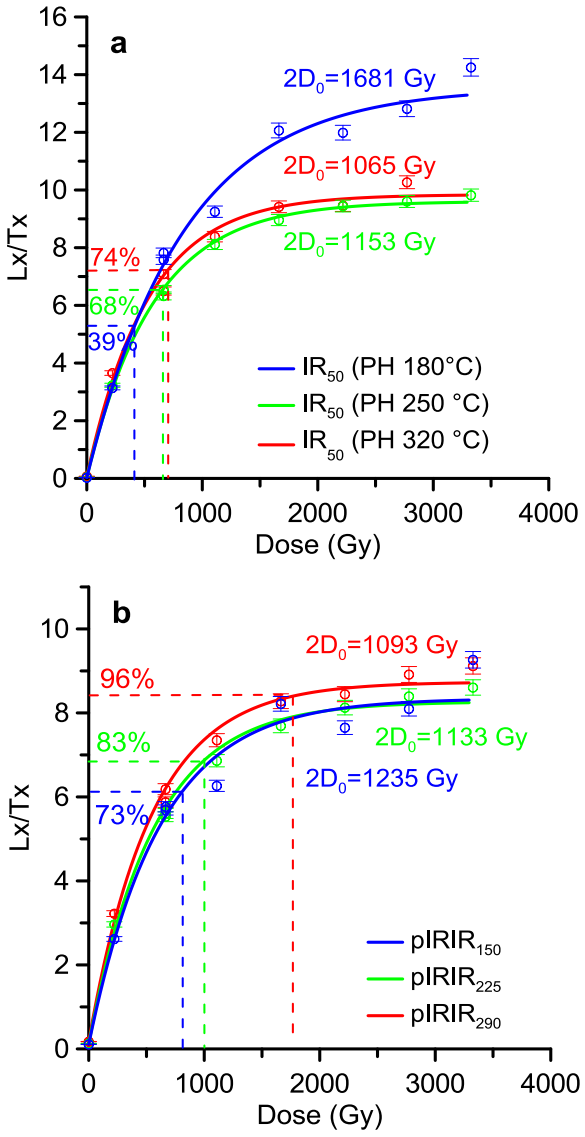

Fig. 5.6 Natural signals and dose response curves for (a) IR_{50} and (b) pIRIR signals obtained from sample LUM-2761. The dose response curve has been fitted with a single saturating exponential function: $I=A\ (1\text{-exp}\ [-(D)/D_0])$. The saturation rate is calculated by dividing L_n/T_n by A.

5.1.7 Comparison of pIRIR ages with independent age control

The fading uncorrected ages of IR_{50}, $pIRIR_{150}$, $pIRIR_{225}$ and $pIRIR_{290}$ are plotted against the corresponding quartz ages (except samples LUM-2746 and LUM-2761) in Fig. 5.7.

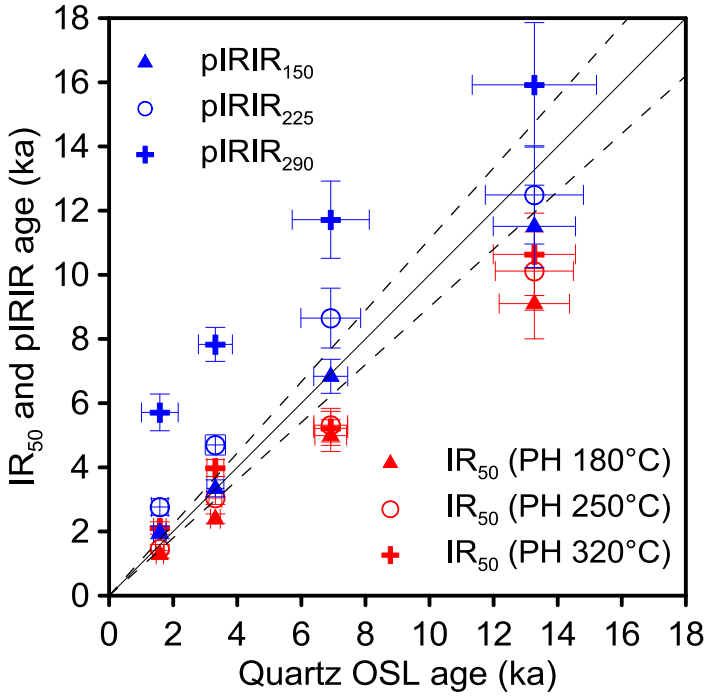

Fig. 5.7 Comparison between the IR_{50} and pIRIR ages and the corresponding quartz OSL ages. The solid line is the 1:1 line and the dashed lines represent ±10% deviation.

The $pIRIR_{150}$ ages show the best agreement with the quartz ages for the samples younger than 8 ka. The higher temperature pIRIR ages overestimate the expected ages for these young samples which probably due to the relatively high residual dose. This suggests that the $pIRIR_{150}$ signals can be used to date young materials (Holocene samples) without any fading correction and/or residual subtraction. For older samples the residual dose would gradually become unimportant, and the effect of anomalous fading would become more significant. Li and Li (2011) showed that a small anomalous fading rate resulted in considerable age underestimations and they therefore suggested that higher elevated stimulation temperatures (>200 °C) are more preferable for dating older samples (>130 ka). Unfortunately, we have no independent age control for such old samples (LUM-2746 and LUM-2761) in our study, so it is not possible to determine which

stimulation temperature gives reliable ages in a wider age range. However, it is noteworthy that the $pIRIR_{150}$ signal starts to slightly underestimate the quartz age at ~13 ka (LUM-2728) and the age obtained by $pIRIR_{225}$ fits better to the independent age than $pIRIR_{150}$. We suggest employing a preheat plateau test with a range of different preheat and stimulation temperatures might be necessary for selecting a suitable temperature combination for the pIRIR protocol. More data are also needed to further investigate the temperature dependency of pIRIR signals.

5.1.8 Conclusions

In this paper we have tested how the preheat and stimulation temperatures affect the luminescence characteristics of pIRIR signals as well as its corresponding IR_{50} signals from feldspar. The variations of residual doses, fading rates and the D_es as a function of preheat and stimulation temperatures were investigated. The results indicate that:

1) The residual doses after 4 h solar simulator bleach are highly dependent on the preheat and stimulation temperatures and variable from sample to sample. They systematically increase with increasing preheat and stimulation temperatures up to ~41 Gy. The pIRIR signals generate higher residual doses than those of the IR_{50} signals. A clear trend of PH180 °C< PH250 °C < PH320 °C in the residual doses has been observed for both IR_{50} and pIRIR signals.

2) The measured fading rates of the pIRIR signal are consistently lower compared to those of the IR_{50} signals and fade by ~55% less than IR_{50}. The fading rates for both IR_{50} and pIRIR signals did not show obvious temperature dependency. General increases of fading rate have been observed in the fading rates for both IR_{50} and pIRIR signals when higher given dose was applied in the fading test.

3) Although the measured fading rates for $pIRIR_{150}$, $pIRIR_{225}$ and $pIRIR_{290}$ are all similar, distinct differences in saturation ratio have been observed for both IR_{50} and pIRIR signals for a field saturated sample and only the $pIRIR_{290}$ signal reached field saturation. This indicates that the laboratory-measured fading rates might be erroneous.

4) By comparing the pIRIR ages with independent age controls, the pIRIR protocol is able to yield reliable ages without any correction, i.e. fading correction and residual subtraction. The $pIRIR_{150}$ ages show the best agreement with the independent age controls for the samples younger than 8 ka. For older samples, higher preheat and stimulation temperatures have to be used to extract stable pIRIR signals.

Acknowledgements. − This research has been supported by a DAAD (Deutscher Akademischer Austauschdienst) PhD scholarship and the Leibniz Institute for Applied Geophysics (LIAG), Hannover. Gudrun Drewes, Sabine Mogwitz, Petra Posimowski and Sonja Riemenschneider (technicians of LIAG-Section S3) are thanked for their technical help during the preparation and measurement of luminescence and gamma samples.

References

Aitken, M.J., 1985. Thermoluminescence Dating. Academic Press, London.

Alappat, L., Vink, A., Tsukamoto, S., Frechen, M. 2010. Establishing the Late Pleistocene-Holocene sedimentation boundary in the southern North Sea using OSL dating of shallow continental shelf sediments. Proceedings of the Geologists' Association 121, 43–54.

Auclair, M., Lamothe, M., Huot, S., 2003. Measurement of anomalous fading for feldspar IRSL using SAR. Radiation Measurements 37, 487−492.

Balescu, S., Lamothe, M., Mercier, N., Huot, S., Balteanu, D., Billard, A., Hus, J., 2003. Luminescence chronology of Pleistocene loess deposits from Romania: testing methods of age correction for anomalous fading in alkali feldspars. Quaternary Science Reviews 22, 967−973.

Balescu, S., Ritz, J-F., Lamothe, M., Auclair, M., Todbileg, M., 2007. Luminescence dating of a gigantic palaeolandslide in the Gobi-Altay Mountains, Mongolia. Quaternary Geochronology 2, 290−295.

Blair, M.W., Yukihara, E.G., McKeever, S.W.S., 2005. Experiences with single- aliquot OSL procedures using coarse-grain feldspars. Radiation Measurements 39: 361−374.

Buylaert, J.P., Murray, A. S., Thomsen, K. J. & Jain, M., 2009. Testing the potential of an elevated temperature IRSL signal from K-feldspar. Radiation Measurements 44, 560−565.

Buylaert, J.P., Jain, M., Murray, A.S., Thomsen, K.J., Thiel, C., Sohbati, R., 2012. A robust feldspar luminescence dating method for Middle and Late Pleistocene sediments. Boreas 41, 435−451.

Buylaert, J.P., Murray, A.S., Gebhardt, A.C., Sohbati, R., Ohlendorf, C., Thiel, C., Wastegårde, S., Zolitschka, B., The PASADO Science Team, 2013. Luminescence dating of the PASADO core 5022-1D from Laguna Potrok Aike (Argentina) using IRSL signals from feldspar. Quaternary Science review 71, 70−80.

Fu, X., Li, S.H., 2013.A modified multi-elevated-temperature post-IR IRSL protocol for dating Holocene sediments using K-feldspar. Quaternary Geochronology 17, 44−45.

Godfrey-Smith, D. L., Huntley, D. J., Chen, W. H., 1988. Optically dating studies of quartz and feldspar sediment extracts. Quaternary Science Reviews 7, 373−380.

Guérin, G., Mercier, N., Adamiec, G., 2011. Dose-rate conversion factors: update. Ancient TL 29, 5−8.

Huot, S., Lamothe, M., 2003. Variability of infrared stimulated luminescence properties from fractured feldspar grains. Radiation Measurements 37, 499−503.

Huntley, D.J., 1997. A proposal for dealing with anomalous fading. Ancient TL 15: 28−29.

Huntley, D. J. & Baril, M. R., 1997. The K content of the K-feldspars being measured in optical dating or in thermoluminescence dating. Ancient TL 15, 11−13.

Huntley, D.J., Hancock, R.G.V., 2001. The Rb contents of the K-feldspars being measured in optical dating. Ancient TL 19, 43−46.

Huntley, D.J., Lamothe, M., 2001. Ubiquity of anomalous fading in K-feldspars and the measurement and correction for it in optical dating. Canadian Journal of Earth Sciences 38, 1093−1106.

Huntley, D. J., Lian, O. B., 2006. Some observations on tunneling of trapped electrons in feldspars and their implications for optical dating. Quaternary Science Reviews 25, 2503−2512.

Jain, M., Ankjaergaard, C., 2011. Towards a non-fading signal in feldspar: insight into charge transport and tunnelling from time-resolved optically stimulated luminescence. Radiation Measurements 46, 292−309.

Kars, R. H., Wallinga, J., Cohen, K. M., 2008. A new approach towards anomalous fading correction for feldspar IRSL dating -tests on samples in field saturation. Radiation Measurements 43, 786-790.

Kars, R. H., Reimann, T., Ankjærgaard, C., Wallinga, J., 2014. Bleaching of the post-IR IRSL signal: new insights for feldspar luminescence dating. Boreas 43, 780−791.

Lamothe, M., Auclair, M., 1999. A solution to anomalous fading and age shortfalls in optical dating of feldspar minerals. Earth and Planetary Science Letters 171, 319−323.

Lamothe, M., Auclair, M., Hamzaoui, C., Huot, S., 2003. Towards a prediction of longterm anomalous fading of feldspar IRSL. Radiation Measurements 37, 493−498.

Li, B., Li, S. H., 2008. Investigations of the dose-dependent anomalous fading rate of feldspar from sediments. Journal of Physics D: Applied Physics 41, 225502 (15pp).

Li, B., Li, S. H., 2011. Luminescence dating of K-feldspar from sediments: a protocol without anomalous fading correction. Quaternary Geochronology 6, 468−479.

Li, B., Li, S. H., 2012. Luminescence dating of Chinese loess beyond 130 ka using the non-fading signal from K-feldspar. Quaternary Geochronology 10, 24−31.

Li, B., Jacobs, Z., Roberts, R.G., Li, S.H., 2014. Review and assessment of the potential of post-IR IRSL dating methods to circumvent the problem of anomalous fading in feldspar luminescence. Geochronometria 41, 178−201.

Li B, Roberts RG and Jacobs Z, 2013. On the dose dependency of the bleachable and non-bleachable components of IRSL from K-feldspar: improved procedures for the dating of Quaternary sediments. Quaternary Geochronology 17, 1−13.

Madsen, A. T., Buylaert, J. P., Murray, A. S., 2011. Luminescence dating of young coastal deposits from New Zealand using feldspar. Geochronometria 38, 378−390.

Mejdahl, V., 1979. Thermoluminescence dating: beta attenuation in quartz grains. Achaeometry 21, 61−73.

Morthekai, P., Jain, M., Gach, G., Elema, D. R., Prip, H., 2013. Dependence of (anomalous) fading of infra-red stimulated luminescence on trap occupancy in feldspars. Journal of Luminescence 143, 704−709.

Murray, A. S., Marten, R., Johnston, A., Martin, P., 1987. Analysis for naturally occuring radionuclides at environmental concentrations by gamma spectrometry. Journal of Radioanalytical and Nuclear Chemistry 115, 263−288.

Murray, A., Wintle, A., 2000. Luminescence dating of quartz using an improved single-aliquot regenerative-dose protocol. Radiation Measurements 32, 57−73.

Murray, A. S., Buylaert, J. P., Thomsen, K. J., Jain, M., 2009. The effect of preheating on the IRSL signal from feldspar. Radiation Measurements 44, 554−559.

Murray, A.S., Schmidt, E.D., Stevens, T., Buylaert, J.-P., Marković, S.B., Tsukamoto, S., Frechen, M., 2014. Dating Middle Pleistocene loess from Stari Slankamen (Vojvodina, Serbia)-Limitations imposed by the saturation behavior of an elevated temperature IRSL signal. Catena 117, 34−42.

Poolton, N.R.J., Ozanyan, K.B., Wallinga, J., Murray, A.S., Bøtter-Jensen, L., 2002. Electrons in feldspar II: a consideration of the influence of conduction band-tail states on luminescence processes. Physics and Chemistry of Minerals 29, 217−225.

Prescott, J. R. & Hutton, J. T., 1994. Cosmic ray contributions to dose rates for luminescence and ESR dating: large depths and long-term variations. Radiation Measurements 23, 497−500.

Reimann, T., Tsukamoto, S., Naumann, M., Frechen, M., 2011. The potential of using feldspars for optical dating of young coastal sediments−a test case from Darss-Zingst peninsula. Quaternary Geochronology 6, 207−222.

Reimann, T., Tsukamoto, S., 2012. Dating the recent past (<500 years) by post-IR IRSL feldspar – Examples from the North Sea and Baltic Sea coast. Quaternary Geochronology 10, 180−187.

Schmidt, E.D., Tsukamoto,S., Frechen, M., Murray, A.S., 2014. Elevated temperature IRSL dating of loess sections in the East Eifel region of Germany. Quaternary International 334-335, 141−154.

Stevens, T., Markovic, S.B., Zech, M., Hambach, U., Sumegi, P., 2011. Dust deposition and climate in the Carpathian Basin over an independently dated last glacial-interglacial cycle. Quaternary Science Reviews 30, 662−681.

Thomsen, K. J., Murray, A. S., Jain, M., Bøtter-Jensen, L., 2008. Laboratory fading rates of various luminescence signals from feldspar-rich sediment extracts. Radiation Measurements 43, 1474−1486.

Thomsen, K.J., Murray, A.S., Jain, M., 2011. Stability of IRSL signal from sedimentary K-feldspar samples. Geochronometria 38, 1−13.

Thiel, C., Coltorti, M., Tsukamoto, S., Frechen, M., 2010. Geochronology for some key sites along the coast of Sardinia (Italy). Quaternary International 222, 36−47.

Thiel, C., Buylaert, J. P., Murray, A., Terhorst, B., Hofer, I., Tsukamoto, S., Frechen, M., 2011a. Luminescence dating of the Stratzing loess profile (Austria)-Testing the potential of an elevated temperature post-IR IRSL protocol. Quaternary International 234, 23−31.

Thiel, C., Buylaert, J.P., Murray, A.S., Tsukamoto, S., 2011b. On the applicability of post-IR IRSL dating to Japanese loess. Geochronometria 38, 369−378.

Thiel, C., Buylaert, P., Murray, A., Elmejdoub, N., Jedoui, Y., 2012. A comparison of TT-OSL and post-IR IRSL dating of coastal deposits on Cap Bon peninsula, north-eastern Tunisia. Quaternary Geochronology 10, 209−217.

Tsukamoto, S., Denby, P.M., Murray, A.S., Botter-Jensen, L., 2006. Time-resolved luminescence from feldspars: new insight into fading. Radiation Measurements 41, 790−795.

Vasiliniuc, S., Vandenberghe, D.A.G., Timar-Gabor, A., Panaiotu, C., Cosma, C., van den Haute, P., 2012. Testing the potential of elevated temperature post-IR IRSL signals for dating Romanian loess. Quaternary Geochronology 10, 75−80.

Visocekas, R., 1985. Tunneling radiative recombination in labradorite: its association with anomalous fading of thermoluminescence. Nuclear Tracks and Radiation Measurements 10, 521−529.

Visocekas, R., Spooner, N. A., Zink, A., Blanc, P., 1994. Tunnel afterglow, fading and infrared-emission in thermoluminescence of feldspars. Radiation Measurement 23, 377–85.

Wacha, L., Frechen, M., 2011. The geochronology of the "Gorjanovic loess section" in Vukovar, Croatia. Quaternary International 240, 87−99.

Wallinga, J., Murray, A., Duller, G., 2000. Underestimation of equivalent dose in single-aliquot optical dating of feldspars caused by preheating. Radiation Measurements 32, 691−695.

Wallinga, J., Murray, A.S., Duller, G.A.T., Törnqvist, T.E., 2001. Testing optically stimulated luminescence dating of sand-sized quartz and feldspar from fluvial deposits. Earth and Planetary Science Letters 193, 617−630.

Wintle, A. G., 1973. Anomalous fading of thermoluminescence in mineral samples. Nature 245, 143−144.

Wintle, A.G., Murray, A.S., 2006. A review of quartz optically stimulated luminescence characteristics and their relevance in single-aliquot regeneraton dating protocols. Radiation Measurements 41, 369−391.

Zhang, J. R., Tsukamoto, S., Grube, A., Frechen, M., 2014. OSL and ^{14}C chronologies of a coastal sedimentary record (Garding-2 core) from the German North Sea coast during the last deglaciation and Holocene. Boreas 43, 856−868.

5.2 D_e plateau and its implications for post-IR IRSL dating of polymineral fine grains

Jingran Zhang[1], Sumiko Tsukamoto[1], Veit Nottebaum[2], Frank Lehmkuhl[2], Manfred Frechen[1]

[1]Leibniz Institute for Applied Geophysics (LIAG), Stilleweg 2, 30655 Hannover, Germany

[2]Department of Geography, RWTH Aachen University, Templergraben 55, 52056 Aachen, German

Quaternary Geochronology, Vol. 30, pp. 147-153.

DOI: http://www.sciencedirect.com/science/article/pii/S1871101415000163

Abstract

In this study, the behaviour of post-IR IRSL (pIRIR) signals from polymineral fine grains (4-11 um) has been systematically investigated under various preheat and stimulation conditions, by using four loess samples from the Qilian Shan in northwestern China. We varied the preheat temperatures from 180 °C to 340 °C with a 20 °C increment and the pIRIR stimulation temperature tracks the preheat temperature by −30 °C, following an IR stimulation at 50 °C (IR_{50}). All pIRIR signals fade much less than the IR_{50} signals and the measured fading rates, ranging between 1.50 ± 0.15 %/decade and −0.29 ± 0.73%/decade, display a general but slight decreasing trend with increasing preheat and stimulation temperatures. For both IR_{50} and pIRIR signals, the residual doses gradually increase towards the higher preheat and stimulation temperatures, indicating that both signals become harder to bleach at higher temperatures. A significant increase in the pIRIR D_es is observed as a function of preheat (stimulation) temperature. A D_e plateau appears between 240 °C and 280 °C preheat temperatures, regardless of expected ages obtained from the quartz D_e from the same samples. After the fading correction, there is a general agreement between the pIRIR and IR_{50} ages obtained from the preheat temperatures

below 260 °C. This may imply that only the lower temperature pIRIR signals were fully bleached before deposition for our samples.

Key words: Post-IR IRSL dating; D_e plateau; Polymineral fine grains; Luminescence intensity; Anomalous fading; Residual dose.

5.2.1 Introduction

The infrared stimulated luminescence (IRSL) dating of feldspar has long been problematic due to one of the intrinsic properties of feldspar minerals known as "anomalous fading" (Wintle, 1973), which is responsible for age underestimation. Thomsen et al. (2008) reported that the post-IR IRSL (pIRIR) signal at an elevated temperature has a lower fading rate compared with the traditional IRSL measured at 50 °C. Thereafter, pIRIR dating has become one of the most widely used techniques in luminescence dating. The pIRIR dating method has been tested by many researchers using different materials under various measurement conditions, demonstrating a great potential of feldspars for dating old samples. The pIRIR signals are most commonly measured after stimulating at 50 °C either at 225 °C ($pIRIR_{225}$, e.g. Buylaert et al., 2009; Alappat et al., 2010; Buylaert et al., 2011; Wacha and Frechen, 2011; Lowick et al, 2012; Sohbati et al., 2012) or at 290 °C ($pIRIR_{290}$, e.g. Thiel et al., 2011a, 2011b, 2012; Stevens et al., 2011; Schmidt et al., 2014; Murray et al., 2014); these protocols are also called as two-step pIRIR. It is noteworthy that Thiel et al. (2011a) observed that the natural $pIRIR_{290}$ signal was in field saturation, suggesting that the $pIRIR_{290}$ signal does not fade in nature. Meanwhile, based on the observation that the fading component in IRSL signal can be progressively eliminated using increasing higher IR stimulation temperatures, Li and Li (2011, 2012) proposed a multi-elevated-temperature pIRIR protocol (MET-pIRIR) as an alternative to the two-step pIRIR protocol for dating feldspar, which reported being able to give reliable age estimation for the Chinese loess up to ~300 ka.

The athermal stability of the pIRIR signal is expected to increase with the preheat and stimulation temperatures (Jain and Ankjærgaard, 2011). High preheat and stimulation temperatures can significantly remove the unstable component and extract less or non-fading feldspar signals compared to the lower temperature IRSL. On the other hand,

signals stimulated at higher temperature become harder to bleach (Buylaert et al., 2009; Li and Li, 2011; Kars et al., 2014a) resulting in considerable residual doses. To date young samples (e.g. Holocene), Reimann et al. (2011) proposed a modified two-step pIRIR protocol using 180 °C stimulation temperature ($pIRIR_{180}$) with preheat temperature of 200 °C for Holocene samples, which is able to significantly reduce the residual dose (<1 Gy) without losing its major advantage of reducing the anomalous fading rate. Subsequently, a $pIRIR_{150}$ (preheat at 180 °C) protocol was also successfully used to date the Holocene samples from various sedimentary environments (e.g. Madsen et al., 2011; Reimann and Tsukamoto, 2012; Long et al., 2014; Long et al., 2015). A modified lower temperature MET-pIRIR protocol has been also proposed by Fu and Li (2013) and applied to date Holocene samples without fading correction. For dating sediments with different age ranges using pIRIR, it is of crucial importance to find a balance between sufficient signal stability and a minimized contribution of residual dose (Kars et al., 2014a). In the MET-pIRIR protocol, a D_e plateau generally presents for both high and lower temperatures which has been explained as an indicator that non-fading signals have been obtained while signals were still bleachable (Fu and Li, 2013; Li et al., 2014). However, for the two-step pIRIR protocol there is still no widely used diagnostic tools to select preheat and stimulation temperatures which are suitable for different dating ranges.

In this study, we aim to investigate the behaviour of the pIRIR signal (as well as the corresponding IR_{50} signal) from polymineral fine grains under a wide range of preheat and stimulation temperatures. A series of measurements, such as the dose recovery, fading and bleachability tests are carried out to examine the pIRIR characteristics. Finally a preheat plateau test is conducted. The ages obtained from a variety of preheat and pIRIR stimulation conditions are compared with quartz optically stimulated luminescence (OSL) ages from the same samples (Zhang et al., 2015). The reliability of the pIRIR "plateau" ages and the possible explanations are discussed.

5.2.2 Samples and experimental details

Four loess samples from Qilian Shan (Northwestern China) were selected for this study: sample LUM-2941, LUM-2940, LUM-2938 and LUM-2952. These samples have been dated using fine-grained quartz minerals with the OSL single-aliquot regenerative-dose

(SAR) protocol, which gave ages of 6.3 ± 0.4 ka, 9.2 ± 0.6 ka, 43.1 ± 3.5 ka and 80.8 ± 5.8 ka, respectively (Zhang et al., 2015). As the quartz OSL signal of sample LUM-2952 might underestimate the real age of the sample (Zhang et al., 2015), 80.8 ± 5.8 ka should be considered as a minimum age of this sample. No other age control is available for these samples. The dosimetric data (Table 5.4) including U, Th, K contents of these samples have been previously presented in Zhang et al. (2015). An a-value of 0.08 ± 0.02 was used according to Rees-Jones et al. (1995) and Frechen et al. (2001) for polymineral fine grains. The cosmic dose rate was calculated according to Prescott and Hutton (1994). The water contents for all samples were estimated to be 5 ± 5%.The calculated dose rates of polymineral fine grains for the four samples (LUM-2941, LUM-2940, LUM-2938 and LUM-2952) are 4.89 ± 0.26 Gy/ka, 4.83 ± 0.26 Gy/ka, 4.60 ± 0.24 Gy/ka and 4.08 ± 0.20 Gy/ka, respectively. Thus, the expected D_es for polymineral fine grains are 31 ± 1 Gy, 46 ± 5 Gy, 198 ± 12 Gy and >330 ± 17 Gy, respectively, according to the corresponding quartz OSL ages.

Table 5.4 The U, Th, K content and the calculated dose rate of the samples under study.

Lab ID	Depth (m)	Uranium (ppm)	Thorium (ppm)	K (%)	Environmental dose rate (Gy/ka)	Cosmic dose rate (Gy/ka)	Total dose rate (Gy/ka)
LUM-2941	0.5	3.39 ± 0.17	11.67 ± 0.59	2.03 ± 0.13	4.58 ± 0.26	0.32 ± 0.03	4.89 ± 0.26
LUM-2940	0.9	3.32 ± 0.17	11.84 ± 0.60	1.97 ± 0.12	4.52 ± 0.25	0.32 ± 0.03	4.83 ± 0.26
LUM-2938	2	3.03 ± 0.15	10.67 ± 0.54	1.98 ± 0.13	4.28 ± 0.24	0.31 ± 0.03	4.60 ± 0.24
LUM-2952	0.47	2.42 ± 0.04	10.22 ± 0.10	1.69 ± 0.02	3.73 ± 0.20	0.35 ± 0.04	4.08 ± 0.20

The fine-grained fraction (4-11 μm) of the samples was extracted according to Stokes' Law, following the description of Frechen et al. (1996). The separated 4-11 μm polymineral fine grains were then mounted on aluminum discs (diameter 9.7 mm) from a suspension in distilled water (2 mg fine grains per disc) for measuring. The luminescence measurements were carried out on an automated Risø TL/OSL DA15 reader with an attached $^{90}Sr/^{90}Y$ beta source. The luminescence signal was stimulated with infrared diodes emitting at 870 nm and detected through a combination of Corning 7-59 and Schott BG39 filters. A modified SAR protocol for pIRIR dating (e.g. Buylaert et al., 2009; Thiel et al., 2011a; Reimann et al., 2011) (Table 5.5) has been applied for all measurements.

Table 5.5 The modified single-aliquot-regenerative-dose (SAR) protocol for post-IR IRSL dating.

Step	Measurement	Observation	Remark
1	Given dose, D_i (i=0,1,2,3…)		
2	Preheat for 60 s (180 °C - 340 °C with 20 °C increment)		
3	IR stimulation, 120 s at 50 °C	L_x	IR_{50}
4	IR stimulation, 240 s (−30 °C tracking the preheat temperature)	L_x	pIRIR
5	Given dose, D_T		
6	Preheat for 60 s (180 °C - 340 °C with 20 °C increment)		
7	IR stimulation, 120 s at 50 °C	T_x	IR_{50}
8	IR stimulation, 240 s (−30 °C tracking the preheat temperature)	T_x	pIRIR
9	Return to step 1		

The preheat temperature was varied from 180 °C to 340 °C with a 20 °C increment. The same preheat conditions were applied prior to the measurements of the natural and/or regenerative dose as well as the test dose. The first IR stimulation was carried out at 50 °C for 100 s (IR_{50}), followed by the second stimulation for 200 s with an elevated temperature (pIRIR) that tracks the preheat temperature by −30 °C. At the start and the end of each IRSL measurement, discs were hold at the stimulation temperature without stimulating with IR (10 s for IR_{50} and 20 s for pIRIR) to monitor and minimize any thermally stimulated signal. The integrated signal intensity over the initial 20 s of the pIRIR signal minus a background of the last 40 s was used while the initial 10 s signal minus a background of the last 30 s was used for the IR_{50}. For residual, fading and dose recovery tests, aliquots were bleached in a Hönle SOL2 solar simulator for four hours prior to measurements. Three samples (LUM-2941, LUM-2940 and LUM-2938) were used for these test measurements, which were conducted on groups of three aliquots per

temperature. For the preheat plateau test, four aliquots per temperature were measured to calculate natural D_es.

5.2.3 Luminescence characteristics

5.2.3.1 Luminescence intensity

The IR_{50} and pIRIR signal intensities obtained from test doses (~45 Gy for LUM-2938 and ~27 Gy for LUM-2941 and LUM-2940) were normalized to the signal obtained under 180 °C preheat temperature (Fig. 5.8a).

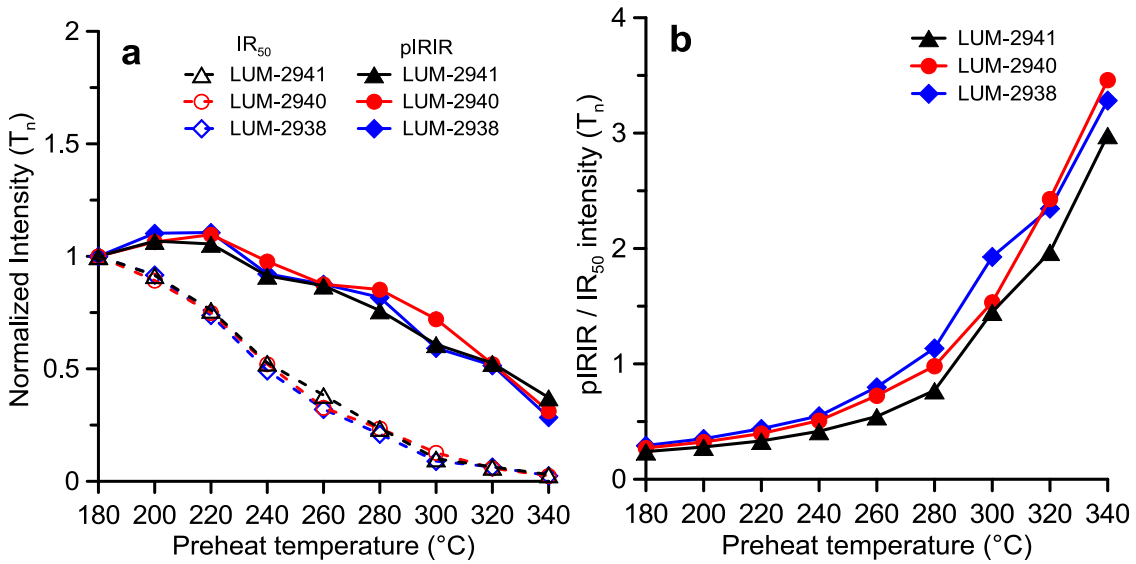

Fig. 5.8 (a) Normalized test dose intensity of the IR_{50} and pIRIR signals. The pIRIR stimulation temperature tracks the preheat temperature by −30 °C. Open symbols indicate for IR50 signals and filled symbols represent pIRIR signals. (b) The ratio between pIRIR and IR_{50} intensities using the same dataset as in (a). The x-axis displays the preheat temperature. Each data point represents the mean of three aliquots.

It clearly shows that the pIRIR signals depleted at much higher temperature than IR_{50} signals, which is consistent with the observation of Thomsen et al. (2011) and Tsukamoto et al. (2012). When comparing the pIRIR intensities with the corresponding IR_{50} signals (Fig. 5.8b), we note that ratios of the pIRIR intensity to the IR_{50} consistently increase from ~0.2–0.3 to ~3–4 as the preheat temperature increased, i.e. the IR_{50} signal was

brighter than the pIRIR signal when the preheat temperature was below 280 °C. In contrast, a reversed trend was shown above 280 °C.

5.2.3.2 Residual dose

The previous studies demonstrated that the residual doses increase as a function of preheat and/or stimulation temperatures (e.g. Reimann et al., 2011; Fu et al., 2012). The bleaching experiment carried out by Kars et al. (2014a) supported this observation that the higher the stimulation temperature, the slower the signals to be bleached. The residual dose in this study refers to the remaining dose after a 4 h bleaching in the solar simulator. Fig. 5.9 shows the residual doses for three samples as a function of preheat temperature. For both IR_{50} and pIRIR signals, the residual doses gradually increase when raising the preheat and stimulation temperatures, Furthermore, larger residual doses were obtained from the samples having larger D_e values, which confirmed the previous observations (e.g. Sohbati et al., 2012; Buylaert et al., 2012).

The residual doses of the IR_{50} signals remain below ~5 Gy for all three samples at all temperatures (Fig. 5.9a). For sample LUM-2938 with an expected D_e of 198 ± 12 Gy, the residual dose of the pIRIR signals range between 1.1 ± 0.1 Gy and 15.1 ± 1.7 Gy, which are all less than 8% of its expected D_e (Fig. 5.9c), indicating that such size of residual dose does not significantly affect the natural D_e measurement at any temperature. Two Holocene samples LUM-2940 and LUM-2941, whose expected D_es are 46 ± 5 Gy and 31 ± 1 Gy, yield much smaller residual doses ranging between 0.26 ± 0.01 Gy and 8.24 ± 0.53 Gy. The residual doses of the $pIRIR_{150}$ signals were less than 1% of the expected D_es after 4 h bleaching (Fig. 5.9d). However, as the preheat and stimulation temperatures were raised, the proportions of the residual dose relative to the expected D_e gradually increase up to ~26% ($pIRIR_{310}$), which can cause severe age overestimation. The result demonstrates that for dating young samples (e.g. Holocene) using a pIRIR protocol, reasonable low preheat and stimulation temperatures should be preferred in order to minimize the effect of residual signals.

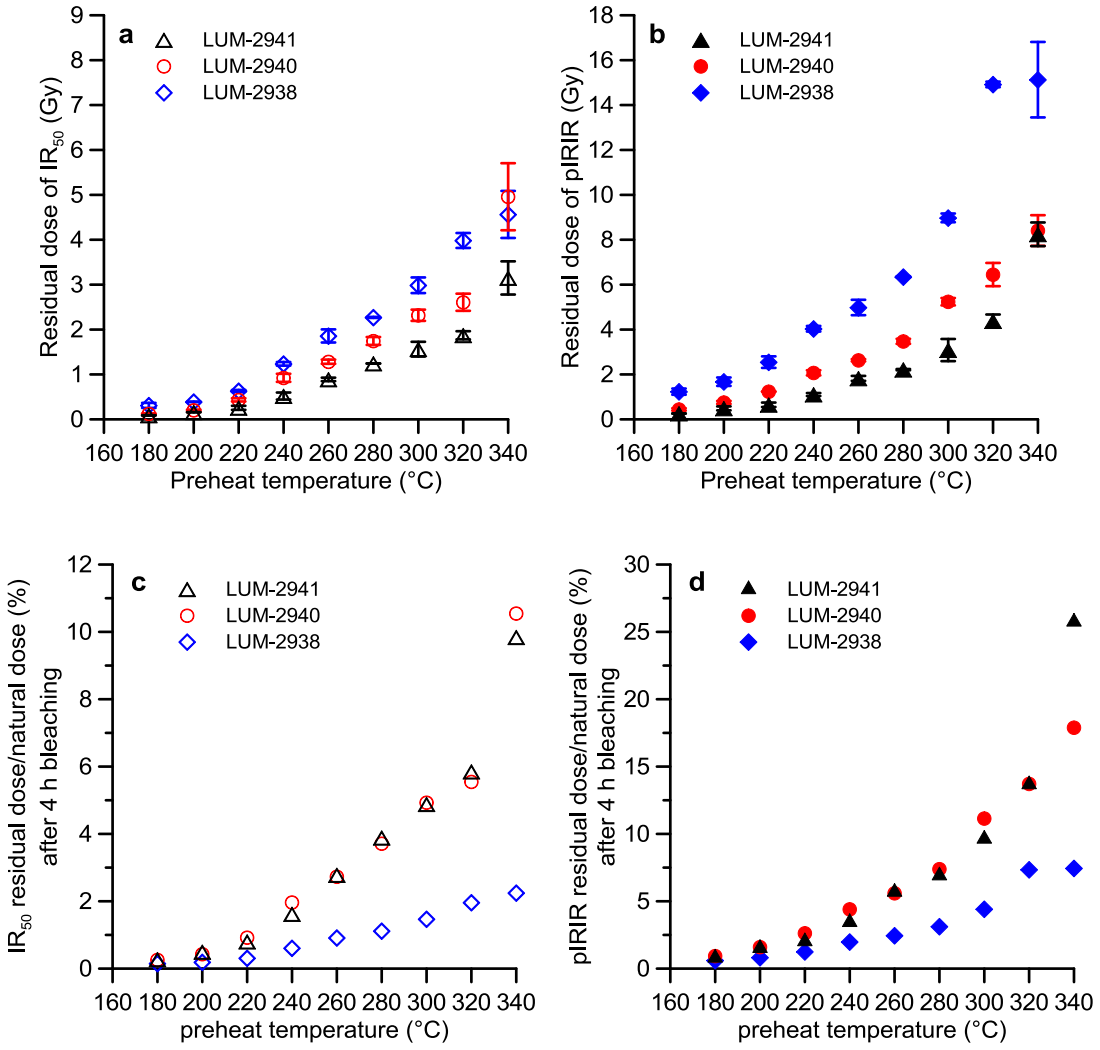

Fig. 5.9 Residual doses of (a) IR_{50} and (b) pIRIR signals measured after 4 h exposure in a Hönle SOL2 solar simulator. Each data point represents the mean of three aliquots with 1sstandard error. The percentage of the remaining dose to the natural dose of (c) IR_{50} signal and (d) pIRIR signal are also shown.

5.2.3.3 Anomalous fading

Li et al. (2014) summarized measured g-values obtained using $pIRIR_{225}$ (n=116) and $pIRIR_{290}$ (n=118) protocols which had been reported in 13 previous studies. It shows that a range of g-values between 0 and ~5 %/decade was observed for different samples from different regions of the world and most values fall between ~0.5 and ~2%/decade. The average fading rates of both signals are not significantly different from each other (1.5 ± 0.1%/decade obtained for the $pIRIR_{225}$ and 1.1 ± 0.1 %/decade for the $pIRIR_{290}$).

The fading rates (g-values) for both the IR_{50} and the pIRIR signals of this study are presented in Fig. 5.10.

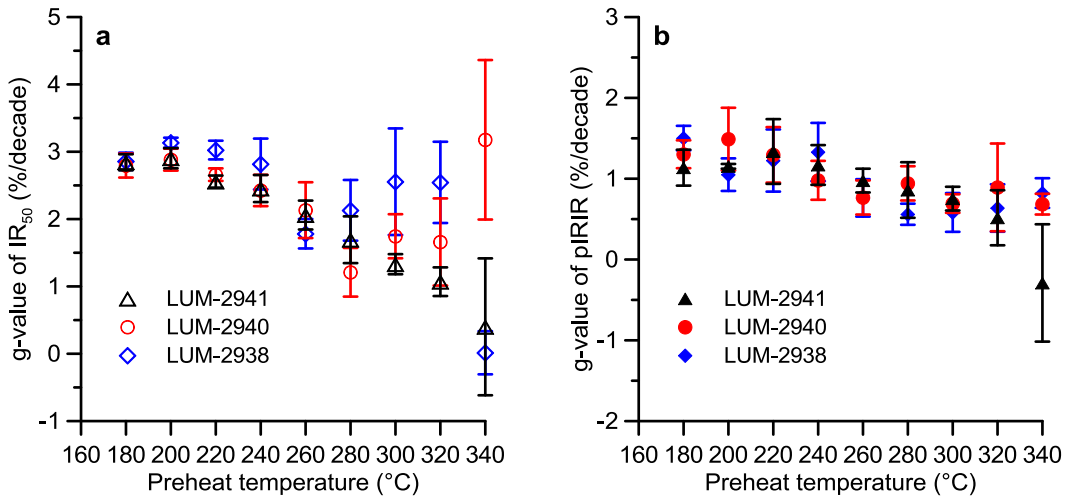

Fig. 5.10 The measured fading rates (g-value) of (a) IR_{50} and (b) pIRIR signals obtained at different preheat (stimulation) temperatures. The regenerative dose of fading measurements was ~26 Gy for all three samples.

The g-values between 3.14 ± 0.07 %/decade and 0.02 ± 0.32 %/decade were observed for different samples from IR_{50} signals, and most of the values fall into the range of ~3−1%/decade. Below 260 °C preheat temperature, the fading rate of the IR_{50} signals for the three samples presented a similar decreasing trend as the function of temperature. From 280 °C to 340 °C, the measured fading rates varied considerably among different samples, i.e. the fading rates of sample LUM-2938 consistently decrease while those of LUM-2940 increase with preheat temperature. The large scatter might be caused by reduced luminescence intensities at higher preheat and stimulation temperatures. Compared with the IR_{50} signals, the pIRIR signals fade much less and the measured fading rates of all three samples appear to generally decrease with increasing preheat (stimulation) temperature, ranging from 1.50 ± 0.15%/decade to −0.29 ± 0.73%/decade.

5.2.3.4 Dose recovery test

The recovered/given dose ratios obtained after subtraction of the residual doses for both IR_{50} and pIRIR signals are plotted in Fig. 5.11. The laboratory administered doses were chosen to approximate the natural doses for each sample, i.e. 26 Gy, 54 Gy and 272 Gy for samples LUM-2941, LUM-2940 and LUM-2938, respectively.

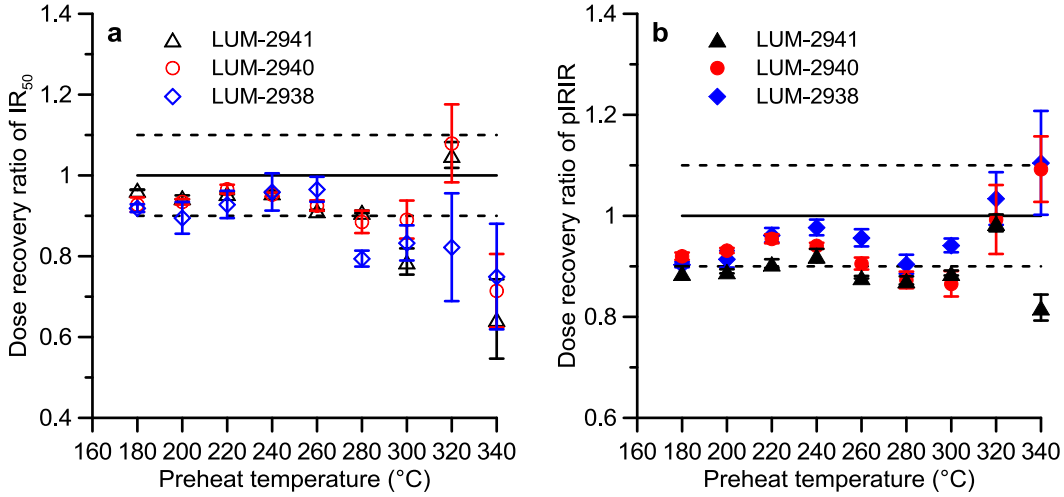

Fig. 5.11 The dose recovery ratios for (a) IR_{50} and (b) pIRIR signals obtained at different preheat (stimulation) temperatures for three samples. Open symbols indicate the dose recovery data of the IR_{50} signal and filled symbols represent the data of the pIRIR signal. The residual doses remaining after 4 h bleaching using a Hönle SOL2 solar simulator are subtracted for each sample. Each data point is the mean of three aliquots, and 1s standard error is shown.

The dose recovery ratios of pIRIR signals are generally within 10% of unity from 180 °C to 320 °C preheat temperature for three samples, indicating that the protocol was able to recover a regenerated dose within 10% of unity. At 340 °C, both inter-aliquot and inter-sample scatterings are significantly increased. For the IR_{50} signals, the laboratory administered doses can be well recovered using preheat temperatures below 260 °C while above this temperature the dose recovery ratio of the IR_{50} shows a larger negative deviation from the unity, as reported by Kars et al. (2014b). The data also become increasingly scattered above 300 °C preheat as indicated by the error bars shown in Fig. 5.11a, because most of the IR_{50} signal was already depleted (Fig. 5.8a).

5.2.4 The pIRIR D_e plateau and its implications

The mean D_e values obtained for the IR_{50} and pIRIR signals for four samples are plotted against the preheat temperature in Fig. 5.12; these data are also presented in Table 5.6. It should be noted that we did not conduct the residual subtraction from the D_es as the measured residual dose does not present the true residual dose in nature (Kars et al., 2014a).

Table 5.6 The D_e (Gy) values obtained from the IR_{50} and pIRIR signals under various preheat temperatures.

Preheat	LUM-2941		LUM-2940		LUM-2938		LUM-2952	
temperature	IR_{50}	pIRIR	IR_{50}	pIRIR	IR_{50}	pIRIR	IR_{50}	pIRIR
180 °C	21.9 ± 0.2	25.7 ± 0.2	38.7 ± 0.2	47.1 ± 0.4	128 ± 1	172 ± 1	399 ± 4	741 ± 28
200 °C	23.3 ± 0.1	26.8 ± 0.1	40.0 ± 0.9	48.5 ± 0.6	136 ± 5	187 ± 0	444 ± 6	758 ± 27
220 °C	25.0 ± 0.2	28.9 ± 0.2	42.8 ± 0.9	51.6 ± 0.5	151 ± 3	205 ± 2	540 ± 7	924 ± 7
240 °C	26.6 ± 0.3	30.9 ± 0.2	44.9 ± 0.8	54.6 ± 0.3	158 ± 5	218 ± 2	601 ± 12	1104 ± 8
260 °C	27.8 ± 0.6	31.6 ± 0.8	46.6 ± 1.4	56.2 ± 0.3	187 ± 10	235 ± 5	591 ± 36	1184 ± 3
280 °C	25.9 ± 0.3	30.6 ± 0.1	45.3 ± 1.1	55.5 ± 0.6	163 ± 17	223 ± 7	632 ± 70	1098 ± 82
300 °C	24.2 ± 0.2	31.7 ± 0.4	44.2 ± 0.9	58.4 ± 1.5	157 ± 7	249 ± 5	727 ± 16	1217 ± 5
320 °C	23.9 ± 0.9	33.5 ± 0.3	41.4 ± 2.7	62.7 ± 1.3	180 ± 32	281 ± 22	550 ± 16	1746 ± 263
340 °C	22.4 ± 0.8	35.5 ± 0.6	42.7 ± 1.0	63.5 ± 1.2	149 ± 6	261 ± 9	356 ± 89	1623 ± 185

The pIRIR D_es show a systematic increasing trend with the increasing preheat and stimulation temperatures and a D_e plateau between 240 and 280 °C can be detected for all samples. A similar trend of D_e variations has been observed by Roberts (2012) for polymineral fine grains when the preheat temperature was above 250 °C. Taking sample LUM-2941 (Fig. 5.12a) as an example, the D_e obtained by $pIRIR_{150}$ (with preheat temperature at 180 °C) is 25.7 ± 0.2 Gy, whereas the $pIRIR_{310}$ signal (preheat 340 °C) yields a D_e value of 35.5 ± 0.6 Gy which is ~38% higher than that of the $pIRIR_{150}$ signal. A pIRIR D_e plateau at ~30 Gy is present between 240 °C and 280 °C preheat temperature. In contrast to the pIRIR signals, the IR_{50} D_es do not show any obvious D_e plateau among the whole preheat temperature range from 180 °C to 340 °C. Below 260 °C (300 °C for sample LUM-2952), the IR_{50} D_es systematically increase for all samples, while an

opposite trend can be seen above 260 °C. The decreasing trend of the IR_{50} D_e at higher temperatures may be a result of inability to recover doses (Fig. 5.11a).

The expected D_es calculated according to the fine-grained quartz OSL ages are marked with 1σ and 2σ standard errors (the gray bars in Fig. 5.12). The IR_{50} D_es overall underestimate the expected D_es except that of the sample LUM-2940. For the youngest sample LUM-2941 (Fig. 5.12a), the pIRIR D_e values obtained from the plateau are in good agreement within uncertainties with the expected D_e, which is promising. However, for samples LUM-2940 and LUM-2938, the "plateau" D_e generally overestimates the expected D_e. The greatest difference was observed for the oldest sample LUM-2952 (Fig. 5.12d), whose pIRIR D_e originated from the plateau are more than three times larger than its expected D_e. Zhang et al. (2015) found that the quartz D_e of ~300 Gy was derived from the additional linear component in the high dose region, which may have caused age underestimation of the sample. This might explain the large discrepancy between the feldspar pIRIR age and the quartz OSL age.

The fading correction was applied to the samples LUM-2941, LUM-2940 and LUM-2938 for both IR_{50} and pIRIR ages (Fig 5.13, Table 5.7) using the R 'Luminescence'-package (Dietze et al., 2013) according to the method of Huntley and Lamothe (2001). After the fading correction, a plateau for the fading corrected pIRIR ages can be still observed between 240 °C and 280 °C. The corrected IR_{50} ages show a good agreement within error with the corrected pIRIR ages when the preheat temperature is below 260°C, especially for sample LUM-2941. This may indicate that both signals were well bleached when a low preheat temperature is applied.

Table 5.7 Summary of pIRIR and IR_{50} ages. The ages named as "Apparent age" are not corrected for anomalous fading.

Preheat temperature	Apparent age (ka)						Fading corrected age (ka)					
	LUM-2941		LUM-2940		LUM-2938		LUM-2941		LUM-2940		LUM-2938	
(°C)	IR_{50}	pIRIR	IR_{50}	pIRIR	IR_{50}	pIRIR	IR_{50}	pIRIR	IR_{50}	pIRIR	IR_{50}	pIRIR
180	4.5 ± 0.04	5.2 ± 0.03	8.0 ± 0.04	9.7 ± 0.1	27.9 ± 0.2	37.5 ± 0.3	5.8 ± 0.63	5.8 ± 0.13	10.4 ± 0.2	10.9 ± 0.2	37.3 ± 0.7	43.1 ± 0.8
200	4.8 ± 0.02	5.5 ± 0.01	8.3 ± 0.19	10.0 ± 0.1	29.7 ± 1.1	40.8 ± 0.1	6.2 ± 0.31	6.0 ± 0.04	10.9 ± 0.3	11.4 ± 0.5	42.2 ± 1.7	44.8 ± 0.9
220	5.1 ± 0.03	5.9 ± 0.04	8.9 ± 0.18	10.7 ± 0.1	32.9 ± 0.6	44.6 ± 0.4	6.5 ± 0.41	6.6 ± 0.25	11.4 ± 0.3	12.0 ± 0.4	45.1 ± 1.3	50.1 ± 2.1
240	5.4 ± 0.06	6.3 ± 0.04	9.3 ± 0.16	11.3 ± 0.1	34.5 ± 1.0	47.5 ± 0.4	6.8 ± 0.78	7.0 ± 0.17	11.6 ± 0.4	12.3 ± 0.3	46.0 ± 2.9	53.9 ± 2.0
260	5.7 ± 0.12	6.5 ± 0.17	9.6 ± 0.29	11.6 ± 0.1	40.7 ± 2.1	51.0 ± 1.2	6.8 ± 0.21	7.0 ± 0.20	11.8 ± 0.6	12.4 ± 0.2	48.5 ± 2.8	54.9 ± 1.9
280	5.3 ± 0.06	6.2 ± 0.02	9.4 ± 0.23	11.5 ± 0.1	35.4 ± 3.8	48.4 ± 1.6	6.1 ± 0.25	6.7 ± 0.18	10.4 ± 0.4	12.5 ± 0.3	43.7 ± 5.1	51.0 ± 1.9
300	4.9 ± 0.04	6.5 ± 0.08	9.1 ± 0.19	12.1 ± 0.3	34.2 ± 1.4	54.2 ± 1.1	5.6 ± 0.10	6.9 ± 0.12	10.8 ± 0.4	12.8 ± 0.4	44.4 ± 5.2	57.0 ± 1.8
320	4.9 ± 0.19	6.8 ± 0.06	8.6 ± 0.56	13.0 ± 0.3	39.1 ± 7.0	61.2 ± 4.7	5.4 ± 0.21	7.1 ± 0.21	9.9 ± 0.9	14.0 ± 0.7	50.8 ± 10.0	65.1 ± 5.2
340	4.6 ± 0.16	7.2 ± 0.11	8.8 ± 0.21	13.1 ± 0.3	32.5 ± 1.3	56.7 ± 2.0	4.7 ± 0.43	7.2 ± 0.11	12.1 ± 2.0	14.0 ± 0.3	32.5 ± 1.7	61.0 ± 2.4

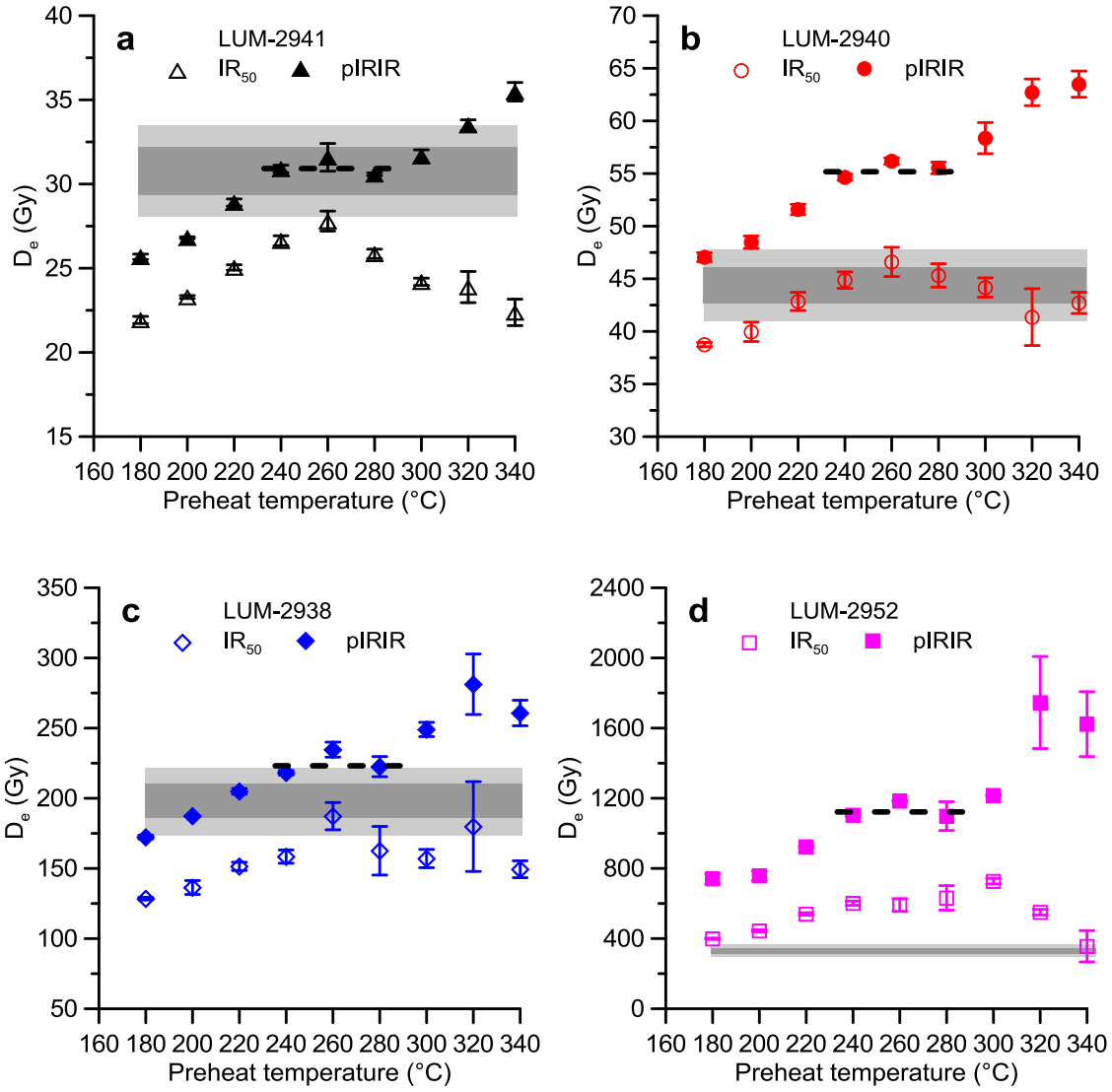

Fig. 5.12 Equivalent dose (D_e) determined for four samples using different measurement conditions. Open symbols indicate for the IR_{50} D_es and filled symbols represent the pIRIR D_es. Each data point represents the mean of 4 aliquots with 1σ standard error. Dashed line represents the position of the plateau of pIRIR D_es. The expected Des calculated according to the corresponding quartz OSL age are shown with 1σ standard error (dark gray bar) and 2σ standard error (light gray bar).

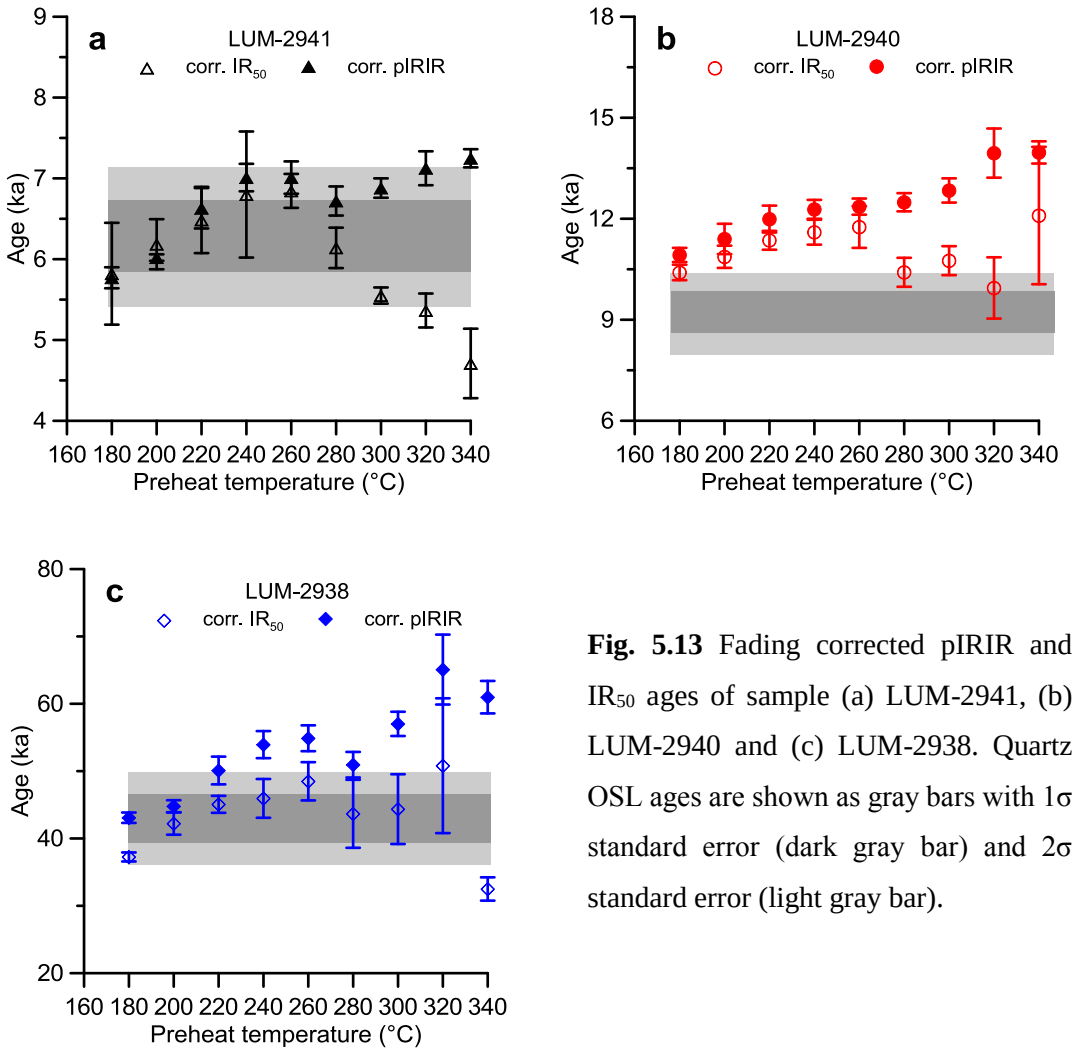

Fig. 5.13 Fading corrected pIRIR and IR_{50} ages of sample (a) LUM-2941, (b) LUM-2940 and (c) LUM-2938. Quartz OSL ages are shown as gray bars with 1σ standard error (dark gray bar) and 2σ standard error (light gray bar).

The D_e plateau has been explained as a balance between fading and bleaching of the pIRIR signal (Li and Li, 2011). The D_e plateau for the MET-pIRIR is located at 200-250 °C (Li and Li, 2011) for older sample while at 140-170 °C (e.g. Fu and Li, 2013) for young samples (e.g. Holocene). From these results we would expect that the two-step pIRIR D_e plateau shifts also as a function of ages, i.e. the young sample reach the D_e plateau at lower temperature range while the older sample presents a D_e plateau at higher temperature range. However, such tendency does not exist in our results. For the four samples in this study, the D_e plateau appears consistently between 240 °C and 280 °C regardless the age of the sample. Furthermore, if the non-fading signal is obtained when the age plateau appears, the relatively small amount of residual dose can not explain the continuously increasing trend of the ages afterward at higher temperatures. The increasing tendency of the pIRIR ages may be explained if the pIRIR signals at higher preheat and stimulation temperatures had not been well bleached before burial, although the luminescence signals from loess is normally thought to be well bleached. Therefore, the

pIRIR age plateaus occurred between 240 °C and 280 °C may be an indicator for a reliable age determination. As there is no external age control apart from the quartz OSL ages available for these samples, we are not able to validate the reliability of the "plateau" age in higher accuracy. Further investigations should be carried out on samples with independent age control concerning this issue.

5.2.5 Conclusions

The behaviour of the pIRIR signal (as well as the corresponding IR_{50} signal) from polymineral fine grains has been investigated under various preheat and stimulation temperatures. The measured residual dose and fading rate confirmed the previous observations that the higher the preheat and stimulation temperatures for the pIRIR signals, the less fading but harder to bleach. The pIRIR D_es show a systematic increasing trend with increasing preheat (stimulation) temperatures. The age plateau between 240 and 280 °C is present for all four samples. After the fading correction, wide agreements are shown between the pIRIR and the IR_{50} ages under lower preheat temperature (<260°C), reflecting the good bleachabilty of the lower temperature pIRIR signals.

Acknowledgements. −This research has been supported by a DAAD (Deutscher Akademischer Austauschdienst) PhD scholarship (J.R. Zhang, A/11/94303). Additionally, we thank the Federal Ministry of Education and Research of Germany (BMBF) for funding in the frame of the project "Supra-regional signal pathways and long-time archives: Quaternary monsoon dynamics at the northern margin of the Tibetan Plateau" (No. 03G0814A) as part of the CAME-program. We would also like to thank the reviewer for constructive comments, which helped to improve this work.

References

Alappat, L, Vink, A., Tsukamoto, S., Frechen, M., 2010. Establishing the Late Pleistocene-Holocene sedimentation boundary in the southern North Sea using OSL dating of shallow continental shelf sediments. Proceedings of the Geologists' Association 121, 43-54.

Buylaert, J.P., Murray, A. S., Thomsen, K. J. & Jain, M., 2009. Testing the potential of an elevated temperature IRSL signal from K-feldspar. Radiat. Meas. 44, 560-565.

Buylaert, J.P., Thiel, C., Murray, A.S., Vandenberghe, D.A.G., Yi, S.W., Lu, H.Y., 2011. IRSL and post-IR IRSL residual doses recorded in modern dust samples from the Chinese Loess Plateau. Geochronometria 38(4), 432-440.

Buylaert, J.P., Jain, M., Murray, A.S., Thomsen, K.J., Thiel, C., Sohbati, R., 2012. A robust feldspar luminescence dating method for Middle and Late Pleistocene sediments. Boreas 41, 435-451.

Dietze, M., Kreutzer, S., Fuchs, M.C., Burow, C., Fischer, M., Schmidt, C., 2013. A practical guide to the R package Luminescence. Anc. TL 31, 11-18.

Frechen, M., Schweitzer, U., Zander, A., 1996. Improvements in sample preparation for the fine grain technique. Anc. TL 14, 15-17.

Frechen, M., van Vliet Lanoe, B., van den Haute, P., 2001. The Upper Pleistocene loess record at Harmignies/Belgium: high resolution terrestrial archive of climate forcing. Palaeogeography, Palaeoclimatology, Palaeoecology 173, 175-195.

Fu, X., Li, B., Li, S.H., 2012. Testing a multi-step post-IR IRSL dating method using polymineral fine grains from Chinese loess. Quat. Geochronol. 10, 8-15.

Fu, X., Li, S.H., 2013. A modified multi-elevated-temperature post-IR IRSL protocol for dating Holocene sediments using K-feldspar. Quat. Geochronol. 17, 44-45.

Huntley, D.J., Lamothe, M., 2001. Ubiquity of anomalous fading in K-feldspars and the measurement and correction for it in optical dating. Canadian Journal of Earth Sciences, 38, 1093-1106.

Jain, M., Ankjaergaard, C., 2011. Towards a non-fading signal in feldspar: insight into charge transport and tunnelling from time-resolved optically stimulated luminescence. Radiat. Meas. 46, 292-309.

Kars, R. H., Reimann, T., Ankjærgaard, C., Wallinga, J., 2014a. Bleaching of the post-IR IRSL signal: new insights for feldspar luminescence dating. Boreas 43, 780-791.

Kars, R.H., Reimann, T., Walling, J., 2014b. Are feldspar SAR protocols appropriate for post-IR IRSL dating?. Quat. Geochronol. 22, 126-136.

Li, B., Li, S. H., 2011. Luminescence dating of K-feldspar from sediments: a protocol without anomalous fading correction. Quat. Geochronol. 6, 468-479.

Li, B., Li, S. H., 2012. Luminescence dating of Chinese loess beyond 130 ka using the non-fading signal from K-feldspar. Quat. Geochronol. 10, 24-31.

Li, B., Jacobs, Z., Roberts, R.G., Li, S.H., 2014. Review and assessment of the potential of post-IR IRSL dating methods to circumvent the problem of anomalous fading in feldspar luminescence. Geochronometria 41, 178-201.

Long, H., Shen, J., Tsukamoto, S., Chen, J.H., Yang, L.H., Frechen, M., 2014. Dry early Holocene revealed by sand dune accumulation chronology in Bayanbulak Basin (Xinjiang, NW China). The Holocene 24, 614-626.

Long, H., Haberzettl, T., Tsukamoto, S., Shen, J., Kasper, T., Daut, G., Zhu, L., Mäusbacher, R., Frechen, M., 2015. Luminescence dating of lacustrine sediments from Tangra Yumco (southern Tibetan Plateau) using post-IR IRSL signals from polymineral grains. Boreas 44, 139-152..

Lowick, S.E., Trauerstein, M., Preusser, F., 2012. Testing the application of post IR-IRSL dating to fine grain waterlain sediments. Quat. Geochronol. 8, 33-40.

Madsen, A.T., Buylaert, J.P., Murray, A.S., 2011. Luminescence dating of young coastal deposits from New Zealand using feldspar. Geochronometria 38, 378-390.

Murray, A.S., Schmidt, E.D., Stevens, T., Buylaert, J.P., Marković, S.B., Tsukamoto, S., Frechen, M., 2014. Dating Middle Pleistocene loess from Stari Slankamen (Vojvodina, Serbia)-Limitations imposed by the saturation behavior of an elevated temperature IRSL signal. Catena 117, 34-42.

Prescott, J. R. & Hutton, J. T., 1994. Cosmic ray contributions to dose rates for luminescence and ESR dating: large depths and long-term variations. Radiat. Meas. 23, 497-500.

Rees-Jones, J., 1995. Optical dating of young sediments using fine-grain quartz. Anc. TL 13, 9-14.

Reimann, T., Tsukamoto, S., Naumann, M., Frechen, M., 2011. The potential of using K-rich feldspars for optical dating of young coastal sediments e a test case from Darss-Zingst peninsula (southern Baltic Sea coast). Quat. Geochronol. 6, 207-222.

Reimann, T., Tsukamoto, S., 2012. Dating the recent past (<500 years) by post-IR IRSL feldspar–Examples from the North Sea and Baltic Sea coast. Quat. Geochronol. 10, 180-187.

Roberts, H.M., 2012. Testing Post-IR IRSL protocols for minimising fading in feldspars, using Alaskan loess with independent chronological control. Radiat. Meas. 47, 716-724.

Schmidt, E.D., Tsukamoto,S., Frechen, M., Murray, A.S., 2014. Elevated temperature IRSL dating of loess sections in the East Eifel region of Germany. Quat. Int. 334-335, 141-154.

Sohbati, R., Murray, A.S., Buylaert, J.P., Ortuno, M., Cunha, P.P., Masana, E., 2012. Luminescence dating of Pleistocene alluvial sediments affected by the Alhama de Murcia fault (eastern Betics, Spain)-a comparison between OSL, IRSL and post-IR IRSL ages. Boreas 41, 250-262.

Stevens, T., Markovic, S.B., Zech, M., Hambach, U., Sumegi, P., 2011. Dust deposition and climate in the Carpathian Basin over an independently dated last glacial-interglacial cycle. Quat. Sci. Rev. 30, 662–681.

Thiel, C., Buylaert, J. P., Murray, A., Terhorst, B., Hofer, I., Tsukamoto, S., Frechen, M., 2011a. Luminescence dating of the Stratzing loess profile (Austria)-Testing the potential of an elevated temperature post-IR IRSL protocol. Quat. Int. 234, 23-31.

Thiel, C., Buylaert, J.P., Murray, A.S., Tsukamoto, S., 2011b. On the applicability of post-IR IRSL dating to Japanese loess. Geochronometria 38, 369-378.

Thiel, C., Buylaert, J.P., Murray, A.S., Elmejdoub, N., Jedoui, Y., 2012. A comparison of TT-OSL and post-IR IRSL dating of coastal deposits on Cap Bon peninsula, north-eastern Tunisia. Quat. Geochronol. 10, 209-217.

Thomsen, K. J., Murray, A. S., Jain, M., Bøtter-Jensen, L., 2008. Laboratory fading rates of various luminescence signals from feldspar-rich sediment extracts. Radiat. Meas. 43, 1474-1486.

Thomsen, K.J., Murray, A.S., Jain, M., 2011. Stability of IRSL signals from sedimentary K-feldspar samples. Geochronometria 38, 1-13.

Tsukamoto, S., Jain, M., Murray, A., Thiel, C., Schmidt, E., Wacha, L., Dohrmann, R., Frechen, M., 2012. A comparative study of the luminescence characteristics of polymineral fine grains and coarse-grained K-, and Na-rich feldspars. Radiat. Meas. 47, 903-908.

Wacha, L., Frechen, M., 2011. The geochronology of the 'Gorjanovic´ loess section' in Vukovar, Croatia. Quat. Internat. 240, 87-99.

Wintle, A. G., 1973. Anomalous fading of thermoluminescence in mineral samples. Nature 245, 143-144.

Zhang, J.R., Nottebaum, V., Tsukamoto, S., Lehmkuhl, F., Frechen, M., 2015. Late Pleistocene and Holocene loess sedimentation in central and western Qilian Shan (China) revealed by OSL dating. Quat. Int. 372, 120-129.

Chapter 6 Conclusions and outlooks

6.1 Conclusions

The aim of this dissertation is to explore the applicability of various luminescence dating techniques to a variety of geological sediment and thereby obtain better chronologies for the selected sedimentary archives. Accordingly, luminescence dating has been applied to three individual sedimentary archives, targeting a coastal sequence from the German North Sea, loess formation at the Qilian Shan from northwestern China, and lacustrine, fluvial sediments, etc. in the Huangqihai Lake basin from northern China, respectively. Quartz fractions are used as primary dosimeter to establish the chronological frameworks, and robustness of the OSL dates was confirmed by internal validation and radiocarbon dates (whenever available) (Chapter 2, 3 and 4). Coupled with stratigraphic, sedimentological and geomorphologic analyses, regional sedimentary responses of the Late Quaternary palaeoenvironmental and palaeoclimatic changes have been illustrated. Using the pIRIR measurement protocol, furthermore, the luminescence behaviours of feldspar have been systematically examined using both sand-sized K-feldspar and polymineral fine grains (Chapter 5), and some suggestions of pIRIR dating application were given.

6.1.1 Luminescence age determination and validation

As reviewed in Chapter 1.1.1.2, both quartz and feldspar show advantages and disadvantages as a dosimeter of luminescence dating. The selection of the most appropriate luminescence technique, such as the choice of mineral, aliquot- and grain-size for dating; analysis of complex equivalent dose distributions, etc., is subject to the materials available for dating, the timescale being considered, and the geological process and depositional setting of the studied materials. The difficulties and the inspiration of luminescence dating for different sedimentary archives are hereby summarized. Different dating procedures have been used according to their own luminescence properties and the encountered problems as well. The applied techniques, protocols, etc, in this dissertation were summarized in Table 6.1.

Table 6.1 Overview of luminescence dating information of three sedimentary archives under study in this dissertation. The applied dating techniques, protocols and the encountered problems of each study are listed.

Archive	Depositional environment/ process	Primary dosimeter	Grain size	Technique	Protocol	Problem	Feldspar measurement
Qilian Shan Loess	aeolian	quartz	4-11 um	blue OSL	SAR	saturation/ dim	yes
Garding-2 core	Coastal/ fluvial	quartz	sand-sized	blue OSL	SAR	saturation / partial bleaching	yes
Huangqihai Lake	lacustine/ beach/ aeolian/ fluvial	quartz	sand-sized	post-IR pulsed OSL	Double SAR	feldspar contamination	no

Of all kind of sedimentary archives, aeolian deposits such as loess have long been considered as the most suitable materials for OSL dating because (1) the zeroing of the potential luminescence signal prior to deposition is most assured during the transport, and (2) the environmental dose rate is relatively stable due to homogenous sedimentation. In Chapter 2.1, we investigate whether OSL dating of fine-grained quartz can be used to establish a reliable chronology for the loess from central and western Qilian Shan area (NW China). For D_e determination, fine grained quartz fraction, the major component of loess sediment (Sun et al., 2000), was used as the primary dosimeter. Different OSL performances were recognized with the standard SAR protocol for different samples. For example, a group of samples show relatively low OSL sensitivity (dim quartz) compared with others, which might relate to different sedimentation history of the particles from the source region to depositional site. However, as such samples didn't present any spatial and temporal pattern, no further inferences could be made for the loess accumulation in the study area. Furthermore, the possible age underestimation of quartz OSL signal obtained from the additional linear component of the growth curve was encountered for three pre-Holocene loess samples, although the SAR protocol performed well for these samples. The age underestimation of these samples was later confirmed by the feldspar pIRIR dating technique (Chapter 5.2). Such behaviour of the quartz OSL signal has been extensively reported for the loess age determination worldwide (e.g. Wang et al., 2006; Buylaert et al., 2007; Timar et al. 2010). The loess samples from the central and western Qilian Shan area confirmed that the quartz OSL ages of the loess tend to underestimate

the real age when the D_e is above ~150–200 Gy. Unfortunately, we are still not able to explain such phenomenon according to the present understanding of these samples.

The airborne sediments, such as loess, are ideal material for OSL dating, since the OSL signal could be sufficiently bleached by sunlight during transport. In contrast, OSL dating of sediments from waterlain environment may be more complex for: (1) containing grains that may have experienced limited exposure to daylight before deposition (i.e. incomplete bleaching); (2) possible variable dose rate through burial time caused by radioactive disequilibrium. The uppermost 26 m Garding-2 core sediment (consisted of tidal flat and fluvial sediments) and the lake deposits from Huangqihai Lake were chosen to test the OSL application of waterlain sediment using sand-sized quartz minerals. For the Garding-2 core sediments (Chapter 3.1), small aliquot (2.5 mm) technique (Duller, 2008) has been applied to detect the bleaching condition. The D_e obtained with large aliquots and small aliquots didn't show significant difference, indicating that the investigated tidal flat sediments were well bleached prior to the deposition. Concerning the dose rate calculation, no radioactive disequilibrium was observed in the thorium and uranium decay chains by the high-resolution gamma spectrometry. The OSL dating results were proved to be reliable by a variety of luminescence characteristics tests and comparison with the radiocarbon dates of shells.

For most of the samples from Huangqihai Lake, feldspar contamination that irremovable after prolonged chemical treatment (e.g. HF etching) which may cause age underestimation, hampered the standard quartz OSL measurement. To deal with this problem, the OSL dating using pulsed stimulation technique has been used to discriminate against the unwanted feldspar signal. Our results confirmed that the pulsed OSL dating technique is able to minimize the unwanted feldspar signal from quartz OSL measurement and therefore offers accurate dose determination (Chapter 4.1). It is noteworthy that quartz OSL measurement of samples from some other sites in the Huangqihai Lake area didn't show significant feldspar contamination (Zhang et al., 2011; 2012). It might be attributed to the different grain sizes and chemical treatments that were applied in these studies. The OSL measurements in Zhang et al. (2011, 2012) were conducted mostly with medium grain-sized fraction (36–68 μm) which was isolated by hydrofluosilicic acid etching for weeks rather than HF with limited time (1 hour in most case). However, several sand-sized quartz samples from Zhang et al. (2012) were also extracted by HF

etching but didn't show significant IR contamination. It could therefore presumably be a result of sample dependence. Such distinction of OSL behaviour of the samples from same area has been reported in previous researches. For example, quartz minerals from Tangra Yum Co (southern Tibet) were reported to be well behaved with the standard SAR protocol and able to provide reliable ages by Long et al., (2012), but not the others from Rades et al. (2015) which argued that their quartz mineral from the same lake suffered from anomalous fading and can not be used as a reliable dosimeter. Such studies reminded us the complexity of the luminescence dating. Great care has to be taken in the evaluation of OSL dates, and certain standards need to be set and met when publishing dating results. The fundamental information of each sample (or each group of samples) of the OSL dating, such as the detailed description of measurement condition, characteristics of luminescence signal, the criteria of the data acceptance, the dose rate calculation and the applied age model, are of crucial important and great interest as well for the data evaluation.

As summarized above, most of the problems associated with the quartz OSL could generally be overcome by selecting the most proper dating procedures according to their luminescence behaviours. In these studies, I could prove that the quartz OSL dating is therefore a powerful dating method, which I applied to determine the ages of various sediments from different geological settings, e.g. loess, coastal and lacustrine sediments in the current studies. However, a serious problem we have encountered in our study is that the quartz OSL signal reaches saturation at relatively low D_e values, which restricted its application to the last glacial period. This problem can not be solved so far by applying any kind of dating procedure using quartz itself. To extend the application of the luminescence dating to the time period over which OSL dating of quartz can reach, feldspar minerals could be used as an alternative dosimeter. The applicability of the feldspar signals using the newly developed pIRIR technique has been therefore systematically tested in Chapter 5, in interest of dating much older materials. The feldspar dating of Garding-2 core sediment was carried out under three intensively tested measurement conditions, namely $pIRIR_{150}$, $pIRIR_{225}$ and $pIRIR_{290}$ protocols (Chapter 5.1). The results confirmed that the pIRIR signals fade much less than the corresponding IR_{50} signals. Nevertheless, the fading rates for both IR_{50} and pIRIR signals did not show obvious temperature dependency but slightly dose dependent. Distinct differences in saturation ratio have been observed for $pIRIR_{150}$, $pIRIR_{225}$ and $pIRIR_{290}$ signals of a field

saturated sample although the measured fading rates are all similar and only the $pIRIR_{290}$ signal reached field saturation. By comparing the pIRIR ages with independent age controls, the $pIRIR_{150}$ ages show the best agreement with the independent age controls for the samples younger than 8 ka. For older samples, higher preheat and stimulation temperatures have to be used to extract stable pIRIR signals. In this case of study, my results show that the pIRIR dating of feldspar yields ages up to more than 400 ka without saturation, which is far beyond the quartz OSL dating limit. To check the performance of the pIRIR signal using polymineral fine grains, four samples with different ages from the Qilian Shan loess (Chapter 5.2) were systematically further investigated with wider temperature range. Significant increases in the pIRIR D_es were observed as a function of preheat (stimulation) temperatures. A D_e plateau appears between 240 °C and 280 °C preheat temperatures for all samples regardless of age. The general agreement between the fading corrected pIRIR and IR_{50} ages obtained below 260 °C preheat temperatures might imply a good bleachability of the feldspar signals. Although the physical mechanisms and dating implications of the pIRIR D_e plateau need further exploration, a preheat temperature below 280 °C should be encouraged for pIRIR measurement using the polymineral fine grain in order to obtain better bleachable signal.

6.1.2 Environmental implications of the obtained chronologies

It is generally concluded that the chronological investigations from the different studies do provide robust new result. It is of great importance to improve the existed geochronological framework for the areas under study. The ages of the three sedimentary archives are restricted to the late Pleistocene and Holocene, which were obtained primarily by quartz OSL dating technique. The records from the Garding-2 core and Huangqihai Lake revealed that both the sea and the lake transgression occurred during the early Holocene, responding to the ameliorating climate condition after the deglaciation. Meanwhile, the loess records from the western and central Qilian Shan started to extensively accumulate at around 13 ka.

6.1.2.1 Late Quaternary aeolian accumulation history in Qilian Shan, northern China

The loess from the central and western Qilian Shan area was OSL dated back to at least ~81 ka, which is remarkably older than previously reported (restricted to the Holocene). No pedogenesis was observed and loess sedimentation existed not only in the glacial period but also in the interglacial period (Holocene). Dust deposition was widespread since the last deglaciation (~13 ka) until ~3.6 ka in the northern piedmont of the central and western Qilian Shan. The existence of suitable environmental conditions (e.g. vegetation cover) for loess accumulation can be deduced in the central and western Qilian Shan for the Holocene. In contrast, the loess during the late glacial period was only episodically and sporadically observed. It is presumed that the sedimentation of the mountain loess might be not only controlled by climate changes (e.g. vegetation cover, wind systems, etc), as previously debated, but also affected by non-climate factors, such as tectonic activities in terms of reshaping the topography and subsequently changing the geomorphology.

6.1.2.2 Late Quaternary sedimentary processes in German North Sea coast

The chronology of the Garding-2 was well built up based on high-resolution OSL as well as AMS ^{14}C dating. It provides a robust coastal record which covers the period from the last deglaciation to the Holocene in a single succession over the German North Sea area. The stratigraphical and chronological evidences illustrated that an estuarine environment dominated in Eiderstedt Peninsula from 16 ka to 13 ka, and a depositional hiatus between 13 ka and 8.3 ka, probably due to erosion during the Holocene transgression. Subsequently, the Holocene transgression initiated, and the sea level rose rapidly until around 3 ka. The fast accumulated (ca. 10 m/ka) foreshore sediments between ~3−2 ka were probably the tidal channel filling deposits own to its relative elevation to the sea level. It might infer the discontinuity of the tidal flat deposits, although the chronologies show no obvious hiatus during this period. After 2 ka, sandy beach deposits accumulated in the sediment succession, and in turn the terrestrial clastic sediment started to

accumulate after 1.5 ka. This sea regression was probably affected by local diking activities which started at around the 11th century (e.g. Kühn and Panten 1989).

6.1.2.3 Late Quaternary lake evolution of Huangqihai in northern China

Five sedimentary outcrops from the Huangqihai Lake basin have been investigated to reconstruct the lake level variations. The pulsed OSL dating technique works well for the study sediments, and the resulting ages are in good agreement with the independent ^{14}C dates. Combining with depositional facies description and the corresponding environmental interpretation on the multiple outcrops, the lake levels of Huangqihai reached a peak during the early Holocene (10−8 ka). Subsequently, the lake level dropped away from the studied elevation during the middle and late Holocene. This pattern of lake-levels was almost synchronous with the variations of the EASM intensity during the Holocene (Wang et al., 2008). In addition, a relatively dry climate was prevailed in Huangqihai basin during 50−11 ka when aeolian sand accumulated and loess formed around this lake, thus a low lake level, compared with that of the early Holocene, was deduced through the entire last glacial period as well.

6.2 Outlooks of the future research

6.2.1 Suggestions regarding luminescence methodology

6.2.1.1 Quartz

As a primary dosimeter, the quartz OSL properties have been systematically investigated in this dissertation with different sedimentary archives using different protocols. One of the major problems of the quartz OSL is the early dose saturation, which hamper its application to dating older materials (D_e>~150–200 Gy). Compared with feldspar pIRIR dating technique, much younger quartz OSL ages were obtained. For example, the pIRIR ages of a sample at 77 m from Garding-2 core were older than 300 ka, while the quartz OSL dating yielded an age of only ~190 ka (Chapter 5.1). The oldest loess sample from western Qilian Shan was dated to be ~80 ka using quartz but at least 180 ka using feldspar

(Chapter 5.2). The OSL performances of these samples generally meet all the acceptance criteria, except the appearance of an additional linear or a second saturating exponential component (with a larger saturation dose) of the growth curve. So far, the underlying mechanisms of the additional high saturation-dose component of the growth curve, which may relate to age underestimation, still remain controversial. It merits further investigation to comprehend such behaviour of quartz OSL. Furthermore, the investigation and application of new technique, such as using the violet (402 nm) stimulated luminescence (VSL) signal of quartz (Ankjærgaard et al., 2013) could be a new direction of extending the quartz OSL dating limit.

6.2.1.2 Feldspar

Concerning feldspar minerals, the pIRIR technique has been intensively tested and applied by many researchers since it was first proposed by Thomsen et al. 2008, showing great potential in dating much older deposits and geological events, compared with quartz OSL. Considerable amount of pIRIR data have been published addressing either methodology or application questions (see review by Li et al., 2014). Nevertheless, there is still a long way to explore the mechanisms of feldspar pIRIR signals in order to obtain more athermally stable but bleachable signal. In Chapter 5, the characteristics of pIRIR signal have been systematically investigated using either sand-sized K-feldspar or polymineral fine grains. It is very inspiring that a pIRIR D_e plateau of polymineral fine grains has been observed. However, the dating implication of the pIRIR D_e plateau is still unclear. For the future work, efforts will be made on more samples (especially on sand-sized K-feldspar) to test whether such D_e plateau is a common existed phenomenon for pIRIR signals or sample dependent. Works will be also focused to explore the dating implication of such D_e plateau in terms of both the thermal and athermal stabilities of pIRIR signals. Samples with reliable chronological control and wide age range (such as Chinese loess) would be ideal material to continue this work. For the application of pIRIR dating, it is also essential and urgent to find standard criteria, such as the commonly accepted preheat plateau test, dose recovery test and etc for quartz OSL dating, to select a proper measurement protocol and validate pIRIR ages besides largely relying on external independent controls.

6.2.2 Further work on Garding drilling project

One of the key issues of the Garding drilling project is to study the geological evolution and the Quaternary climate change in northern Germany. To fulfill this research aim, chronology is of crucial importance. In this dissertation, a robust chronostratigraphy of Garding-2 core has been established for only the uppermost 26 m deposits (back to ~16 ka) using quartz OSL dating technique. The further work on Garding-2 core is to establish the chronostratigraphy for the rest of the core and thereby make comparison and correlation with other sedimentary records in Europe. It has been shown that the OSL dating of quartz is a powerful tool for dating coastal sediments of the Garding-2 core. However, below 26 m of the Garding-2 core, the sediments are majorly consisted of glacial or glacio-fluvial deposits. The age determination for the rest part of the Garding-2 core could be much more complex. Some pre-test revealed that there is significantly scatter in D_es from such deposits, which might be a result of partial bleaching. For such samples, a larger amount of D_e measurements is required and statistical analysis (e.g. minimum age model (Galbraith et al., 1999)) should be conducted. Furthermore, the quartz OSL signal might be already saturated at the depth around 40 m. Downward, feldspar mineral would be the only applicable luminescence dosimeter for the age determination. The pioneering work of feldspar pIRIR dating (Chapter 5.1) has been conducted with few samples from the core, showing that the pIRIR dating is able to provide ages back to ~500 ka.

Reference

Ankjærgaard, C., Jain, M., Wallinga, J., 2013. Towards dating Quaternary sediments using the quartz Violet Stimulated Luminescence (VSL) signal. Quaternary Geochronology 18, 99−109.

Buylaert, J.P., Vandenberghe, D., Murray, A.S., Huot, S., De Corte, F., Van den haute, P., 2007. Luminescence dating of old (470 ka) Chinese loess: a comparison of single-aliquot OSL and IRSL techniques. Quaternary Geochronology 5, 9−14.

Duller, G.A.T., 2008. Single-grain optical dating of Quaternary sediments: why aliquot size matters in luminescence dating. Boreas 37, 589–612.

Galbraith, R.F., Roberts, R.G., Laslett, G.M., Yoshida, H., Olley, J.M., 1999. Optical dating of single and multiple grains of quartz from Jinmium Rock Shelter, northern Australia: Part 1, experimental design and statistical models. Archaeometry 41, 339–364.

Kühn, H. J., Panten, A. 1989. Der frühe Deichbau in Nordfriesland: Archäologisch-historische Untersuchungen. 127 pp. Neumann, Bredstedt.

Li, B., Jacobs, Z., Roberts, R.G., Li, S.H., 2014. Review and assessment of the potential of post-IR IRSL dating methods to circumvent the problem of anomalous fading in feldspar luminescence. Geochronometria 41, 178−201.

Long, H., Lai, Z., Frenzel, P., Fuchs, M., Haberzettl, T., 2012.Holocenemoist period recorded by the chronostratigraphy of a lake sedimentary sequence fromLake Tangra Yumco on the south Tibetan Plateau. Quaternary Geochronology 10, 136–142.

Rades, E., Tsukamoto, S., Frechen, M., Xu, Q., Ding, L., 2015. A lake-level chronology based on feldspar luminescence dating of beach ridges at Tangra YumCo (southern Tibet). Quaternary Research 83, 469–478.

Sun, Y.B., Lu, H.Y., An, Z.S., 2000. Grain size distribution of quartz isolated from Chinese loess/paleosol. Chinese Science Bulletin 45, 2296–2298.

Thomsen, K. J., Murray, A. S., Jain, M., Bøtter-Jensen, L., 2008. Laboratory fading rates of various luminescence signals from feldspar-rich sediment extracts. Radiation Measurements 43, 1474−1486.

Timar, A., Vandenberghe, D., Panaiotu, E.C., Panaiotu, C.G., Necula, C., Cosma, C., van den haute, P., 2010. Optical dating of Romanian loess using fine-grained quartz. Quaternary Geochronology 5, 143−148.

Wang, X.L., Lu, Y.C., Zhao, H., 2006. On the performances of the single- aliquot regenerative-dose (SAR) protocol for Chinese loess: fine quartz and polymineral grains. Radiation Measurements 41, 1−8.

Wang, Y.J., Cheng, H., Edwards, R.L., Kong, X.G., Shao, X.H., Chen, S.T., Wu, J.Y., Jiang, X.Y., Wang, X.F., An, Z.S., 2008. Millennial- and orbital-scale changes in the East Asian monsoon over the past 224,000 years. Nature 451, 1090−1093.

Zhang JR, Jia YL, Lai ZP, Long H, Yang LH. 2011. Holocene evolution of Huangqihai Lake in semi-arid northern China based on sedimentology and luminescence dating. The Holocene 21, 1261−1268.

Zhang, J.R., Lai, Z.P., Jia, Y.L., 2012. Luminescence chronology for late Quaternary lake levels of closed Huangqihai lake in East Asia monsoon marginal area in northern China. Quaternary Geochronology 10, 123−128.

Appendix 1: Curriculum vitae

For reasons of data protection, the curriculum vitae is not published in the electronic version.

Appendix 2: Publications

(First author)

1. **Zhang, J.R.,** Tsukamoto, S., Jia, Y.L., Frechen, M., **2016**. Lake level reconstruction of Huangqihai Lake in northern China since MIS 3 based on pulsed optically stimulated luminescence dating. Journal of Quaternary Science 31, 225-238. DOI: 10.1002/jqs.2861.
2. **Zhang, J.R.,** Tsukamoto, S., Nottebaum, V., Lehmkuhl, F., Frechen, M., **2015**. D_e plateau and its implications for post-IR IRSL dating of polymineral fine grains. Quaternary Geochronology 30, 147-153.
3. **Zhang, J.R.,** Nottebaum, V., Tsukamoto, S., Lehmkuhl, F., Frechen, M., **2015**. Late Pleistocene and Holocene loess sedimentation in central and western Qilian Shan (China) revealed by OSL dating. Quaternary International 372, 120-129.
4. **Zhang, J.R.,** Tsukamoto, S., Grube, A., Frechen, M. **2014**. OSL and 14C chronologies of a coastal sedimentary record (Garding-2 core) from the German North Sea coast during the last deglaciation and Holocene. Boreas 43, 856–868.
5. **Zhang, J.R.,** Lai, Z.P., Jia, Y.L., **2012**. Luminescence chronology for late Quaternary lake levels of Huangqihai lake in East Asian monsoon marginal area in northern China, Quaternary Geochronology 10, 123–128.
6. **Zhang, J.R.,** Jia, Y.L., Lai, Z.P., Long, H., Yang, L.H., **2011**. Holocene evolution of Huangqihai Lake in semi-arid northern China based on sedimentology and luminescence dating. The Holocene 21(8), 1261–1268.

(co-author)

7. Nottebaum, V., Stauch, G., Hartmann, K,. **Zhang, J.R.,** Lehmkuhl, F., **2015**. Unmixed loess grain size populations along the northern Qilian Shan (China)–Relationships between geomorphologic, sedimentologic and climatic controls. Quaternary International 372, 151-166.
8. Long, H., Lai, Z.P., Fuchs, M, **Zhang, J.R.,** Li, Y., **2012**. Timing of Late Quaternary palaeolake evolution in Tengger Desert of northern China and its possible forcing mechanisms. Global and Planetary Change 92/93:119–129.
9. Cao, G.C, Long, H., **Zhang, J.R.,** Lai, Z.P., **2012**. Quartz OSL dating of last glacial sand dunes near Lanzhou on the western Chinese Loess Plateau: A comparison between different granulometric fractions, Quaternary Geochronology 10, 32–36.

10. Jia, Y.L., Lai, Z.P., **Zhang, J.R.**, Peng, X.M., Zhang, B., Zhang, Z., Wang, P.L., 2012. Chronology and provenance of aeolian sediments from Poyang Lake area in the middle reaches of the Yangtze River in China, Quaternary Geochronology 10, 44-49.

11. Long, H., Lai, Z.P., Fuchs, M, **Zhang, J.R.**, Yang, L.H., 2012. Palaeodunes intercalated in loess strata from the western Chinese Loess Plateau: Timing and palaeoclimatic implications.Quaternary International 263, 37–45.

Appendix 3: Conference contributions

(Orals)

1. **Zhang, J.R.,** Tsukamoto, S., Grube, A., Frechen, M., Oral: Reconstructing Holocene transgression history and sedimentary processes by a robust chronostratigraphic record from German North Sea coast. XIX INQUA Congress in Nagoya, Japan, 26th July-2nd Aug 2015.
2. **Zhang, J.R**., Tsukamoto, S., Frechen, M., Oral: Bleaching properties of post-IR IRSL signals at different preheat and stimulation temperatures. 2014 German Luminescence and ESR conference (LED) in Gießen, Germany, 14^{th}-16^{th} November 2014.
3. **Zhang, J.R**., Tsukamoto, S., Frechen, M., Oral: Loess sedimentation in the northern piedmont of Qilian Shan (China): timing and process revealed by luminescence dating. 2014 International Luminescence and ESR conference (LED) in Montreal, Canada, 07^{th}-14^{th} July 2014.
4. **Zhang, J.R**., Tsukamoto, S., Frechen, M., Oral: Luminescence and ^{14}C chronologies of a coastal sedimentary record (Garding-2 core) from the German North Sea coast during the last Deglaciation and Holocene. 2013 German Luminescence and ESR conference (LED) in Freiberg, Germany, 25^{th}-27^{th} October 2013.
5. **Zhang, J.R**., Tsukamoto, S., Frechen, M. Oral: Which Combination of Preheat and Stimulation Temperatures of pIRIR Should We Use for Different Age Ranges?−A Case Study from Northern Germany. UK LED 2013, 27^{th}-30^{th} August 2013, St Andrews, UK.
6. **Zhang, J.R.** Oral: Timing and possible forcing mechanisms of Huangqihai Lake fluctuations in semi-arid northern China since the late Glacial. XVIII INQUA Bern, Switzerland, 21^{st}-27^{th} July 2011.

(Posters)

7. **Zhang, J.R.,** Tsukamoto, S., Grube, A., Frechen, M. 2013. The transgression and sediment accumulation history in the coastal area of German North Sea since 16 ka−based on the high resolution luminescence and radiocarbon dating of Garding Core. EGU 2013, Vienna, Austria.

8. **Zhang, J.R.**, Jia, Y.L., Lai, Z.P., Long, H. Holocene lake evolution of Huangqihai Lake in semi-arid northern China based on sedimentology and luminescence dating. The 2nd PAGES Global Monsoon Symposium, in Shanghai, China, September 2010.

Appendix 4: Eidesstattliche Erklärung

Hiermit erkläre ich, dass ich die vorgelegte Arbeit selbständig und ohne fremde Hilfe verfasst habe. Die Beiträge der Co-Autoren der wissenschaftlichen Veröffentlichungen sind im Rahmen der Danksagung (Acknowledgements) dargelegt. Ich erkläre, dass die Arbeit erstmalig am Fachbereich Geowissenschaften der Freien Universität Berlin eingereicht wurde und somit noch keiner anderen Fakultät oder Universität zur Prüfung vorgelegt wurde. Der Inhalt der dem Verfahren zugrunde liegenden Promotionsordnung ist mir bekannt.

Jingran Zhang

Hannover, 20. Mai. 2015